NEW DEHYDRATION AND PRETREATMENT PROCESS FOR

ETHANOL PRODUCTION FROM BIOMASS

A Thesis
Presented to
The Academic Faculty

by

Pakkapol Kanchanalai

In Partial Fulfillment
of the Requirements for the Degree
Doctor of Philosophy in the
School of Chemical & Biomolecular Engineering

Georgia Institute of Technology
May 2015

NEW DEHYDRATION AND PRETREATMENT PROCESS FOR

ETHANOL PRODUCTION FROM BIOMASS

Approved by:

Dr. Matthew J. Realff, Advisor
School of Chemical & Biomolecular
Engineering
Georgia Institute of Technology

Dr. Yoshiaki Kawajiri, Advisor
School of Chemical & Biomolecular
Engineering
Georgia Institute of Technology

Dr. Martha Grover
School of Chemical & Biomolecular
Engineering
Georgia Institute of Technology

Dr. Pradeep K. Agrawal
School of Chemical & Biomolecular
Engineering
Georgia Institute of Technology

Dr. Scott Sinquefield
Renewable Bioproducts Institute
Georgia Institute of Technology

Date Approved: [March 24, 2015]

This thesis is dedicated to my father and my mother.

ACKNOWLEDGEMENTS

TABLE OF CONTENTS

Page

LIST OF TABLES

LIST OF FIGURES

LIST OF SYMBOLS

A	Membrane area
A_C	Cross sectional area
B	Biomass concentration
b_v	Biomass porosity
C	Component concentration in liquid phase
C^{eq}	Equilibrium component concentration in liquid phase
D	Diameter of reactor/TMB column
E	Total molar flow of fuel-grade ethanol
ε	Bed porosity of TMB column
F^A	Fresh acid consumption
F	Molar feed flow rate
Fe	Molar feed flow rate of each finite element
f	Biomass fraction
H	Adsorption Henry's coefficient
k	Kinetic constant
$\bar{k}_f$	Mass transfer coefficient of adsorption
KP	Total number of pervaporation membrane stage
KR	Total number of RO membrane stage
L	Length
M^B	Biomass throughput
$\mathrm{M}_w, \mathrm{M}_e$	Molar permeate flux

n	Exponent of acid concentration in kinetic model
P	Kinetic pre-factor
PUR	Purity of component at extract stream
p	Pressure
Q	Membrane permeance
q	Component concentration in solid adsorbent
R	Recycle stream flow rate
Rec	Ethanol recovery
S^s	Sugar selectivity
T	Temperature
t	time
u	liquid velocity
v	Solid velocity
w	Liquid mass fraction
x	Liquid mole fraction
xe	Liquid mole fraction in each finite element
Y	Sugar yield
y	Vapor mole fraction
γ	Activity coefficient
Γ	Gas constant
δ	Binary variable
π	Osmotic pressure

LIST OF SUBSCRIPTS AND SUPERSCRIPTS

A	*Acid component*
B	*Byproduct component*
D	*Desorbent stream*
D-PV	*Distillation-membrane-pervaporation unit*
E	*Extract stream*
FR	*Outlet stream from reactor*
FT	*Feed stream to TMB*
f	*Feed stream*
G	*Glucose component*
int	*intermediate stream*
PV	*Pervaporation unit*
p	*Permeate stream*
R	*Raffinate stream*
RO	*RO unit*
REP	*Recycle stream to ethanol production process*
RER	*Recycle stream to reactor*
RET	*Recycle stream from TMB column*
r	*Retentate stream*
S	*Sugar component*
W	*Water component*
X	*Xylose component*

LIST OF ABBREVIATIONS

CCR   *Countercurrent Reactor*

D-PV   *Distillation-Membrane-Pervaporation*

GAMS   *General Algebraic Modeling System*

MINLP   *Mixed-Integer-Non-Linear-Programming*

NRTL   *Non-Random Two-Liquid Model*

OECD   *Organization For Economic Co-Operation And Development*

PBR   *Progressing Batch Reactor*

RO   *Reverse Osmosis*

SPRSS   *Solid Phase Reactive Separation System*

SMB   *Simulated Moving Bed*

TMB   *True Moving Bed*

SUMMARY

The cost of pretreatment of biomass for saccharification and dilute ethanol purification are significant components of the overall cost for fuel grade ethanol production through fermentation or other biological routes. This thesis addresses three main topics: first, the optimization of a novel hybrid pretreatment process for a dilute bioethanol purification process; second, experimental determination of reaction kinetic parameters for the concentrated acid hydrolysis of cellulose and hemicellulose; third, the development of a novel solid-phase reactive chromatographic separation system for biomass saccharification via acid hydrolysis. All of these use optimization approaches to seek the best process configurations, process operation, and for parameter estimation.

For dilute ethanol purification, a reverse osmosis (RO) membrane process is introduced as a potential pretreatment for bioethanol purification in order to concentrate an ethanol-water mixture to an intermediate concentration. This is to reduce the distillation energy consumption and hence cost of dilute ethanol purification. It is confirmed that for dilute ethanol feeds, the steam used in the distillation reboiler dominates both the energy and the cost of the overall system. Installing the RO system reduces the steam usage at the expense of larger capital investment in membrane modules, which, given the cost equations used in this thesis, is found to be optimal for dilute feeds below 3 wt% ethanol. The optimal number of membrane stages and the feed location of individual RO modules change at different feed concentrations and ethanol recoveries.

For concentrated acid hydrolysis using sulfuric acid, the kinetics parameters are estimated for four main reaction paths including pure cellulose (Avicel), xylan hydrolysis

as well as xylose and glucose decomposition from four sets of batch experiments at different temperature and acid concentration. These parameters can be used as part of models to predict the concentration of sugars from biomass saccharification via a concentrated acid hydrolysis process as well as to investigate reactor and reactive separation process performance. In addition, it is found that the initial crystallinity index of the cellulose has a significant effect on the rate of hydrolysis reaction, where the lower initial crystallinity index of the cellulose has a much higher rate of cellulose hydrolysis.

Finally, a new reactive separation process concept termed solid-phase reactive separation system (SPRSS) is proposed and applied for biomass saccharification via acid hydrolysis. This process integrates the progressing batch reactor and the simulated moving bed chromatography processes where both systems employ similar principles of the movement of the liquid feed to imitate the countercurrent movement of solid and liquid phases. It is found that the key advantage of the SPRSS process is its flexibility in varying the acid concentration and liquid flow rate within the reactor system without any dilution to hydrolyze different portions of the biomass which have different hydrolysis reaction rates. The continuous model as well as the dynamic model of the SPRSS are formulated. The benefits of the SPRSS design are explored for both the dilute and concentrated acid hydrolysis processes. It is found that there is a potential improvement of the sugar yield as well as less byproduct formation by changing the acid concentration using the SPRSS configuration design.

CHAPTER 1

INTRODUCTION

1.1 Lignocellulosic material - a source for bioethanol production

The world is dependent on fossil fuels such as petroleum, natural gas, and coal to fulfill energy demands. Global energy needs continue to grow driven by economic development and population growth especially in countries outside the Organization for Economic Co-operation and Development (non-OECD countries) as shown in Figure 1.1[1] The burning of fossil fuels leads to the release of acid gases such as nitrous and sulphurous oxides and heavy metals and of most recent specific concern carbon dioxide. CO_2 emissions have been increasing over the last 150 years, causing a change in the atmospheric concentrations from 280 ppm to 365 ppm,[2] and are predicted to increase by 28% by 2030.[3]
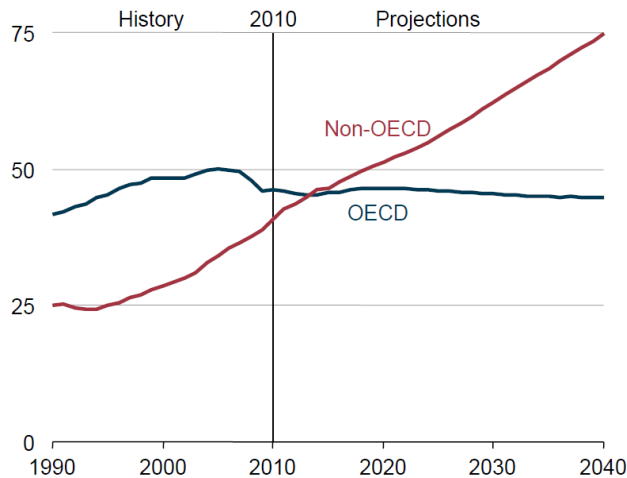
Figure 1.1. OECD and non-OECD petroleum and other liquid fuels consumption in million barrels per day (taken from EIA, 2014[4])

More evidence has been reported on the change in global atmosphere caused by an increase in the amount of CO_2 emission. Increased energy demand and concern about energy security as well as CO_2 impacts on climate have driven interest in the development of alternative fuels based on renewable feed stocks. The world energy outlook shows substantial growth of renewable energy sources in the next 20 years driven both by markets for CO_2 emission limitation and by government subsidy.[1, 5] However, it is challenging to produce these renewable fuels cost effectively and with relatively low energy input.

Bioethanol has been considered as a promising and potentially sustainable fuel since it can be used as a gasoline oxygenate, both to increase the octane number and provide a cleaner combustion, as well as being produced from carbon fixed from the atmosphere over relatively short time periods.[6] Over the lifecycle, the production and combustion of the bioethanol generally leads to a lower emission of fossil CO_2, carbon monoxide (CO), and nitrogen oxides for a given quantity of energy.[2] Large scale production of ethanol is based on first generation feedstocks such as sugarcane in Brazil or corn starch in USA. The production of sugarcane-based ethanol has increased in several countries mainly in tropical region. As for the bioethanol from corn starch, the production capacity cannot be increased significantly as this would compete with demand from the food industry.[7] Bioethanol can be produced via the lignocellulosic material, a second generation feedstock, which can avoid impacts on the food market. A key advantage of lignocellulosic material feedstock is its availability from sources such as grasses, sawdust, sugarcane bagasse, and corn stover which are generally residues from agricultural industries, although harvesting these secondary sources cost effectively is still a challenge.

1.2   Biomass composition

Biomass contains cellulose, hemicellulose, lignin, and other small components where the compositions vary by source. The typical composition of biomass is illustrated in Figure 1.2. Cellulose is generally the most abundant portion in the biomass accounting for 32 – 54 wt% in the biomass. Cellulose is present mainly in crystalline phases and small fractions in an amorphous phase.[8] Glucose is the hexose sugar that forms cellulose in a linear polymer structure where the degree of polymerization is typically around 2000 – 27000 units. Hemicellulose, the second main component in biomass, accounting for 11-37 wt% in biomass, is in a branched amorphous form which is easier to hydrolyze compared to the crystalline cellulose. The monosaccharides contained in hemicellulose include both hexoses and pentoses[9] such as xylose, mannose, glucose, galactose, arabinose, etc. Lignin, the third main component, accounting for 17 – 32 wt % in the biomass, is a complex polymer of phenylpropane units linked in a three-dimensional structure.[10] These components are extremely resistant to the hydrolysis reaction. There are some other small components in the biomass such as ash and extractives (e.g. fat, waxes, and inorganic compounds).[11]

1.3   Overall bioethanol production process from acid hydrolysis

Bioethanol production via hydrolysis of lignocellulosic materials can proceed through different pathways depending on the selection of pretreatment technology and the hydrolysis step. Two well-known hydrolysis technologies are the enzymatic and acid
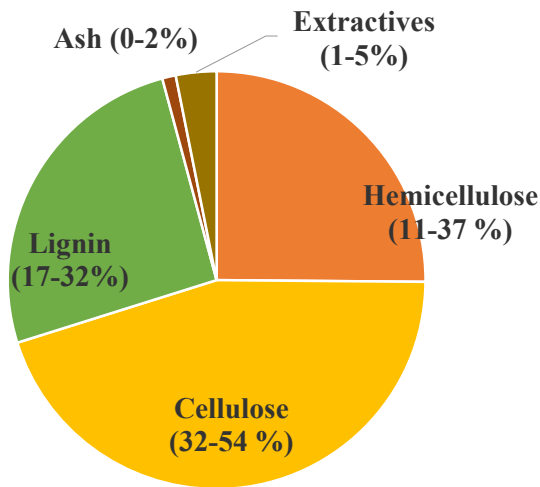
Figure 1.2. Composition of lignocellulosic materials.

hydrolysis.[9] The high sugar yield can be achieved from the enzymatic hydrolysis but its main drawbacks are the high enzyme cost as well as the slow reaction rate. Acid hydrolysis process has faster reaction but could generate byproducts that inhibit the fermentation process. This research focuses on the hydrolysis via an acid catalyst where the simplified overall bioethanol production process from lignocellulosic material is illustrated in Figure 1.3.[11] The biomass is milled to reduce the particle sizes to allow the acid to penetrate and hydrolyze to get the sugar solution in the next step. Sulfuric acid is the most preferred acid catalyst based on its price, corrosivity, and toxicity. Cellulose and hemicellulose are mostly converted into sugars, while lignin remains as solid residual which can be burned to produce steam for the process due to its high energy value. Several byproducts could be generated during the acid hydrolysis which require detoxification step to achieve the fermentable sugars. Glucose and xylose are generally the main products from the

hydrolysate, products from hydrolysis, which can be converted by separated fermentation or by a co-culture process using two microorganisms specific for each sugars.[12] For example, the commonly used microorganisms are *Saccharomyces cerevisiae* and *Zymomonas mobilis* for glucose fermentation and *Pichia stipites* and *Candida shehatae* for xylose fermentation.[13] Since the fermentation process for xylose is not as efficient as that for glucose, many recent researchers have endeavored to increase the xylose utilization for ethanol production via metabolic engineering.[14-16] After the fermentation, the bioethanol product is purified to achieve a fuel-grade ethanol at the purity of greater than 99 wt%.

Lignocellulosic material → Milling & size reduction → Acid hydrolysis

Fermentable sugar ← Detoxification ← **Sugar solutions**

Fermentation → Purification → **Bioethanol**
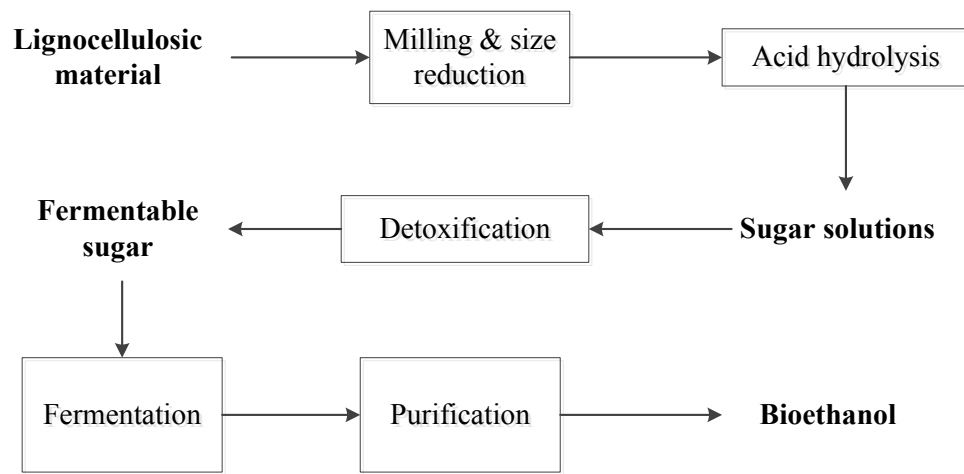
Figure 1.3. Overall process for bioethanol production from lignocellulosic material via acid hydrolysis.[11]

1.3.1 Biomass saccharification via acid hydrolysis

Acid hydrolysis can be done in two ways using either dilute or concentrated acid. The advantage of acid hydrolysis is its ability to penetrate lignin without pretreatment and its faster reaction rate compared to enzyme hydrolysis. However, there are several primary problems of the acid saccharification process. For the dilute acid hydrolysis process, a high
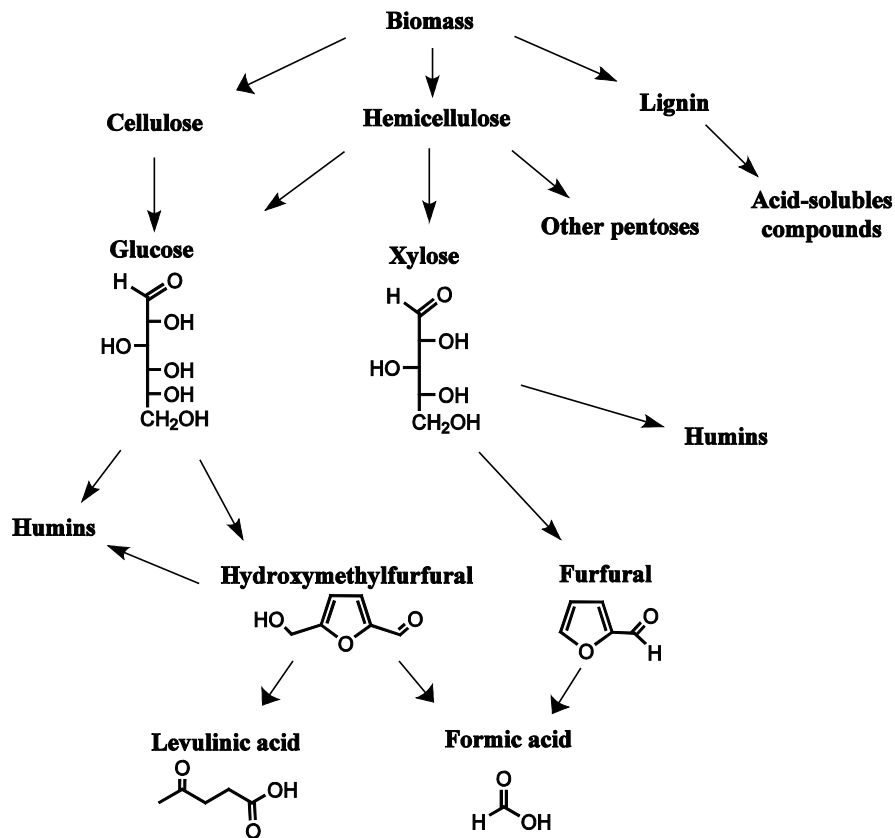
Figure 1.4. Possible reaction pathways for biomass acid hydrolysis achieved from Girisuta et al. [17]

operating temperature is required to break down the structure of the material: approximately 200-240 °C for cellulose and 140-160 °C for hemicellulose. However, these severe conditions also cause sugar decomposition and generate side products such as furfural, hydroxymethylfurfural (HMF), formic acid, and levulinic acid where the possible reaction scheme of the biomass hydrolysis is illustrated in Figure 1.4.[17] These generated byproducts strongly inhibit the fermentation process for bioethanol production process.[11, 18-20] The concentrations of furfural, the decomposed product from xylose, at 0.5, 1.0 and 2.0 g/L can reduce *Pichia stipites*, a common fermentation yeast, growth by 25%, 47% and

6

99%, respectively. Likewise, the concentration of HMF, the decomposed product from glucose, at 0.5, 0.75, 1.5 g/L decrease the growth rate of *Pichia stipites* by 43%, 70%, and 100%.[21] These byproducts must be detoxified before going through the fermentation step such as removal via evaporation of the volatile component, and precipitation of heavier toxic compounds.[22] The byproduct can also be removed via advanced separation technology such as chromatographic separation.[18] The acid contained in the hydrolysate must also be neutralized leading to a substantial generation of solid byproduct salts. All of these detoxification processes result in additional cost for bioethanol production.

For the concentrated acid hydrolysis process, a lower operating temperature, lower pressure, and a smaller amount of sugar degradation and less byproduct formation are its advantages over the dilute acid hydrolysis. However, the main drawbacks are the expensive process equipment to prevent corrosion and a significant cost of acid recovery.[11, 23] To reduce the cost of process acid, the acid must be separated and recycled which can be done via chromatography.[24] The concentrated acid hydrolysis process from Arkenol is considered an economically viable method for biomass saccharification.[25] This process contains two stages of hydrolysis where the biomass is treated at high acid concentration around 70 wt% in the first stage to decrystallize cellulose and hemicellulose followed by the hydrolysis reaction at acid concentration around 20 – 30 wt% at the temperature of 80 – 100 °C at atmospheric pressure to produce sugars where the reaction takes generally two to six hours. The acid in the hydrolysate is separated using the cation-exchange resin and the acid can be concentrated and recycled. The separation technology could be further enhanced by using the simulated moving bed chromatography (SMB) to recover fermentable sugars as well as recycling the acid which has been investigated in several

papers.[26-27] An improvement in separation process efficiency could potentially make concentrated acid hydrolysis process more economically viable.

1.3.2 Ethanol purification process

The purification of the bioethanol is generally an energy-intensive process. Fuel-grade bioethanol requires the separation of the ethanol-water mixture across the azeotropic point at around 95.6 wt%. Therefore, the separation is usually divided into two steps where the first step performs the main ethanol separation by ordinary distillation to achieve the purity close to the azeotropic point while the second step is to dehydrate the bioethanol across the azeotropic point to produce fuel-graded bioethanol.[6] There are several technologies used in the second step of separation. For example, azeotropic or extractive distillation alters the separation factor in the distillation system by adding a third component such as liquid solvent, dissolved salt, or ionic liquid. Adsorption is another technique which can be done in a vapor phase such as molecular sieves[28] and silica gel[29], and liquid phase such as starch-based adsorbents.[30]

The technique that has been recently considered the most effective and energy efficient is the membrane separation process. This includes membrane pervaporation systems[31-32] where the component with high permeability in the liquid feed is permeated through the membrane and evaporated into the vapor phase, and gas permeation where the system is all in the gas phase.[33]

Several papers describe the overall ethanol-water separation process using the hybrid distillation membrane approach to further reduce the energy consumption such as hybrid distillation-membrane-pervaporation[34] and steam-stripping-gas-permeation[35]

which are illustrated in Figure 1.5. It has been shown that different ethanol feed concentration may change the optimal choices of the separation process.[36]

(a)   (b)
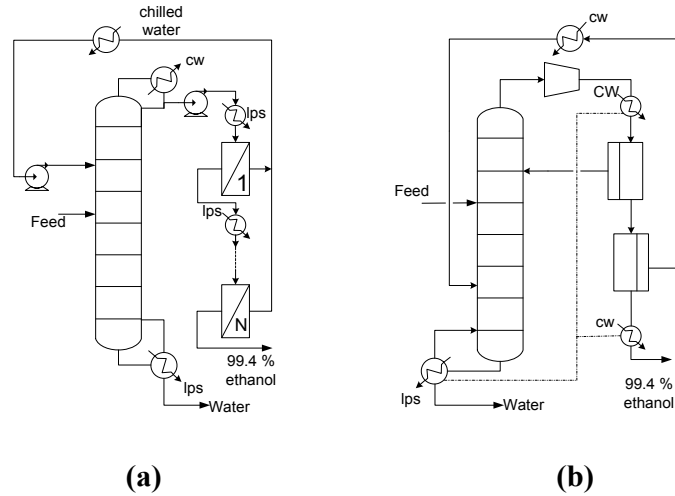
Figure 1.5. Hybrid distillation-membrane separation system (a) pervaporation (b) gas permeation.

1.4   Economics of the bioethanol production from lignocellulosic material

The US market price of ethanol has been fluctuating between $1.30 USD/gal and $3.40 USD/gal over the past 5 years, and the price in February 2015 was approximately 1.45 USD/gal.[37] In designing a bioethanol production process, the minimum ethanol selling price (MESP) must be lower than the market price in order to make the process economically attractive. The economic analysis of bioethanol production from lignocellulosic biomass has been investigated in several past studies.[38-40] The relatively high capital cost and the feedstock as well as logistic costs of the biomass resources are the main barrier for the commercial implementation of this process. The pretreatment step of

the biomass saccharification is one of the critical components that could significantly change the economics of the bioethanol production. A study from Tao et al. [41] found that MESP varies from $2.74 to $4.09 per gallon due to different biomass pretreatment process implementations. The ethanol yield is found to be the most important factor in determining the MESP, which is largely based on the sugar yield achieved in the pretreatment step and ensuring that inhibitory by-products are minimized.

Distillation is an energy-intensive process where the cost could increase significantly when the ethanol feed concentration from the fermentation decreases.[35] This also depends on the sugar concentration generated from the pretreatment and the hydrolysis steps. Thus, there is a tradeoff between the cost of the pretreatment technology and that of the purification process. For instance, two-stage dilute acid pretreatment may offer an economic advantage over the enzymatic path due to the expensive cost of the enzyme.[40] However, the yield from such an acid pretreatment technique is lower, resulting in a lower concentration of fermentable sugars, as well as bioethanol which ultimately increases the purification cost.

It is essential to develop an economic and efficient technology to convert second generation biomass feedstocks to produce fermentable sugars as well as an energy-effective separation technology for bioethanol production especially when the feed concentration is low. These are the main motivation for, and the objective of, this thesis.

CHAPTER 2

SCOPE OF THESIS

The overarching goal of this work is to reduce the cost of bioethanol production from biomass by developing novel pretreatment processes based on available mathematical modeling and optimization methods. Two processes including the bioethanol separation and the acid hydrolysis are the main focuses of this work as illustrated in Figure 2.1. Experimental work is also conducted in this work to provide essential information for the mathematical modeling. There are three main objectives in this work.

1. To identify the optimal separation process configuration with feed pretreatment via reverse osmosis for dilute bioethanol purification processes.
2. To model the kinetics of concentrated acid hydrolysis reactions of cellulose and hemicellulose.
3. To conceptualize and design a novel optimal solid phase reactive chromatographic separation system for biomass saccharification using a rigorous optimization strategy.

The first objective is the topic of Chapter 3 which synthesizes a bioethanol purification process for a dilute (1-5 wt%) feed. The reverse osmosis membrane system is introduced to pretreat the feed where the overall separation process configuration is modeled and optimized using the superstructure formulation to seek the best configuration and operating scheme. The comparisons of the cost and energy consumption of the separation process between the ones with and without reverse osmosis membrane pretreatment are illustrated. The optimal configurations of the overall separation process are presented at different feed concentrations.
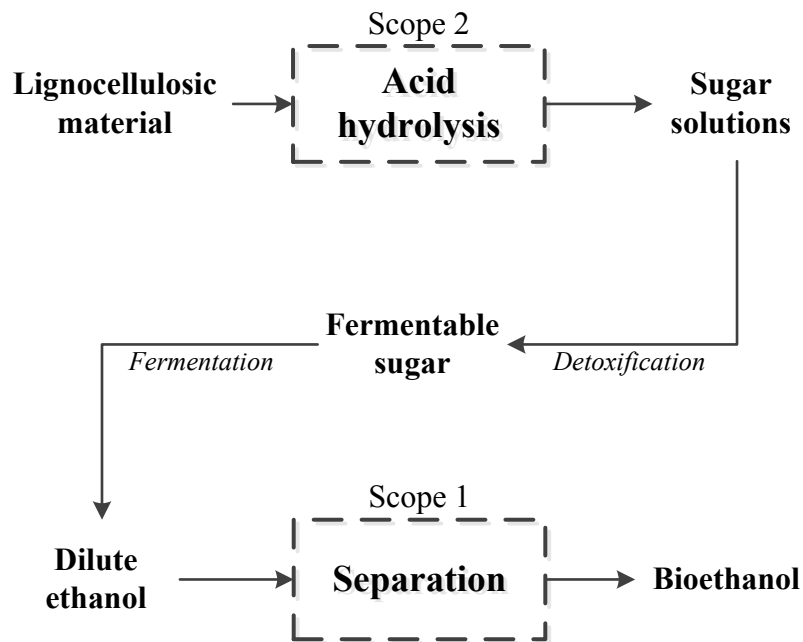
Figure 2.1. Scope of thesis

The second objective is the topic of Chapter 4 which shows the experimental work and the parameter estimation on the reaction kinetics of concentrated acid hydrolysis of cellulose and hemicellulose, as represented by Avicel and Xylan from Sigma Aldrich. In this chapter, the effect of the initial crystallinity index on the kinetics of the cellulose hydrolysis is illustrated. Furthermore, the kinetic parameters of the four main reaction paths of cellulose hydrolysis, xylan hydrolysis, glucose decomposition, and xylose decomposition are estimated using the method of least square minimization from four sets of batch experiments at different reaction temperatures and sulfuric acid concentrations.

The final objective is the topic of Chapter 5, Chapter 6, and Chapter 7 which illustrates a novel solid-phase reactive separation system (SPRSS). The new process is proposed and applied for the system involving the solid reactants like biomass which is aimed to increase the sugar yield and minimize byproduct formation from the acid hydrolysis reaction. The progressing batch reactor and simulated-moving bed chromatographic separation are combined where both systems have similar principles

which imitate the solid phase movement by switching the liquid inlet and outlet ports in the direction of the liquid flow. The advantages of SPRSS are investigated using the optimization strategy with the simplified continuous models of countercurrent reactor and true-moving-bed chromatography. The SPRSS with the kinetic parameters from the dilute acid region and from the concentrated acid hydrolysis achieved in Chapter 4 are explored in Chapter 5 and Chapter 6, respectively. Chapter 7 presents the dynamic model of SPRSS and specifically focuses on the progressing batch reactor where the simulation results are compared with the countercurrent reactor.

Altogether this thesis develops new pretreatment processes for bioethanol production from biomass and searches for the best process designs using optimization techniques based on superstructures that capture many possible configurations. The benefits of the new process designs could partially reduce the overall cost of the bioethanol production from biomass. Furthermore, the proposed reactive separation process may find other applications beyond bioethanol production.

CHAPTER 3

NEW PROCESS DESIGNS FOR DILUTE BIOETHANOL

PURIFURCATION

3.1   Motivation

Bioethanol is a well-established alternative fuel produced from various biomass sources. The primary production route is via fermentation of sugars from corn and sugarcane that leads to an ethanol in water solution whose concentration is limited by the initial concentration of the sugars and the toxicity of ethanol and other feed constituents to the fermentation organism. These first generation feed stocks are being supplemented by other second and third generation sources of ethanol derived from lignocellulosic material and from algae process.[42-44] These sources lead to ethanol concentrations of significantly lower than those from sugars. Fuel grade bioethanol has purity above 99 wt% and requires ethanol purification across the ethanol-water azeotropic point around 95 wt%. Several technologies have been used for ethanol dehydration such as membrane pervaporation, adsorption, extractive distillation, or the hybrid distillation-membrane separation.[6, 45] The choice of optimal separation technology may change depending on the feed concentration and throughput.[36, 46]

The ethanol concentration derived from the lignocellulosic material and algae process can be very low. The conversion using simultaneous saccharification and fermentation from lignocellulosic material can produce bioethanol of a concentration less than 5 wt%.[42, 47] Likewise, the processes based on growing algae can generate bioethanol at a very low concentration. One alternative route, for example, is a cyanobacteria (blue-

14

green algae) based process uses photosynthesis to produce ethanol which is then collected from closed photobioreactors by evaporation and condensation driven by the diurnal thermal cycle.[43-44, 48] However, ethanol production from this route can be very dilute, ranging from 0.5–5 wt%, and would require high energy consumption using conventional purification technology.[35, 48] Figure 3.1 depicts the energy consumption for ethanol purification to fuel grade at 99.4 wt% for different ethanol feed concentration using the optimal design of hybrid distillation-membrane-pervaporation (D-PV) system derived from previous work.[36] The value includes the sensible heat to preheat the stream at different feed temperatures and the ethanol purity of the stream leaving from the bottom of the distillation column must be less than 0.02 wt% to constrain on ethanol recovery. It can be seen that the energy requirement for ethanol purification to fuel grade increases rapidly with decreasing ethanol inlet concentration and exceeds the ethanol high heating value (HHV) which is around 30 MJ/kg-ethanol[35] when the ethanol feed purity is in the 1–2 wt% range. This implies that generating the fuel requires more energy than can be released from its combustion. Thus, this hybrid separation process, with current membrane material properties, is inadequate for dilute ethanol purification, and further reduction in energy consumption must be pursued. This motivates introducing a pretreatment process specifically suited to produce ethanol at an intermediate purity before feeding to the main separation to reduce significantly the separation cost and energy consumption for dilute ethanol purification.

In this work, we will focus on the optimal design of dilute ethanol purification with reverse osmosis (RO) membrane pretreatment technology from feeds that purify the
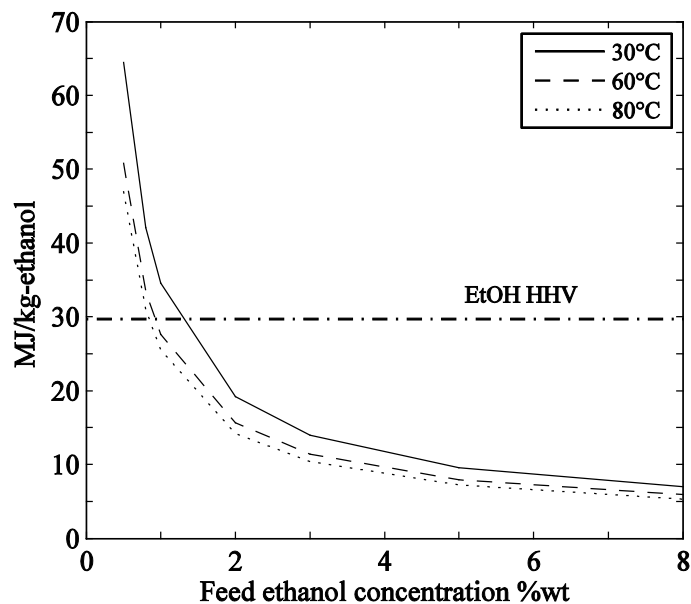
Figure 3.1. Energy consumption in MJ/kg-ethanol for D-PV for ethanol dehydration at different feed temperatures.

very dilute concentrations of ethanol. The superstructures of the hybrid distillation-membrane pervaporation with pretreatment are modeled as Mixed-Integer Nonlinear Programming (MINLP) problems to find the optimal process configurations by minimizing the total separation cost, subjected to a recovery constraint on the ethanol.

This chapter is organized as follow: section 3.2 describes the superstructure of the overall separation technologies including the hybrid D-PV and RO membrane pretreatment. The effect of ethanol recovery on RO membrane, the separation partition between RO membrane and D-PV, and the cost and energy savings from the RO membrane pretreatment are discussed in section 3.3.
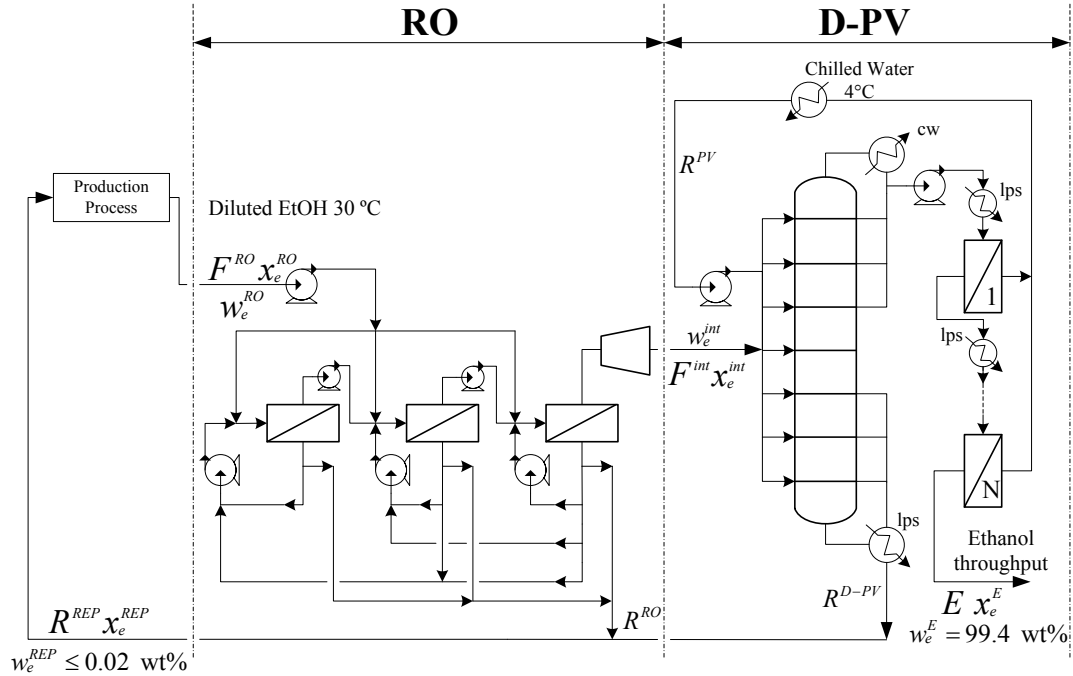
Figure 3.2. Superstructure of ethanol purification process.

3.2   Superstructure of separation technologies

A design methodology and process operation for the hybrid distillation-membrane system has been widely studied.[49-51] A distillation column can be combined with gas permeation or pervaporation membrane, each of which each has its own advantages. A comparison of the performance of gas permeation and pervaporation has been addressed based on the same basis.[52] Lipnizki et al.[53] and Koczka et al.[54] reviewed several configurations and arrangement of D-PV for ethanol dehydration. Huang et al.[55-56] and Vane et al.[57] developed a new hybrid distillation-gas-permeation with vapor compression for ethanol purification which enables heat integration within the system. Our previous work shows that the hybrid D-PV membrane is favored over the gas-permeation system at

a low ethanol feed concentration.[36] Therefore, the D-PV system is chosen as the main separation for bioethanol dehydration in this work. Superstructures for the D-PV have been proposed as a rigorous MINLP model to minimize the total annual cost of separation.[34, 58-60] In this study, the pervaporation membrane is placed at the top of the distillation column to purify the mixture across the azeotropic point and the RO pretreatment is added before the main separation unit after the ethanol production process to produce a stream with intermediate ethanol concentration. Figure 3.2 shows the superstructure of the hybrid separation technology to purify dilute ethanol to fuel grade ethanol.

Water removed from both the pretreatment step and the main distillation column is recycled to the ethanol production process which can be any types. A constraint is placed on the recycled ethanol concentration to be lower than 0.02 wt% to constrain on the ethanol recovery. The optimizer will decide how much ethanol should be removed or recovered from each subsystem. Thus, the ethanol recovery is one of the main decision variables for the optimization of overall separation process.

3.2.1 Hybrid distillation-membrane pervaporation

The main distillation column is modeled as a MINLP proposed by Viswanathan and Grossmann[61-62] where the non-random two-liquid (NRTL) phase equilibrium model for ethanol-water mixture is used at atmospheric pressure. The column model variables are the number of column stages, feed stage, the distillate flow rate, and the top column purity. The top distillate passes through the pump and the heat exchanger respectively to increase the pressure to maintain the flow in a liquid phase and increase the temperature before feeding to the membrane system.
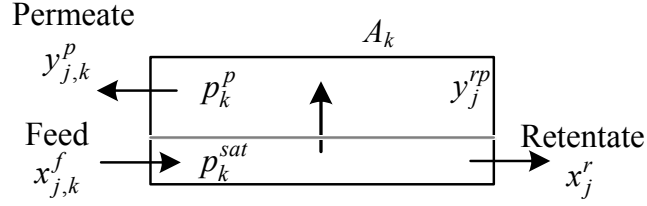
Figure 3.3. Hollow fiber pervaporation membrane modeling each stage.

Previous studies have addressed the design and operation of pervaporation membrane for ethanol dehydration.[31, 63] Ethanol is concentrated to fuel grade at 99.4 wt% while the water permeates are combined and cooled by chilled water before feeding back to the distillation column at the appropriate stage decided by the optimizer. The membrane model can vary the membrane area, the ethanol outlet concentration for each membrane stage, the feed temperature, and the permeate pressure which is controlled by the temperature of the chilled water.

The hollow fiber pervaporation membrane model is counter-current flow (see Figure 3.3) with mass and energy balance around each membrane stage. We define a set $NPS = \{1, 2, \ldots, KP\}$ to denote the number of pervaporation membrane stage and another set $NC = \{e, w\}$ to denote the ethanol and water component. The standard solution-diffusion mass transfer model is used to calculated the permeate flux of each stage where the pressure driving force mainly depends on the vapor pressure of the feed and the permeate[64-66]

$$y_{j,k}^{p} F_{k}^{p} = Q_{j,k} \overline{\left(\gamma_{j,k} x_{j,k} p_{k}^{sat} - y_{j,k} p_{k}^{p} \right)} A_{k} \qquad j \in NC, k \in NPS \qquad (2.1)$$

19

where $y_{j,k}^{p}$ is the species molar composition in the permeate, F_{k}^{p} is the total vapor molar

permeate flow, and A_{k} is the membrane area of each stage. A polyvinyl alcohol membrane

material is used where the species permeance ($Q_{j,k}$) is expressed as a function of ethanol

concentration.[66-67] The remaining term is the pressure driving force which is evaluated by

using the log-mean average vapor pressure difference between the feed and the permeate

side at both inlet and outlet of the membrane.[66]

$$\overline{\gamma_{j,k} x_{j,k} p_{k}^{sat} - y_{j,k} p_{k}^{p}} = \frac{\left(\gamma_{j,k}^{f} x_{j,k}^{f} p_{k}^{sat} - y_{j,k}^{p} p_{k}^{p} \right) - \left(\gamma_{j,k}^{r} x_{j,k}^{r} p_{k}^{sat} - y_{j,k}^{rp} p_{k}^{p} \right)}{\ln \left(\dfrac{\gamma_{j,k}^{f} x_{j,k}^{f} p_{k}^{sat} - y_{j,k}^{p} p_{k}^{p}}{\gamma_{j,k}^{r} x_{j,k}^{r} p_{k}^{sat} - y_{j,k}^{rp} p_{k}^{p}} \right)} \qquad (2.2)$$

$$j \in NC, k \in NPS$$

The evaluation of logarithm terms may cause numerical problems in an

optimization model. Therefore, the Chen approximation is implemented to approximate

the log-mean pressure driving force.[66, 68]

$$\frac{\Delta_{1} - \Delta_{2}}{\ln \left(\dfrac{\Delta_{1}}{\Delta_{2}} \right)} \approx \left(\Delta_{1} \Delta_{2} \left\{ \frac{\Delta_{1} + \Delta_{2}}{2} \right\} \right)^{\frac{1}{3}} \qquad (2.3)$$

The vapor pressure driving force depends on the temperature of the feed, which is

reduced along the module by the latent heat of evaporation of the permeate flow.

Intermediate heating of the retentate between membrane stages is therefore required to

increase the driving force.[31, 63] The total number of stages KP was varied and cost was a

monotonically decreasing function of KP with increasingly small changes as KP was

increased. Therefore, the number of stage was chosen by manually increasing KP until no

significant improvement on the objective function was observed. Four membrane stages

with four interstage heaters were found sufficient and fixed as the number of stages for the

rest of the study (*KP*=4). The heaters increase the membrane feed temperature of each stage up to 90°C, assumed to be below the maximum operating temperature of the pervaporation membrane.[56]

3.2.2   RO membrane pretreatment

RO membranes have been widely used in waste water treatment and desalination as they offer several benefits such as low energy consumption, moderate cost, and operation at ambient temperature.[69-70] Several past studies considered ethanol purification using RO membranes.[71-72] Optimal configurations and the superstructures of RO membrane system have been previously addressed.[73-75] El-Halwagi[76] proposed a state-space approach including RO units, pumps, energy-recovery devices, and stream distribution which has been used and modified by several authors.[77-79] Our system which contains a binary mixture is required to achieve both a certain ethanol purity and ethanol recovery. We consider a membrane system adapted from a countercurrent cascade which contains enriching and stripping section similar to a distillation column.[80-82] The superstructure of RO membrane is shown in Figure 3.4.

The superstructure allows the number of RO membrane to vary. In this superstructure, we limit the system to a maximum of three membrane stages in order to reduce the computation time and avoid some redundant local solutions which will be described in the results. RO systems normally operate at a high pressure to increase the driving force which is assumed to have a maximum value of 83 bar. The feed is pressurized and its location chosen to be between any of the three membrane stages. The model allows the permeate to be pressurized and recycled back to any of the previous stages for ethanol recovery, or it can be removed from the membrane system at any stage. The model can

choose to have an interstage pump to increase retentate pressure before feeding to the next stage. The stream with intermediate ethanol purity from the final membrane stage passes through to an energy recovery device[83] to reduce it to atmospheric pressure and it is fed to the main dehydration step, while the water removed from the membrane system is returned to the ethanol production process and water recovery.
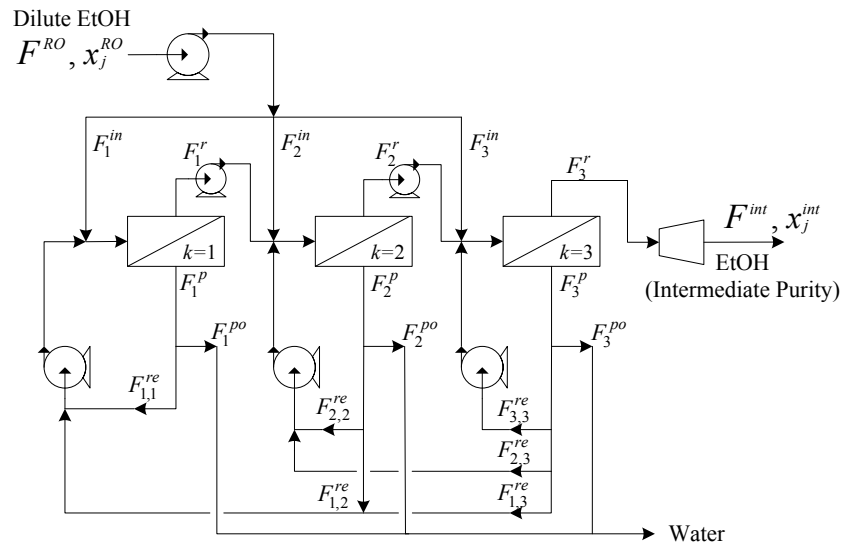
Figure 3.4. Superstructure of RO membrane.
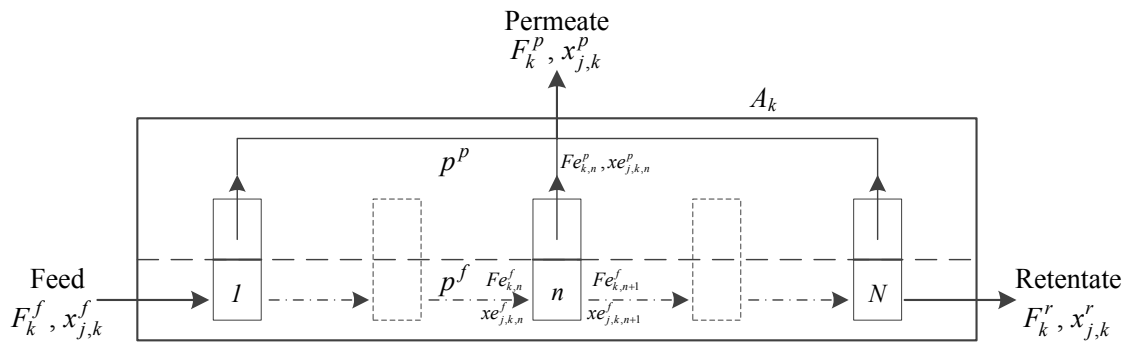
Figure 3.5. Spiral wound cross flow model with finite elements for RO membranes.

The area of the RO membrane is relatively large up to approximately 150 times of the pervaporation membrane area in dehydration step. Each membrane stage is therefore discretized equally into 30 finite elements to increase the accuracy of optimization results (see Figure 3.5). Let $NE = \{1,2,\ldots,N\}$ be a set of the number of finite element and $NRS = \{1,2,\ldots,KR\}$ be a set of RO membrane stage where $N = 30$ and $KR = 3$. The mole and component balance equations of a mixing of feed streams for each membrane stage are[73]

$$F_1^f = F_1^{in} + \sum_{l=1}^{KR} F_{1,l}^{re} \tag{2.4}$$

$$x_{j,1}^f F_1^f = x_j^{RO} F_1^{in} + x_{j,1}^{re} \sum_{l=1}^{KR} F_{1,l}^{re} \qquad j \in NC \tag{2.5}$$

$$F_k^f = F_k^{in} + F_{k-1}^r + \sum_{l=k}^{KR} F_{k,l}^{re} \qquad k \in NRS - \{1\} \tag{2.6}$$

$$x_{j,k}^f F_k^f = x_j^{RO} F_k^{in} + x_{j,k-1}^r F_{k-1}^r + x_{j,k}^{re} \sum_{l=k}^{KR} F_{k,l}^{re} \qquad j \in NC, k \in NRS - \{1\} \tag{2.7}$$

where F_k^f is the total molar feed rate at each stage, F_k^{in} is the feed entering stage k, and F_k^r is the retentate outlet from stage k. $F_{k,l}^{re}$ is the recycle stream from the permeate stage l to stage k which is allowed to enter only the current stage and all previous stages ($k \le l$), and x_j is the species liquid mole fraction of the corresponding stream. The mole and component balances of each membrane element are

$$F_k^f = Fe_{k,2}^f + Fe_{k,1}^p \qquad k \in NRS \tag{2.8}$$

$$x_{j,k}^f F_k^f = xe_{j,k,2}^f Fe_{k,2}^f + xe_{j,k,1}^p Fe_{k,1}^p \qquad j \in NC, k \in NRS \tag{2.9}$$

$$Fe_{k,n}^f = Fe_{k,n+1}^f + Fe_{k,n}^p \qquad k \in NRS, n \in NE - \{1, N\} \tag{2.10}$$

$$xe_{j,k,n}^f Fe_{k,n}^f = xe_{j,k,n+1}^f Fe_{k,n+1}^f + xe_{j,k,n}^p Fe_{k,n}^p$$
$$j \in NC, k \in NRS, n \in NE - \{1, N\} \tag{2.11}$$

$$Fe_{k,N}^f = F_k^r + Fe_{k,N}^p \qquad k \in NRS \tag{2.12}$$

$$x_{j,k}^f Fe_{k,N}^f = x_{j,k}^r F_k^r + xe_{j,k,N}^p Fe_{k,N}^p \qquad j \in NC, k \in NRS \tag{2.13}$$

23

$$\sum_{j \in NC} xe^{p}_{j,k,n} - \sum_{j \in NC} xe^{r}_{j,k,n} = 0 \qquad k \in NRS, n \in NE \qquad (2.14)$$

where $Fe^{f}_{k,n}$, $Fe^{p}_{k,n}$, are molar flow rates of the feed and permeate stream of each membrane element at stage k respectively, xe_j is the corresponding species mole fraction. The permeate of each membrane stage is the sum of permeate from all membrane elements.

$$F^{p}_{k} = \sum_{n=1}^{N} Fe^{p}_{k,n} \qquad k \in NRS \qquad (2.15)$$

$$x^{p}_{j,k} F^{p}_{k} = \sum_{n=1}^{N} xe^{p}_{j,k,n} Fe^{p}_{k,n} \qquad j \in NC, k \in NRS \qquad (2.16)$$

The permeate of each membrane stage is allowed to recycle to the previous stage or to be removed from the membrane system, which is a decision represented by logic constraints as follows.

$$\sum_{\bar{k}=1}^{k} F^{re}_{\bar{k},k} + F^{po}_{k} = F^{p}_{k} \qquad k \in NRS \qquad (2.17)$$

$$\sum_{l=k}^{KR} x^{p}_{j,l} F^{re}_{k,l} = x^{re}_{j,k} \sum_{l=k}^{KR} F^{re}_{k,l} \qquad j \in NC, k \in NRS \qquad (2.18)$$

$$\sum_{\bar{k}=1}^{k} F^{re}_{\bar{k},k} = \delta^{p}_{k} F^{p}_{k} \qquad k \in NRS \qquad (2.19)$$

F^{po}_{k} is the permeate removed from stage k and δ^{p}_{k} is the binary variable indicating the permeate recycle. The logic constraints for the feed location are

$$F^{RO} = \sum_{k=1}^{KR} F^{in}_{k} \qquad (2.20)$$

$$F^{in}_{k} \leq \delta^{f}_{k} F^{RO} \qquad k \in NRS \qquad (2.21)$$

$$\sum_{k=1}^{KR} \delta^{f}_{k} = 1 \qquad (2.22)$$

where F^{RO} is the total feed flow rate and δ_k^f is the binary variable for choosing the feed

location. The existence of membrane stage is determined by the binary variable.

$$L\delta_k^{A_k} \leq A_k \leq U\delta_k^{A_k} \qquad k \in NRS \tag{2.23}$$

$$\delta_k^{A_k} \leq \delta_{k-1}^{A_k} \qquad k \in NRS - \{1\} \tag{2.24}$$

$$\delta_k^f \leq \delta_k^{A_k} \qquad k \in NRS \tag{2.25}$$

L and U are lower and upper bounds of the membrane area and $\delta_k^{A_k}$ is the binary

variable representing the existence of a membrane stage. We restrict membrane stages after

the first stage to be added consecutively by including the logic constraint, Eq. (3.24). The

feed is restricted to be located only at an existing membrane stage (Eq. (3.25)). These logic

constraints are added to avoid non-unique solutions.

The RO membrane module is modeled as a spiral wound cross flow model where

the permeate side is assumed well mixed. A mass transfer solution-diffusion model is

chosen where the water driving forces depend on the liquid pressure and the osmotic

pressure of both feed and permeate side. The ethanol permeate flow is relatively small

compared to water permeate flow and is modeled using a concentration gradient[66, 80] rather

than a pressure driving force. The permeate flow and the driving force of each component

are given as follows.

Water permeate flow and driving force:

$$xe_{w,k,n}^p Fe_{k,n}^p = M_w \left\{ \overline{\left(\Delta p^f - \Delta \pi \right)}_{k,n} \right\} \frac{A_k}{N} \qquad k \in NRS, n \in NE \tag{2.26}$$

$$\overline{\left(\Delta p^f - \Delta \pi \right)}_{k,n} = \left(p_k^f - p^p \right) - \left(\overline{\pi}_{k,n} - \pi_{k,n}^p \right) \qquad k \in NRS, n \in NE \tag{2.27}$$

Ethanol permeate flow and driving force:

$$xe_{e,k,n}^p Fe_{k,n}^p = \mathrm{M}_e \left\{ \overline{\left(C_e - C_e^p \right)}_{k,n} \right\} \frac{A_k}{N} \qquad k \in NRS, n \in NE \qquad (2.28)$$

$$\overline{\left(C_e - C_e^p \right)}_{k,n} = \left(\overline{C}_{e,k,n} - C_{e,k,n}^p \right) \qquad k \in NRS, n \in NE \qquad (2.29)$$

where A_k is the total membrane area of each stage, and N is the total number of finite

elements. Thus, each stage has 30 equivalent elements where the area of each element for

each stage depends on the optimal total membrane area A_k. M_W and M_e are the permeate

flux of water and ethanol, which are functions of its driving force. ΔP and $\Delta \pi$ are the

pressure and osmotic pressure difference of the feed and the permeate, respectively. P_k is

the feed pressure of each membrane stage, p is the atmospheric permeate pressure, and C_e

is the molar ethanol concentration (kmol.m^{-3}). The osmotic pressure and the ethanol

concentration of the permeate side is constant under the well-mixed assumption while those

of feed side denoted $\overline{\pi}$ and $\overline{C}_e$ are approximated between the feed inlet and retentate outlet

using the log-mean average with the Chen approximation. The correlation to estimate the

osmotic pressure used in the model assuming the ideal solution is[82]

$$\pi = iC_e \Gamma T \qquad (2.30)$$

where i is the Van't Hoff factor which is equal to one for an ethanol-water mixture, Γ is

the gas constant and T is the temperature which is assumed at 303 K. We assume a

polyacrylamide membrane where the mass transfer across the membrane is fitted to

experimental data[84] and express the permeate flux as a linear function for a specified range

(see Figure 3.6).
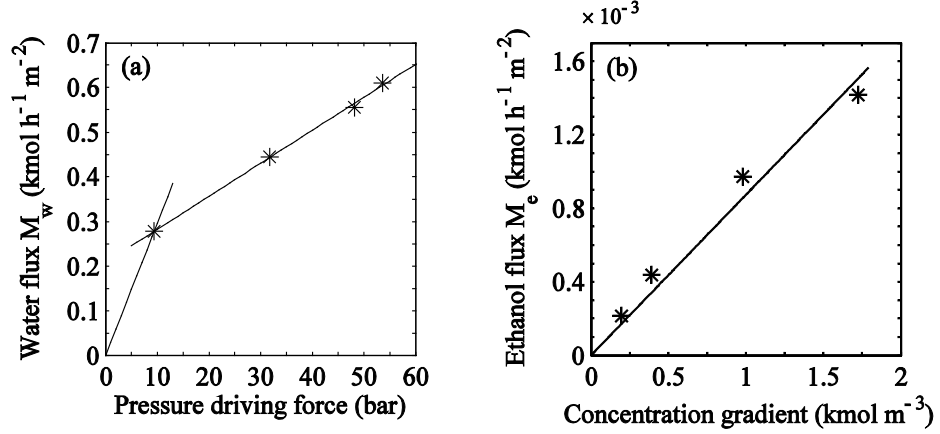
Figure 3.6. Molar flux of water (a) and ethanol (b) through polyacrylamide.

$$M_w = \begin{cases} 0.0296\left(\overline{\Delta p^f - \Delta \pi}\right) & \overline{\Delta p^f - \Delta \pi} < 10 \text{ bar} \\ 0.0074\left(\overline{\Delta p^f - \Delta \pi}\right) + 0.2083 & \overline{\Delta p^f - \Delta \pi} \geq 10 \text{ bar} \end{cases} \qquad (2.31)$$

$$M_e = 8.74 \times 10^{-4}\left(\overline{C_e - C_e^p}\right) \qquad \left(\overline{C_e - C_e^p}\right) \leq 1.8 \text{ kmol} \cdot \text{m}^{-3} \qquad (2.32)$$

The effect of concentration polarization is assumed negligible. In addition, we define the ethanol recovery of RO system, D-PV, and total separation as

$$Rec^{RO} = \frac{x_e^{int} F^{int}}{x_e^{RO} F^{RO}} \qquad (2.33)$$

$$Rec^{D-PV} = \frac{x_e^E E}{x_e^{int} F^{int}} \qquad (2.34)$$

$$Rec^T = Rec^{RO} Rec^{D-PV} = \frac{x_e^E E}{x_e^{RO} F^{RO}} = 1 - \frac{x_e^{REP} R^{REP}}{x_e^{RO} F^{RO}} \qquad (2.35)$$

where x_e^{int} and F^{int} are the ethanol composition and molar flow of the intermediate stream feeding to D-PV unit, x_e^{RO} and F^{RO} are those of RO feed, and E is the ethanol product stream with corresponding x_e^E (see Figure 3.2). The total recovery in Eq. (3.35) can be expressed from the mole balance in terms of the composition and the flow of the recycle

stream to ethanol production process denoted by x_e^{REP} and R^{REP}, respectively. The details of the model assumptions are shown in Table 3.1.

The optimization model is solved to minimize the ethanol separation cost per unit fuel ethanol throughput. This consists of the total annualized capital cost (TCC) and the total operating cost (TOC) for different ethanol feed concentrations and throughputs.

$$\min \; z = \text{EtOH Cost} = \frac{\text{TCC+TOC}}{E} \qquad (2.36)$$

The weight purity of ethanol product stream is set as an equality constraint at fuel grade.

$$w_e^E = 0.994 \qquad (2.37)$$

There is additional constraint for recovery which will be discussed in the results. All equipment costs and sizing are modeled using the correlations from Sieder et al.[85] while the RO membrane cost is from Baker and Lokhandwala.[86] A process life cycle is assumed to be 15 years for all equipment except for a 5-year-life of both pervaporation and RO membranes and a discount rate of 8%. A summary of all equipment and utilities used in optimization model is shown in Table 3.2.

The model is non-convex with many possible local solutions; therefore, different initial guesses have been investigated to get the best optimal solution, but global optimality is not guaranteed. All of the model decisions are listed in Table 3.3.

Table 3.1. Model assumptions of hybrid D-PV with RO membrane pretreatment for dilute ethanol purification

Model parameter	Assumption
Ethanol production process	
Maximum ethanol concentration of recycle stream[35]	0.02 wt%
Ethanol feed temperature	30 °C
Distillation column	
Phase equilibrium model	NRTL
Tray efficiency	75%
Operating pressure	1.01 bar with no pressure drop
Column limitation diameter[85]	7.3 meters (24 feet)
Pervaporation membrane	
Membrane type	Polyvinyl alcohol – hollow fiber
Mass transfer model and flow type[64-66]	Solution-diffusion; counter-current with Chen approximation for log-mean driving force
Membrane interstages	4 stages
Maximum membrane operating temperature[56]	90 °C
Water permeance[66]	$0.314 x_e^{-0.374}$ (kmol h^{-1}m^{-2}bar^{-1})
Selectivity water/ethanol[66]	$890 x_e^{2.83}$
Membrane cost in module[85]	409 $/m^2 (38 $/ft^2)
Membrane cost in module and skid[a]	1,292 $/m^2 (120 $/ft^2)
Life cycle	5 years
RO membrane pretreatment	
Maximum membrane interstages	3 stages
Membrane type[84]	Polyacrylamide – spiral wound
Mass transfer model and flow type[64-66]	Solution-diffusion; cross flow with Chen approximation for log-mean driving force
Maximum operating pressure	83 bar
Membrane area upperbound (Eq. (3.23))	7×10^6 m^2
Membrane area lowerbound (Eq. (3.23))	100 m^2
Water flux[84]	Linear function expressed in Eq. (3.31)
Ethanol flux[84]	Linear function expressed in Eq. (3.32)
Membrane cost in module[86]	15 $/m^2
Membrane cost in module and skid[86]	50 $/m^2
Life cycle	5 years
Other equipment	
Heat transfer coefficient of reboiler[b]	2.27 kW m^{-2} °C^{-1} (400 Btu h^{-1} ft^{-2} °F^{-1})
Heat transfer coefficient of condenser[c]	0.57 kW m^{-2} °C^{-1} (100 Btu h^{-1} ft^{-2} °F^{-1})
Efficiency of RO energy recovery device[d]	97 %

Table 3.1 (continued). Model assumptions of hybrid D-PV with RO membrane pretreatment for dilute ethanol purification

Model parameter	Assumption
Utilities[85]	
Cooling water temperature	30 °C
Cooling water cost	2×10^{-5} $/kg
Chilled water temperature	4 °C
Chilled water cost	4×10^{-6} $/kJ
Steam temperature	120 °C
Steam cost	6.6×10^{-3} $/kg
Electricity cost	0.06 $/(kW.h)
Economic assessment	
Discount rate	8 %
Separation plant life cycle	15 years
Operating days per year	330 days

[a]The membrane in module and skid is approximated by multiplying the bare module factor which is assumed equivalent to that of shell-and-tube heat exchangers at 3.17[85] The cost with skid is for the capital cost while the cost without skid is for the maintenance operating cost.

[b]Based on steam condensing–water[85]

[c]Based on alcohol vapor–water[85]

[d]Isobaric positive displacement mechanism is used for energy recovery devices[83] where the reciprocating pump cost model is used to estimate the cost.[85]

Table 3.2. Summary of process equipment and utilities used in optimization model

Separation Unit	Process Equipment	Utilities
Distillation column	Column	Cooling water for condenser
	Condenser	Steam for reboiler
	Reflux drum	
	Reboiler	
	Recycle pumps	
Pervaporation	Feed pump	Steam for interstage heaters
	Pervaporation membrane	Chilled water from vacuum condenser
	Interstage heaters	Electricity for all pumps
	Vacuum condenser	
	Vacuum drum	
	Recycle pump	
RO membrane	RO membrane	Electricity for all pumps
	Feed pumps and interstage pumps	
	Energy recovery device	

Table 3.3. List of model decisions

Distillation column	Pervaporation	RO membrane
Number of stages	Membrane area	Number of stages
Feed stage	Feed temperature of each stage	Feed stage
Recycle stage	Permeate pressure	RO membrane area
Reflux ratio	Vacuum condenser area	Recycle stage
Distillate flow rate		Feed pressure of each stage
Condenser area		Existence of power recovery unit
Reboiler area		

3.3   Results and discussions

All of the MINLP models of the superstructure of separation technologies are formulated and solved in GAMS 23.7.3 using SBB/CONOPT 3.15A solver, and the optimizations are run on six-Core 2.4 GHz AMD Opteron(tm) Processor with 8GB of RAM. Several equipment cost models were extrapolated beyond their stated ranges especially at a high throughput. For instance, the areas of a reboiler, a condenser, the volumetric flow rate, and a head of several pumps exceed the valid range of the equipment cost equations.[85] Multistage heat exchangers and pumps may be necessary in practice, but would add unnecessary complexity to the MINLP because the costs of these units account for a small fraction of the total separation cost, and therefore have negligible impact on the optimal solutions. The extrapolated results are also compared with other different cost models[87] and very small differences in the optimal solutions were found. The accuracy of Chen approximation for the driving force of the mass transfer model was investigated separately. We found negligible difference of the estimated membrane area and the separation cost compared between an exact and the approximate model.

3.3.1 Effect of ethanol recovery on optimal configuration of RO system

The ethanol recovery is one of the main decision variables for the overall separation process. We first solved a sub-problem of the RO system to study the impact of ethanol recovery on the optimal configuration of the RO system. In this case study, the RO is used to purify dilute ethanol from 0.8 wt% ($w_e^{RO} = 8.0 \times 10^{-3}$) to an intermediate concentration of 7.0 wt% ($w_e^{RO} = 0.07$) at 426 Mgal/yr (volumetric flow corresponding to F^{int}) which is approximately equivalent to a throughput of fuel ethanol (99.4 wt%) at 30 Mgal/yr. In addition, the model includes additional constraint on ethanol recovery of RO.

$$Rec^{RO} \geq Rec^{min} \qquad\qquad (2.38)$$

where Rec^{min} is the minimum RO recovery which is set at different values ranging from 80% to 100%. The optimal results from our superstructure reveal that the RO configurations are reducible into three stages or less for our investigated ranges of feed purity and throughput. Figure 3.7a shows the ethanol unit cost for each corresponding optimal membrane configuration in Figure 3.7b at different ethanol recoveries. At Rec^{min} = 82–85%, only one optimal stage is sufficient to achieve the recovery (see Figure 3.7b-I). Some amount of ethanol is therefore allowed to exit with the permeate and no further recovery is required. In Figure 3.7b-II, the number of membrane stages increases to three when increasing the Rec^{min} to 87–95%. This configuration has two enriching stages and one stripping stage, which indicates a higher emphasis on ethanol purification than ethanol recovery. The dilute ethanol is mixed with the retentate of the same purity from the stripping stage and fed to the first enriching stage where a significant amount of water is removed before further separation at the next enriching stage. The second enriching stage purifies the stream to achieve the final concentration and to allow the permeate to recycle

to the stripping stage for ethanol recovery. At $Rec^{\min} = 98$ %, the optimizer reduces the total number of stage to two, comprising one enriching and stripping stage as shown in Figure 3.7b-III. This shows that the separation task for ethanol purification and ethanol recovery is approximately equivalent. When increasing the ethanol concentration to almost full recovery at $Rec^{\min} = 99\%$, the optimizer adds another stripping stage to a total of two while remaining enriching section at one stage as can be seen in Figure 3.7b-IV. The optimizer partitions the separation task for ethanol recovery in the stripping section more than that for ethanol purification in enriching stage. In this configuration, the dilute ethanol is fed to the enriching stage to achieve final concentration and the permeate is recycled to the first stripping stage to remove significant amount of water. The second stripping stage purifies ethanol to mix with the dilute feed with similar purity and recycle ethanol in the permeate to the first stripping stage. From Figure 3.7a, the separation cost for the RO membrane increase rapidly especially at almost full ethanol recovery. Even though the optimizer has already changed the optimal configuration, the membrane area still increases significantly at high recoveries making the separation cost relatively expensive.

3.3.2   Optimal partition of separation work on recovery between RO and D-PV

Here, we consider the overall separation process where the RO system is included before the D-PV for the pretreatment of ethanol purification. The overall process model has an additional constraint on the weight purity of the recycle stream, which consists of the stream removed from the RO and from the bottom of the distillation column as previously described (see Figure 3.2).

$$w_e^{REP} \leq 2 \times 10^{-4} \qquad\qquad (2.39)$$

(a)
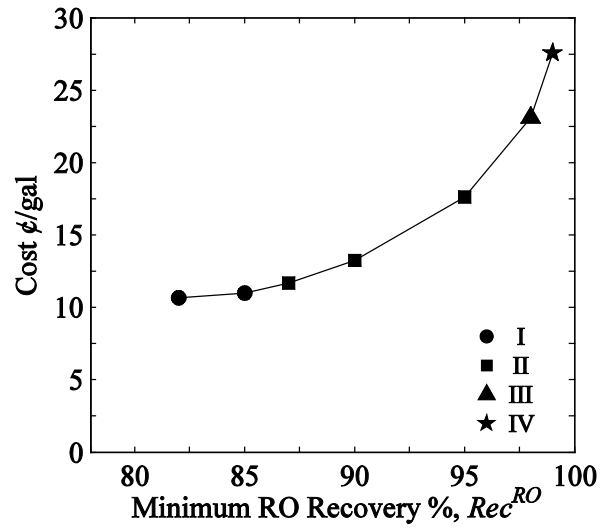
(b)
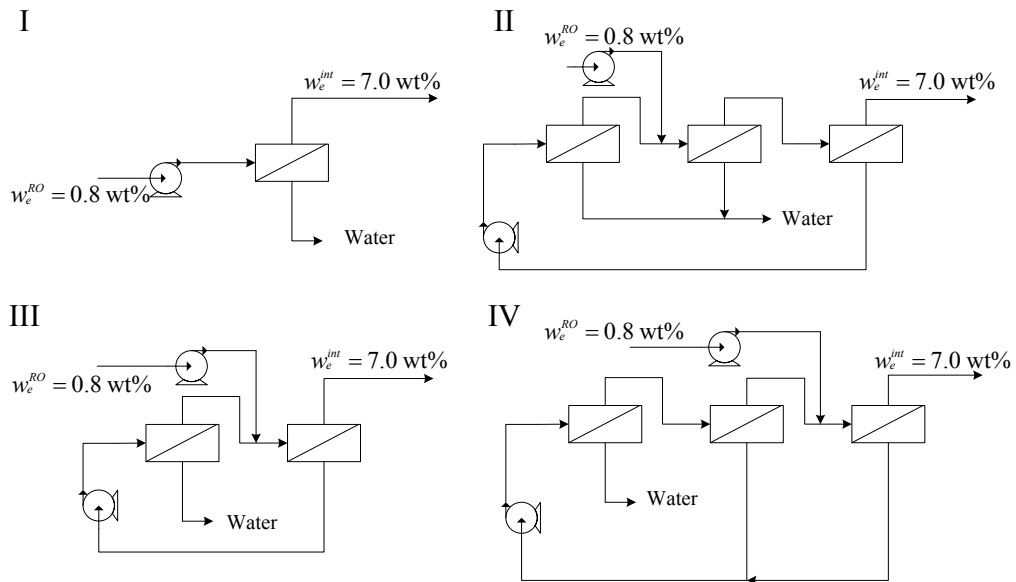
Figure 3.7. Optimal RO membrane system for different RO ethanol recovery: (a) ethanol unit cost of optimal configurations (b) different optimal configurations.

From previous investigation, three RO membrane stages have been set as a maximum in order to reduce the size of the model and avoid some local solutions. The model of the superstructure of the overall separation technology consists of 2000 variables

with approximately 120 integer variables, and the computation times are between 1–5 minutes. Optimization results show that the RO membrane pretreatment has advantages for ethanol purification at a very dilute ethanol feed. Table 3.4 illustrates the optimal ethanol recovery between the RO membrane and the D-PV unit for different ethanol feed purities at the ethanol throughput of 30 Mgal/yr. It can be seen that the total ethanol recovery rises with an increase in the feed concentration. At the optimal solutions, the constraint in Eq. (3.39) is always active at all feed condition as it reduces the total recovery of the separation system to achieve a lower separation cost. Furthermore, the ratio of R over F^{RO} is almost constant since both are changed concomitantly with increased feed purity. Thus, from Eq. (3.35), increasing the feed purity directly reduces the ethanol recovery of the overall separation system.

From Table 3.4, the optimizer partitions the recovery task between RO and D-PV where Rec^{RO} increases from 96 to 99 % while Rec^{D-PV} is almost constant around 100% at $w_e^{RO} = 0.5$–2.0 wt%. Since the cost of RO membrane increases rapidly at high recoveries, the optimizer therefore minimizes the ethanol recovery from the RO membrane and recovers more ethanol at the D-PV unit to minimize the total separation cost. When w_e^{RO} is increased to greater than 2.0 wt%, the ethanol recovery of RO increases to achieve the overall recovery until having RO membrane is not optimal. Thus, introducing RO pretreatment will be of benefit when the feed concentration is very low.

Table 3.4. Optimal ethanol recovery of each separation unit for different feed purity (w_e^{RO}) at ethanol throughput of 30 Mgal/yr

Unit	0.5 wt%	0.8 wt%	1.0 wt%	2.0 wt%	3.0 wt%	5.0 wt%
Rec^{RO}	96	97.5	98	99	-	-
Rec^{D-PV}	~ 100	~ 100	~ 100	~ 100	99.3	99.5
Rec^{T}	96	97.5	98	99	99.3	99.5
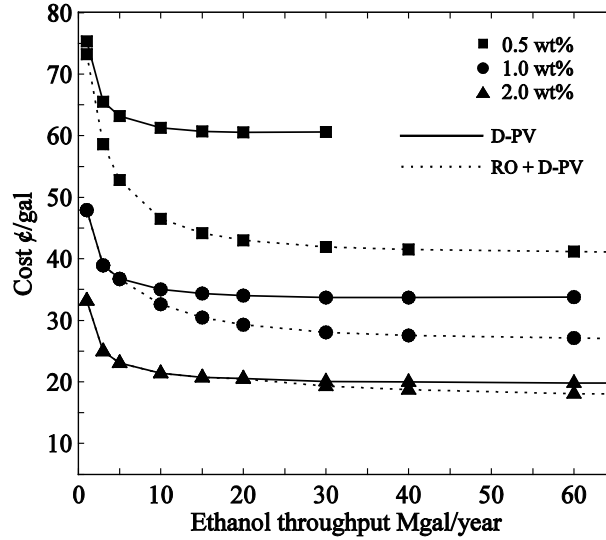
Figure 3.8. Ethanol unit cost, ¢/gal, of optimal configurations of overall ethanol separation for different feed purities (w_e^{RO}) and throughputs.

3.3.3   Cost and energy savings by RO pretreatment

Figure 3.8 demonstrates the separation cost savings when adding the RO membrane pretreatment. At the throughput of 30 Mgal/yr, the ethanol unit cost is reduced from 61 ¢/gal to 42 ¢/gal at w_e^{RO} = 0.5 wt% and from 34 ¢/gal to 28 ¢/gal at w_e^{RO} =1.0 wt%. The cost is almost equal at w_e^{RO} = 2.0 wt% and the RO will be eliminated when w_e^{RO} is greater than 3.0 wt%. The results also reveal that the volumetric throughput has an effect on the optimal technology. We believe this is because of the different equipment usage at different scales. In addition, there is a limitation of a scale for a single hybrid separation process due to a distillation column size where the diameter cannot exceed the maximum of 7.3 meters.[85] The figure shows that the single hybrid separation unit has a limited capacity at around 30 Mgal/yr for w_e^{RO} = 0.5 wt% and 60 Mgal/yr for w_e^{RO} =1.0 wt%. It requires a higher feed flow rate F^{RO} to achieve a similar ethanol production of 99.4 wt% at a low

feed ethanol concentration. The RO pretreatment allows the significant amount of water to be removed before feeding to the distillation column. The pretreatment is consequently necessary for a large plant capacity. The detailed of annualized capital and operating costs of each component at throughput of 30 Mgal/yr are summarized in Table 3.5.

From Table 3.5, the total separation cost of D-PV is sensitive to the operating cost since it accounts for the highest portion at 76–85%. An increase in feed concentration directly decreases the energy consumption and operating cost of the distillation column and therefore substantially reduces the separation cost due to its high contribution to the overall cost. The table also shows a negligible change in the cost fraction of annualized capital cost of distillation while both the annualized capital cost and operating cost fraction of pervaporation moderately increases. This is because the separation partition more separation work to the pervaporation membrane as the feed concentration increases which has been described in our previous work.[36]

It can be seen from Table 3.5 that introducing the RO membrane significantly reduces the operating cost portion of the distillation column from 76–85 % to 19–32 %, and the total cost of RO system now is the largest contributor to overall cost. This indicates the main advantage of introducing RO membranes at very dilute feeds is the reduction in energy consumption of the distillation. Figure 3.9 shows the comparison of energy consumption between a single D-PV and that with RO pretreatment where the number is based on the ethanol purification of dilute feed with a temperature of 30°C from ethanol production process to produce fuel grade ethanol at throughput of 30 Mgal/yr. The energy consumption in the hybrid unit consists of the heat used in the reboiler, interstage heaters, and the electricity used for pumps and a chilled water unit while the RO membrane

Table 3.5. Annualized cost of separation process equipment and utilities at ethanol throughput of 30 Mgal/yr

Annualized cost (%)	$w_e^{RO} = 0.5$ wt%		$w_e^{RO} = 1.0$ wt%		$w_e^{RO} = 2.0$ wt%	
	D-PV	RO + D-PV	D-PV	RO + D-PV	D-PV	RO + D-PV
Distillation						
Tower	4.0	2.5	5.0	3.0	6.0	4.0
Condenser and reflux drum	0.5	0.5	1.0	1.0	1.5	1.0
Reboiler	5.5	1.0	5.0	1.5	4.0	2.0
All utilities	85.0	19.5	82.0	24.5	76.0	32.0
TAC of distillation	11.0	4.0	11.0	5.5	11.5	7.0
TOC of distillation	85.0	19.5	82.0	24.5	76.0	32.0
Pervaporation						
Membrane	2.5	4.0	4.5	6.0	7.5	8.5
Vacuum condenser and drum	< 0.5	< 0.5	< 0.5	0.5	1.0	1.0
Vacuum system	< 0.5	< 0.5	< 0.5	< 0.5	< 0.5	< 0.5
Interstage heaters and pumps	< 0.5	< 0.5	< 0.5	< 0.5	< 0.5	< 0.5
Membrane maintenance	1.0	1.5	1.5	2.0	2.5	3.0
All utilities	< 0.5	< 0.5	< 1	0.5	0.5	1.0
TAC of pervaporation	3.0	4.5	5.0	6.5	9.5	10.0
TOC of pervaporation	1.0	1.5	2.0	2.5	3.0	4.0
RO membrane						
RO membrane		20.5		18.5		12.0
High pressure pumps	-	2.5	-	4.0	-	6.0
Energy recovery device		0.5		0.5		1.0
Membrane maintenance		7.0		6.0		4.0
All utilities		40.0		32.0		24.0
TAC of RO membrane	-	23.5	-	23.0	-	19.0
TOC of RO membrane		47.0		38.0		28.0
Ethanol Unit cost (¢/gal)	**61.0**	**42.0**	**34.0**	**28.0**	**22.0**	**19.5**
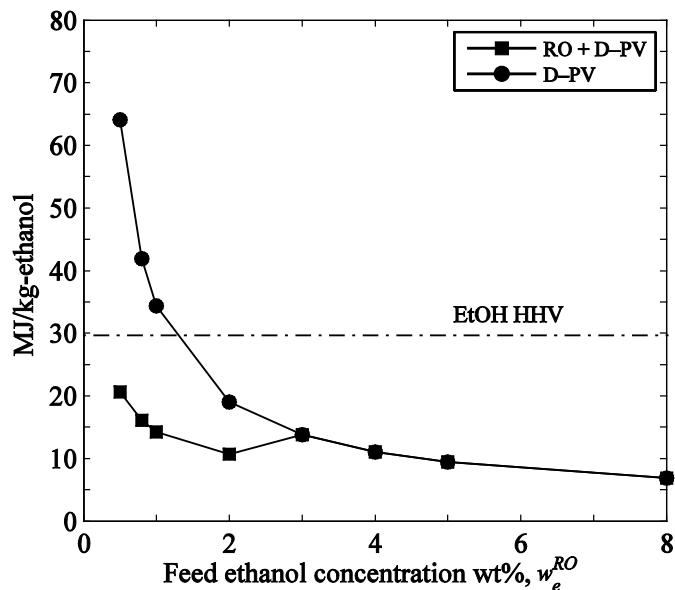
Figure 3.9. Energy consumption, MJ/kg-ethanol, of optimal configurations for ethanol purification for different ethanol feed concentrations at ethanol throughput of 30 Mgal/yr.

consumes electrical energy from the pumps inside the membrane system. The energy is shown as fuel equivalents where reboiler heat duty is assumed having 90% efficiency, 3.0 MJ-fuel can produce 1.0 MJ electrical energy, and 4.0 °C chilled water requires 0.53 MJ-fuel per MJ heat removed.[35] It can be seen that RO membrane highly reduces the energy consumption to below the HHV of ethanol when w_e^{RO} is lower than 3.0 wt% — around 10-20 MJ/kg-ethanol. In Figure 3.9, no energy saving occurs when w_e^{RO} is higher than 3.0 wt% at 30 Mgal/yr, the RO system becomes expensive and outweighs the cost savings from the reduction of energy consumption. Table 3.6 shows the breakdown of energy consumption of all main units for different feed concentration at throughput of 30 Mgal/yr. It can be seen that the largest energy consumption of the separation comes from the reboiler of the distillation column where the energy usage increase rapidly when reducing w_e^{RO} from 2.0% to 0.5%. After introducing the RO membrane for dilute feed pretreatment, the

Table 3.6. Details of energy consumption at ethanol throughput of 30 Mgal/yr for different feed concentrations

Energy Consumption [MJ/kg]	w_e^{RO} = 0.5 wt%		w_e^{RO} = 1.0 wt%		w_e^{RO} = 2.0 wt%	
	D-PV	RO+D-PV	D-PV	RO+D-PV	D-PV	RO+D-PV
Reboiler	63.84	9.88	34.10	8.30	18.77	7.48
Interstage Pervaporation heater	0.19	0.20	0.18	0.20	0.18	0.21
Chilled Water	0.09	0.09	0.08	0.10	0.08	0.10
Electrical energy of Pumps in RO membrane system	-	10.49	-	5.62	-	2.91
Total	64.12	20.66	34.36	14.22	19.03	10.70

energy consumption of the reboiler declines in exchange for a smaller increase in that from electricity demand for powering the pumps in the RO membrane system. The optimizer also decides to have the energy recovery device for further decreasing energy usage as the membrane system is always chosen to operate at a very high pressure. The reduction in energy consumption explains the reduction of operating cost of distillation. Accordingly, adding RO membrane pretreatment can be considered as a more energy efficient way for dilute ethanol purification compared to a single D-PV hybrid separation.

3.4   CONCLUSIONS

Optimal process configurations of dilute bioethanol purification using D-PV including RO membrane pretreatment were investigated. The effect of ethanol recovery on the optimal configurations of an individual RO system was analyzed where the cost of RO membranes was found to be very sensitive to the ethanol recovery, especially at almost full recovery, due to the high membrane area required. The optimal solution shows a change in the number of membrane enriching and stripping stages with increased ethanol recovery. Increasing the feed purity increases the overall ethanol recovery while maintaining the constraint of ethanol purity on the recycle to the ethanol production process. The optimal overall bioethanol separation process allows more ethanol to leave from the RO units to the recycle stream than from the D-PV process due to the expensive cost of RO system at a high recovery. RO pretreatment saves costs for dilute ethanol feeds and high throughputs where the pretreatment enables the constraint on the size of a distillation column to be met. An analysis of cost fraction of separation cost shows the largest portion of the operating cost is distillation. Including the RO pretreatment significantly reduces the portion of the operating cost of distillation. The RO pretreatment reduces the energy consumption of the reboiler when the ethanol feed purity is very low. Improving the RO membrane technologies for a lower membrane cost may improve the RO pretreatment to be more attractive in a wider range of feed concentrations.

CHAPTER 4

REACTION KINETICS OF THE CONCENTRATED-ACID HYDROLYSIS FOR CELLULOSE AND HEMICELLULOSE AND EFFECT OF CRYSTALLINITY

4.1   Motivation

The concentrated acid hydrolysis process has been reported to have several advantages such as a lower operating temperature and pressure, a higher sugar yield, and less byproduct formation compared to the dilute acid hydrolysis, which is favorable for the fermentation for bioethanol production. However, it requires a specialized material to prevent the corrosion as well as an acid recovery process which can significantly increase the cost of saccharification and this has reduced its economic viability.[11] Despite these disadvantages, the concentrated acid hydrolysis process has continued to be of interest due to improvement in sugar-acid recovery technology such as simulated-moving-bed chromatographic separation.[24, 26] Commercially, the concentrated acid hydrolysis is being developed by Blue Fire Renewable using chromatographic separation technology which can efficiently recover the sugar without the dilution.[88]

The complex structure of the biomass and its variability in composition make it difficult to predict the kinetics of the hydrolysis reaction. In enzymatic hydrolysis pathway, for instance, the lignin and hemicellulose content can reduce the catalyst accessibility and reduce hydrolysis rates.[89] Furthermore, biomass with different crystallinity index (CrI) can significantly change the kinetics of the hydrolysis reaction. Previous work has illustrated a

strong correlation between the initial rates of the enzymatic hydrolysis reaction of the cellulose and the initial CrI where the more amorphous sample is hydrolyzed much faster than a higher crystalline cellulose.[90] In the case of acid hydrolysis, the kinetic parameters of the reactions varies significantly depending on several factors such as different sources of biomass and the different reaction conditions including temperature and acid concentration.[91-93] Owing to these uncertain factors, the modeling of the kinetics of the biomass hydrolysis reactions is still a challenge.

The concentrated acid hydrolysis process of biomass has been addressed in only a few studies.[23, 94-95] The biomass in these studies contains various compositions of cellulose, hemicellulose, lignin, and has a different CrI which could interfere the hydrolysis rate of each composition leading to different reported values of the kinetic parameters. Camacho et al. [96] have reported the kinetic parameters of the concentrated acid hydrolysis of pure cellulose (Merck 2330) and glucose decomposition reactions in the low temperature range of 25 – 40 °C and 30 – 70 %w/v H_2SO_4 acid. However, this does not include experimental work on the kinetics of the C5 reaction paths. Furthermore, the concentrated acid hydrolysis process is usually performed at a higher temperature range of 80 – 100 °C,[97] and the kinetics in this temperature range should be investigated more carefully.

The purpose of this chapter is to present the experimental data and a model of the kinetics of the hydrolysis of cellulose and hemicellulose as well as the glucose and xylose decomposition reactions via concentrated sulfuric acid. Pure microcrystalline cellulose (Avicel) and xylan, the major component in hemicellulose, are used in the experiment to investigate the kinetics of the C5 and C6 reaction paths separately. Complex substrates were not used to avoid confounding the kinetics and to limit the influence of mass transfer.

The hydrolysates components including the sugars and several main decomposed byproducts from the batch experiments are characterized at different temperature between 80 – 100 °C and at different acid concentration between 10 – 50 wt% (10 – 70 %w/v). In addition, the effect of the initial CrI of the cellulose on the rate of the hydrolysis reaction is explored where Avicel samples with different crystallinities are generated by exposure to phosphoric acid solutions at different concentrations, which is referred as "decrystallization".

This chapter is organized as follow: section 4.2 discussed the material and analytical methods used in this work including the concentrated acid hydrolysis, the analysis using high performance liquid chromatography (HPLC), X-ray diffraction (XRD), and the pretreatment method using phosphoric acid at different concentrations. The kinetic model used to fit the reactions is also discussed. The experimental results from the concentrated acid hydrolysis from different samples as well as the fitting of the kinetic parameters are shown in section 4.3. Additionally, the effect of the pretreatment of the cellulose on the rate of the concentrated acid hydrolysis is discussed in this section.

4.2   Materials and methods

4.2.1 Chemicals

The xylan from beechwood (Catalog No. x-4252; Batch No. BCBM5311V), microcrystalline cellulose, Avicel PH-101 (Catalog No. 11365; Batch No. BCBJ8498V), xylose, furfural, HMF, levulinic acid, and phosphoric acid (85 wt%) were purchased from Sigma-Aldrich. Formic acid and glucose are purchased from Alfa Aesar, acetone was

purchased from BDH, and sulfuric acid (>95%) was purchased from MACRON. These chemicals were used for the hydrolysis reaction, cellulose decrystallization, and as standards for high-performance-liquid-chromatography (HPLC) analysis.

4.2.2   Concentrated acid hydrolysis

The batch experiments for the concentrated acid hydrolysis of biomass are carried out to estimate the kinetic parameters of four main reaction paths including the generation and decomposition of the C5 and C6 sugars. Four sets of batch experiments of the concentrated acid hydrolysis reactions are employed for four different samples including xylan, xylose, Avicel, and glucose. Each set of experiment contains six batch experiments at various temperature and H_2SO_4 concentration where five of these are used to estimate the parameters and the remaining one is used to validate the kinetic model which is discussed in detail in section 4.3.3. Table 4.1 summarizes the set of batch experiments with the sample preparation and the reaction conditions performed in this work.

All solid samples and the acid are preheated separately before starting the reaction to avoid the temperature drop after mixing. The total reaction times for all batch hydrolysis experiments were seven hours where the mixture is stirred constantly using a mechanically or magnetic stirrer at the speed around 360 rpm, and the reactor flasks are constantly heated using a temperature controlled heat bath or heating mantle. All samples were taken at various reaction times and filtered into the HPLC vials using the polyethersulfone (PES) membrane syringe filter with the pore size of 0.45 μm from VWR (Catalog No. 28145-505). The HPLC vials were immediately stored in the ice bath to quench subsequent reaction before HPLC analysis.

Table 4.1. Batch experiments for concentrated acid hydrolysis

Batch experiment	Set 1	Set 2	Set 3	Set 4
Reactions	Xylan hydrolysis	Xylose decomposition	Avicel (cellulose) hydrolysis	Glucose decomposition
Initial Concentration (g/L)	40	30	100	30
Batch size				
Reactant (grams)	4.0	3.0	15.0	4.5
H_2SO_4 (mL)	100	100	150	150
Batch reaction conditions ($H_{(acid\ wt\%)}$-$T_{(°C)}$)				
For parameter fitting				
1	H_{20}-T_{80}	H_{20}-T_{100}	H_{20}-T_{100}	H_{20}-T_{100}
2	H_{40}-T_{80}	H_{30}-T_{100}	H_{30}-T_{100}	H_{30}-T_{100}
3	H_{10}-T_{80}	H_{50}-T_{100}	H_{50}-T_{100}	H_{50}-T_{100}
4	H_{10}-T_{90}	H_{40}-T_{80}	H_{40}-T_{80}	H_{40}-T_{80}
5	H_{10}-T_{100}	H_{40}-T_{90}	H_{40}-T_{90}	H_{40}-T_{90}
For model validation				
6	H_{30}-T_{80}	H_{40}-T_{100}	H_{40}-T_{100}	H_{40}-T_{100}

4.2.3   Phosphoric acid pretreatment for cellulose

The effect of initial CrI of Avicel on the kinetic of hydrolysis reaction was also investigated. This work uses phosphoric acid to pretreat the Avicel to generate the samples with different CrI to examine the effect on the hydrolysis reaction. Phosphoric acid solvent has been popularly used for cellulose decrystallization due to its nontoxic, non-corrosive and safe compared other inorganic acids.[98] It has also been shown that the ice-cold phosphoric pretreatment has insignificant impact on the degree of polymerization.[99]

The phosphoric acid pretreatment procedure was modified and scaled up from Hall et al. [90] In this study, 3 mL of deionized water was added to 10 grams of Avicel to make a slightly moistened substrate. The Avicel was then mixed with 150 mL of ice-cold phosphoric acid (77 – 85 wt%, 0 °C) and held for 60 minutes in an ice bath with manually constant stirring. After the pretreatment, 200 mL of ice-cold Acetone (0 °C) was added to the mixture in order to regenerate cellulose. The mixture was then vacuum-filtered using

coarse fritted filtered- funnel, and washed three times with 200 mL of ice-cold acetone (0 °C) and four times with 1 L of deionized water until the pH of the filtrate is around 2.6 – 3.0. The pretreated cellulose was lyophilized for two days until the weight of the cellulose changed by less than 0.5 grams. The weight of the samples was slightly over the initial dry weight (10 grams) which is assumed to be due to residue water. The cellulose was sampled for X-ray diffraction measurement and the remaining was proceeded for the concentrated sulfuric acid hydrolysis. The pretreated Avicel samples of approximately 10 grams were preheated to 50 °C and hydrolyzed with 150 ml of 40 wt% sulfuric acid at 80 °C.

4.2.4 Degree of cellulose crystallinity using X-ray diffraction

The CrI measurement of all samples using XRD follows the procedure described by Kang et al. [100] XRD patterns of lyophilized samples were recorded with an X'pert PRO X-ray diffractometer (PANanalytical BV, Almelo, the Netherlands) using Cu=Kα_1 irradiation (1.54 A˚) at 45 kV and 40 mA. The scattering angle (2θ) ranged from 10˚ to 40˚ with a scan speed of 0.021425 s^{-1} and step size of 0.0167˚.

4.2.5 HPLC Chemical analyses

The sugar and byproduct components from the hydrolysate from the reaction samples were analyzed by HPLC from Shimadzu. A Bio-Rad Aminex HPX-87H column was used where the analysis was conducted at 50 °C using the eluent of 0.005 mol/L H_2SO_4 at 0.6 mL/min. The injection volumes are 20 μL for all the samples and 3 μL for the samples from hydrolysis of pretreated Avicel using the corresponding calibration curves. All the samples were stored at 5 °C in the autosampler SIL-20AC during the analysis to stop

47

possible decomposition reactions. The sugars including glucose and xylose are detected using Refractive index RID-10A while the byproducts including formic acid, levulinic acid, HMF, furfural are detected by UV-Photodiode Array SPD-M20A at the wavelength of 207 nm, 207 nm, 270 nm, and 310 nm, respectively

4.2.6 Kinetic model

In the present study, the kinetic expression proposed by Saeman [101] was used to fit the kinetic of concentrated acid hydrolysis for all reaction paths where two homogeneous consecutive first-order reactions were assumed in both cellulose and hemicellulose hydrolysis (see Figure 4.1). The kinetic models for sugar concentration from each set of experiment are shown as follows.

Biomass hydrolysis reaction (experiment set 1 and set 3):

$$\frac{dB^j}{dt} = -k_1 B^j \quad j \in \{\text{xylan, Avicel}\} \tag{3.1}$$

$$\frac{dC^k}{dt} = k_1 B^j - k_2 C^k \quad (j,k) \in \{(\text{xylan, xylose}), (\text{Avicel, glucose})\} \tag{3.2}$$

B and C is the concentration of biomass and sugar, respectively, and the analytical solution for the sugar concentration is

$$C^k = \frac{C_{eq}^{k,0} k_1}{k_1 - k_2} \left(e^{(-k_2 t)} - e^{(-k_1 t)} \right) \quad k \in \{\text{xylose, glucose}\} \tag{3.3}$$

where

$$C_{eq}^0 = \frac{\text{initial mass of biomass} \times f_s}{\text{volume of solution}} \times \frac{\text{MW}_{\text{sugar}}}{\text{MW}_{\text{anhydrous sugar}}} \tag{3.4}$$

48

Eq. (4.4) shows the expression for initial equivalent sugar concentration (C_{eq}^0)

where f_s is the fraction of sugar consisting in the biomass.

Sugar decomposition reaction (experiment set 2 and set 4):

$$\frac{dC^k}{dt} = -k_2 C^k \quad k \in \{\text{xylose, glucose}\} \tag{3.5}$$

The analytical solution of the above differential equation is given by:

$$C^k = C^{k,0} e^{-k_2 t} \quad k \in \{\text{xylose, glucose}\} \tag{3.6}$$

The Arrhenius expression was used to estimate the kinetic constant which depends on the temperature and the effect of acid concentration is included in the pre-exponential factor[102] as follows.

$$k_j = k_j^0 \left(C^A\right)^{n_j} e^{-\left(\frac{Ea_j}{RT}\right)} \quad j = \{1, 2\} \tag{3.7}$$

Biomass $\xrightarrow{k_1}$ Sugars $\xrightarrow{k_2}$ Decomposed products
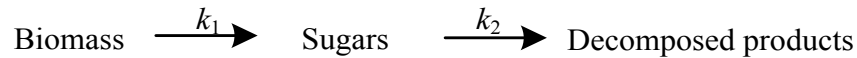
Figure 4.1. Reaction pathway for biomass hydrolysis

4.3   Results and discussion

Experiments outlined in Table 1 are carried out to investigate the reaction kinetics. In all sets of experiments, the color of the mixture turns into yellow, and dark brown, respectively, where the dark insoluble humin particles keep forming owing to the sugars (xylose and glucose) decomposition reactions where the xylan hydrolysis samples are

49

shown in Figure 4.2 as an example. In addition, it is observed that the Avicel is much more difficult to solubilize into the liquid mixture compared to the xylan due to the more crystalline structure.
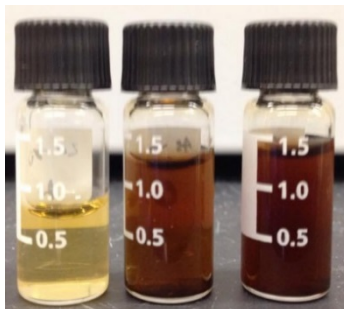
Figure 4.2. Hydrolysate of xylan at different reaction time

4.3.1 Xylan hydrolysis and xylose decomposition

Figure 4.3 depicts the xylose concentration of xylan hydrolysis over different reaction time from the experiments set 1. It can be seen that almost all reaction conditions, the xylose concentration rises rapidly to its maximum and then reduces due to the sugar decomposition reaction. The effect of temperature can be seen Figure 4.3a where the H_2SO_4 concentration is constant at 10 wt%. In this figure, the xylose concentration increases slowly over seven hours of reaction at 80 °C. At a higher temperature in 90-100 °C, it increases more rapidly within the first 60 minutes to reach the maximum around 28 – 29 g/L, and then stay almost constant with a slight reduction which indicates a low xylose decomposition reaction.

The effect of acid concentration can be clearly seen in Figure 4.3b where increasing the concentration of H_2SO_4 increases the rate of xylose generation rapidly at a constant temperature of 80 °C. It can be seen that at 40 % H_2SO_4, the xylose concentration increases

significantly to the maximum in the first 15 minutes and began to decrease faster compared to other conditions which indicates a higher xylose decomposition rate.

The xylose yield C/C_{eq}^0 can be calculated from Eq. (4.3) where f_s is obtained by solving the optimization problem which is discussed in section 4.3.3. It is found that a very high xylose yield can be achieved up to more than 95 % with an appropriate reaction time.

The rate of xylose decomposition is further investigated in the batch experiments set 2, a more severe reaction condition compared to the xylan hydrolysis and shown in Figure 4.4. The concentrations of byproducts including the furfural and formic acid are also shown in Figure 4.5 and Figure 4.6, respectively. In Figure 4.4a, increasing the temperature at 10 wt% H_2SO_4 significantly increase the decomposition rate of xylose which is completely consumed at around 300 minutes for 100 °C. Likewise, increasing the H_2SO_4 concentration significantly increases the decomposition rate of xylose at 100 °C as shown in Figure 4.4b. At the severest condition (50 wt% H_2SO_4, 100 °C), the xylose concentration decreases significantly and completely decomposes at around 90 minutes.

The decomposition can be confirmed from the furfural concentration illustrated in Figure 4.5 where the concentration increases rapidly at high temperature (Figure 4.5a) and H_2SO_4 concentration (Figure 4.5b). From the figure, it can be seen that at most of the conditions, the concentration of furfural increases at a slower rate until the concentration reaches the maximum, and then reduces significantly due to the subsequent decomposition to form formic acid. There are also other byproduct such as humins and other unknown byproducts which are not quantified.

Figure 4.3. Xylose concentration as a function of hydrolysis reaction time from experiment set 1 (a) 80-100 °C at 10 wt% H_2SO_4 and (b) 10-40 wt% H_2SO_4 at 80 °C.

Figure 4.4. Xylose concentration as a function of hydrolysis reaction time from experiment set 2 (a) 80-100 °C at 40 wt% H_2SO_4 and (b) 20-50 wt% H_2SO_4 at 100 °C.
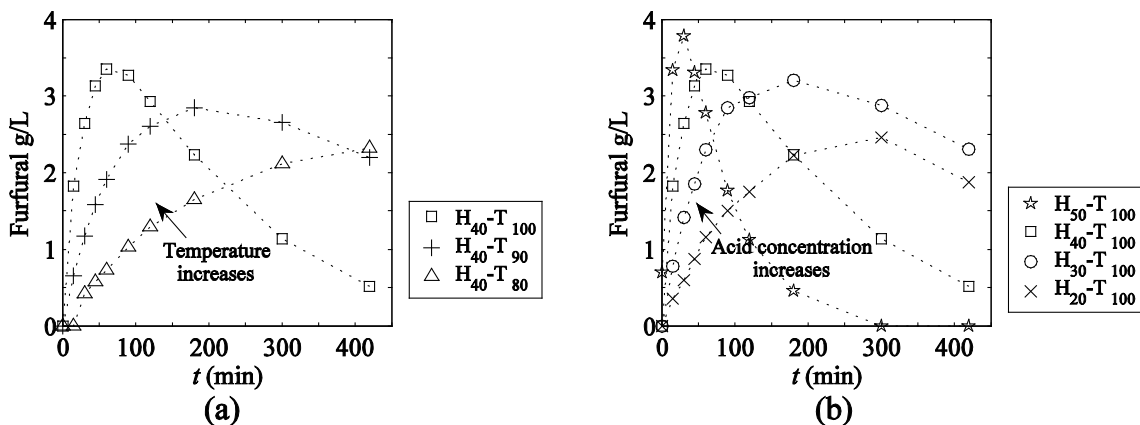
Figure 4.5. Furfural concentration as a function of hydrolysis reaction time from experiment set 2 (a) 80-100 °C at 40 wt% H_2SO_4 and (b) 20-50 wt% H_2SO_4 at 100 °C.
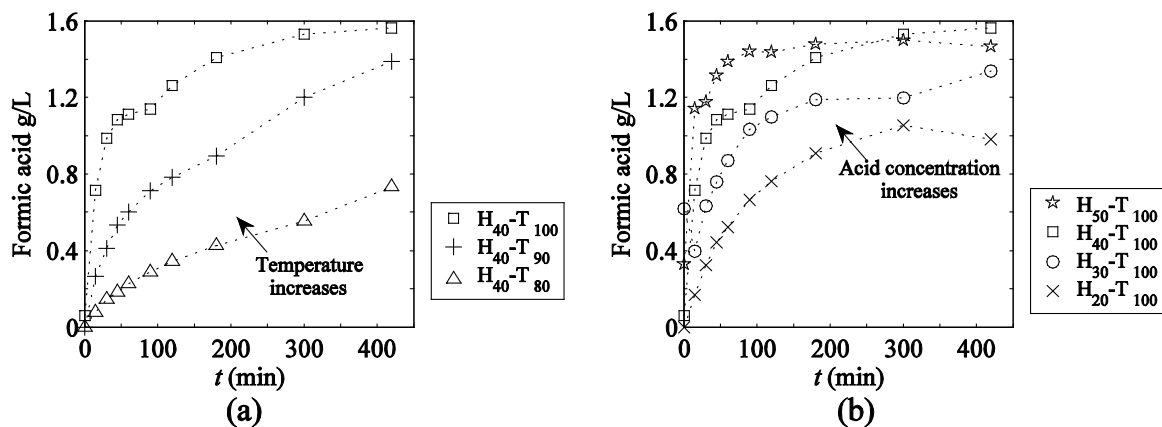
Figure 4.6. Formic acid concentration as a function of hydrolysis reaction time from experiment set 2 (a) 80-100 °C at 40 wt% H_2SO_4 and (b) 20-50 wt% H_2SO_4 at 100 °C.

4.3.2 Cellulose hydrolysis and glucose decomposition

The glucose concentration of the Avicel hydrolysis over different reaction time from set 3 experiments are illustrated in Figure 4.7. From the figure, a similar trend is observed for the glucose concentration to the xylose concentration from experiment set 1 where the sugar concentration increases with reaction time for most reactions conditions. Figure 4.7a compares the glucose concentration at different temperature at 40 wt% H_2SO_4 where the glucose concentration increases with temperature.

The effect of changing the H_2SO_4 concentration on the rate of Avicel hydrolysis can be directly seen in Figure 4.7b at the reaction temperature of 100 °C. The glucose concentration increases with acid concentration between 20 wt% and 40 wt%. However, at 50 wt% H_2SO_4, the glucose concentration increases with reaction time and reaches its maximum of 29.0 g/L at around $t = 120$ minutes before reducing afterwards due to the relatively fast glucose decomposition reaction.

It should be noted that the glucose yield C/C_{eq}^0 at these reaction conditions is around 10 – 26 % which is relatively low compared to the xylose yield from the xylan hydrolysis. This relatively low yield indicates a much slower reaction rate for the cellulose hydrolysis reaction due to the crystalline structure.

The glucose concentration in the glucose decomposition reaction as a function of reaction time from set 4 experiments are shown in Figure 4.8. It can be seen that the glucose concentration reduces when increase the temperature (see Figure 4.8a) at the constant acid concentration of 40 wt%, as well as when the acid concentration is increased (see Figure 4.8b) at a temperature of 100 °C. By comparing the glucose concentration in Figure 4.8 and xylose concentration in Figure 4.4, it can be seen that the glucose decomposes at a significantly slower rate than xylose does. The change in the rate of glucose decomposition from this set of experiment can be confirmed by the byproduct concentrations including the HMF, formic acid, and levulinic acid which are illustrated in Figure 4.9, Figure 4.10, and Figure 4.11, respectively. It can be seen from Figure 4.9 that the concentration of HMF is relatively low and tends to decrease faster at a high temperature and high acid concentration which indicates a low stability to the reaction conditions. In contrast, the concentration of formic acid and levulinic acid, which are the decomposed product from HMF, are more stable as can be seen from the higher concentrations in Figure 4.10 and Figure 4.11. It has been reported that HMF decomposes into formic and levulinic acid with the molar ratio of 1:1.[103] However, it is found that the molar concentration of the formic acid is slightly higher than that of the levulinic acid up to 30% at the end of the experiment. This could be due to potential error in the HPLC

54

analysis where some unknown impurities overlapped the peak of formic acid, or unknown reaction paths. Further experiment should be performed to investigate this observation.
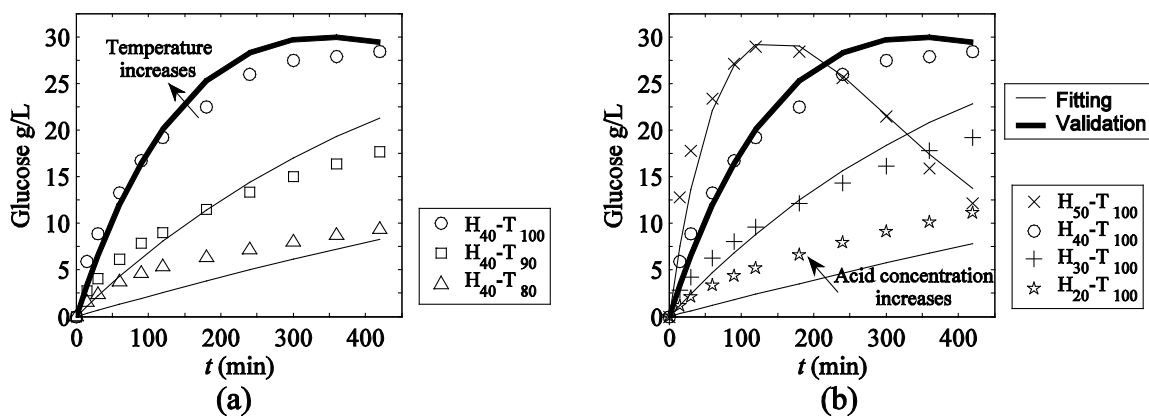
Figure 4.7. Glucose concentration as a function of hydrolysis reaction time from experiment set 3 (a) 80-100 °C at 40 wt% H_2SO_4 and (b) 20-50 wt% H_2SO_4 at 100 °C.
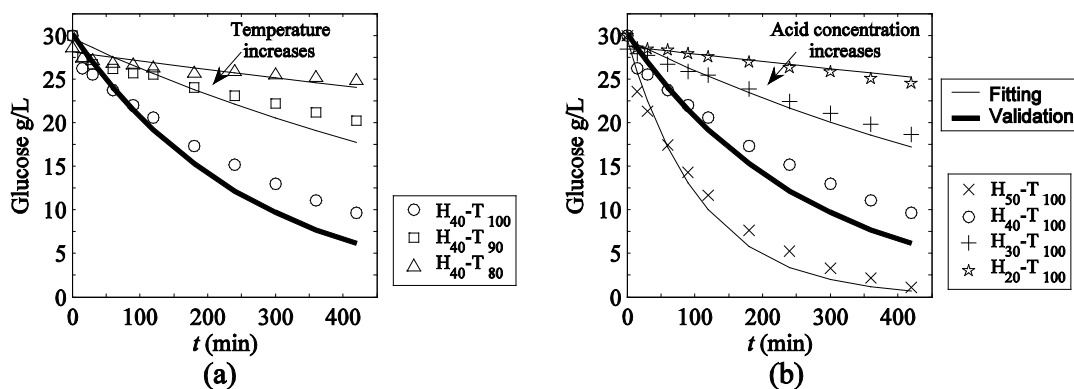
Figure 4.8. Glucose concentration as a function of hydrolysis reaction time from experiment set 4 (a) 80-100 °C at 40 wt% H_2SO_4 and (b) 20-50 wt% H_2SO_4 at 100 °C.
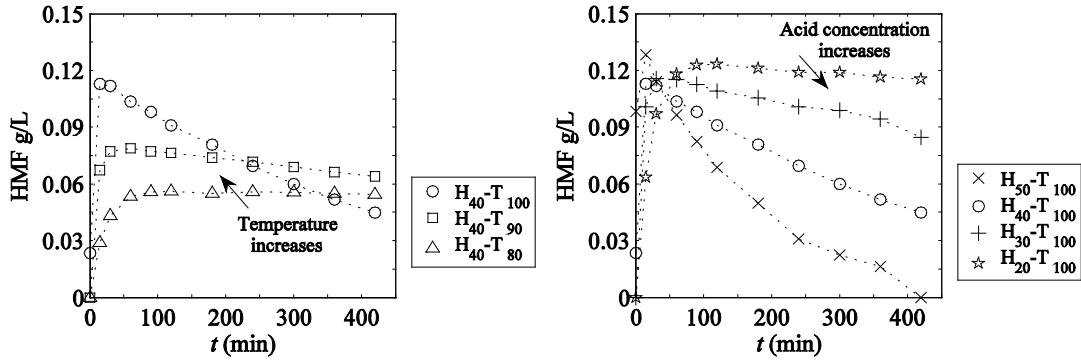
Figure 4.9. HMF concentration as a function of hydrolysis reaction time from experiment set 4 (a) 80-100 °C at 40 wt% H_2SO_4 and (b) 20-50 wt% H_2SO_4 at 100 °C
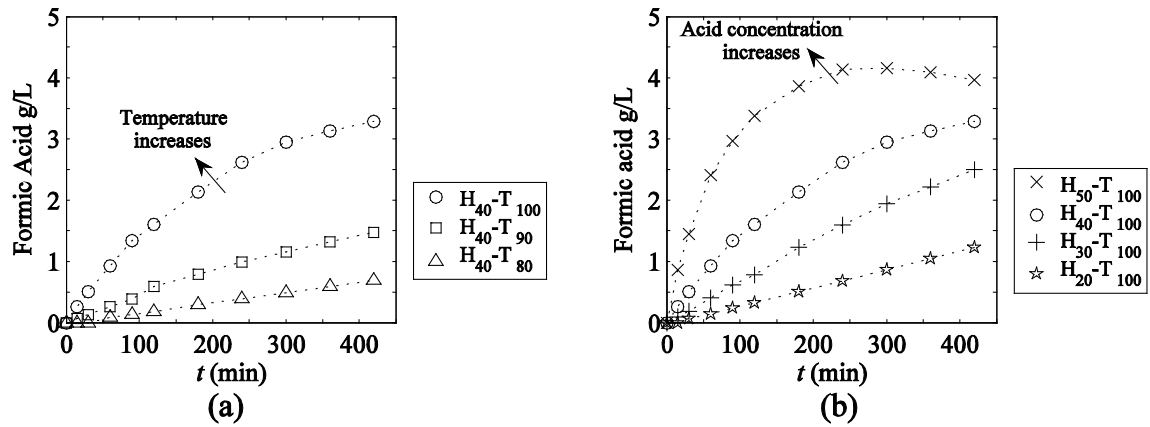
Figure 4.10. Formic acid concentration as a function of hydrolysis reaction time from experiment set 4 (a) 80-100 °C at 40 wt% H_2SO_4 and (b) 20-50 wt% H_2SO_4 at 100 °C
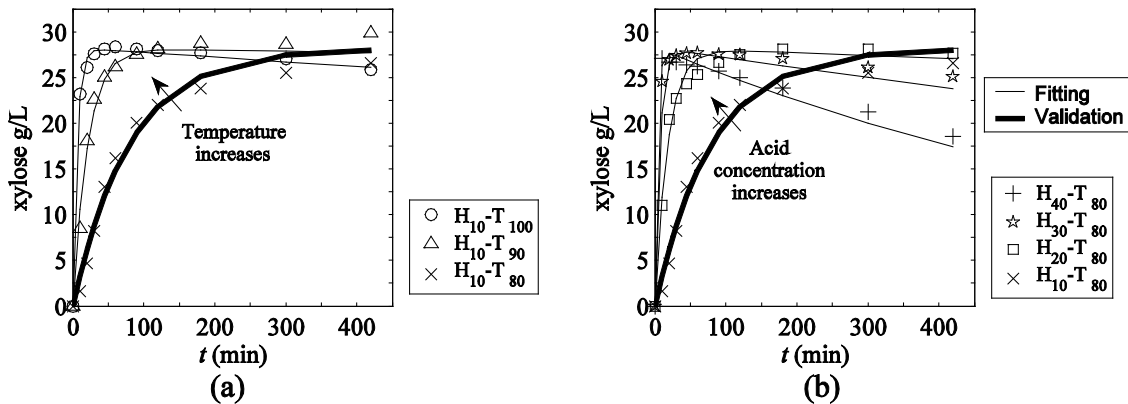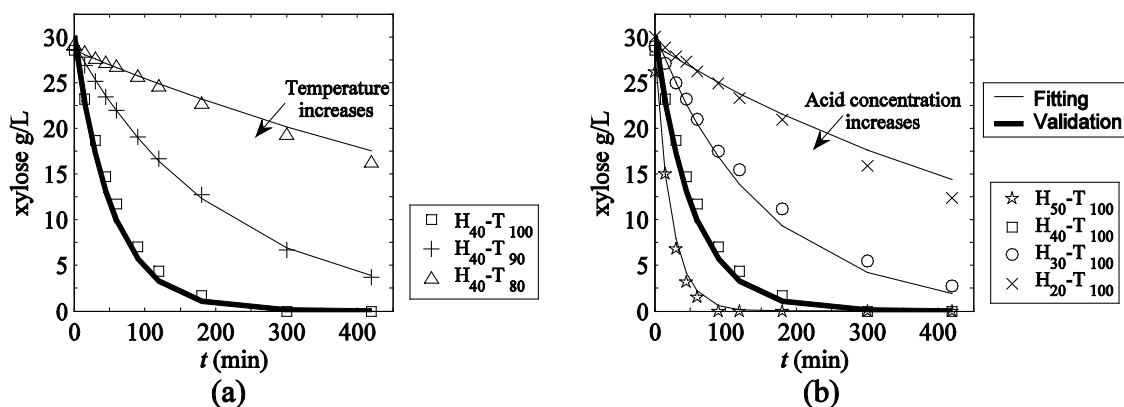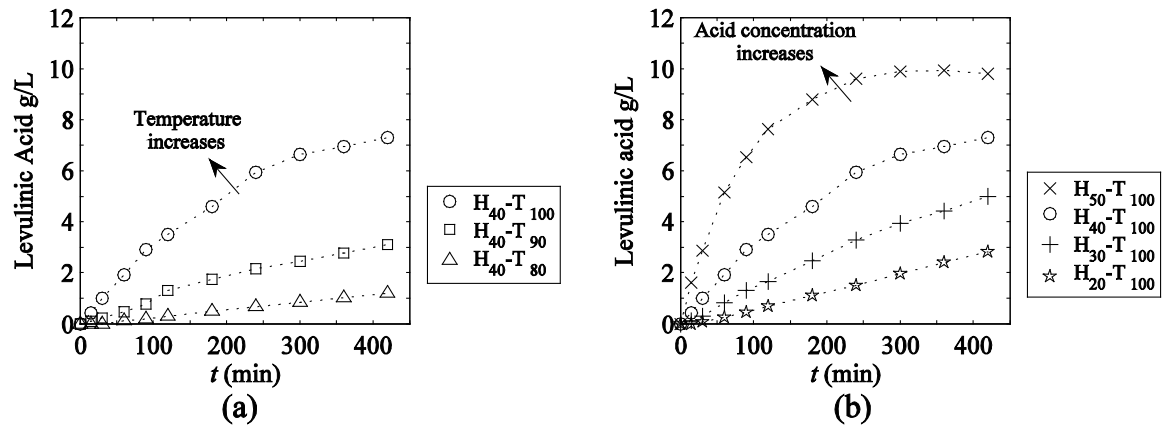

Figure 4.11. Levulinic concentration as a function of hydrolysis reaction time from experiment set 4 (a) 80-100 °C at 40 wt% H_2SO_4 and (b) 20-50 wt% H_2SO_4 at 100 °C

4.3.3 Kinetic model fitting for the concentrated acid hydrolysis

The kinetic parameters of the concentrated acid hydrolysis for both C5 and C6 can be estimated by least-square minimization. Two optimization problems are set up for the reaction paths of C5 and C6 where the objective function is given as follows.

$$
\min z = \sum_{j \in S_1} \left(\sum_i \left(C_{exp,i,j} - C_{cal,i,j} \right)^2 \right)
$$
$$
+ \sum_{j \in S_2} \left(\sum_i \left(C_{exp,i,j} - C_{cal,i,j} \right)^2 + \rho \left(C_j^{in} - C_{prep}^{in} \right)^2 \right)
$$

(3.8)

In this objective function, the sum of the squared error of the sugar concentration is minimized where $C_{exp,i}$ is the concentration of sugar at the ith data point of each experiments j^{th} and C_{cal} is the sugar concentration found from the kinetic model in Eq. (4.3) -(4.6). In this fitting, five batch experiments of the biomass hydrolysis (S_1) and five batch experiments of sugar decomposition (S_2) are used to fit k_1 and k_2 for C5 and C6 sugars (see Figure 4.1). The remaining one batch experiment from each set are excluded from the minimization to validate the kinetic parameters (see Table 4.1).

It should be noted that the fraction of xylose consisting in the biomass (f_s in Eq. (4.3)) in xylan is not measured; however, the composition analysis from Kumar et al. [104] for the same product catalog from the same manufacturer shows that this beechwood xylan contain around 69.6% xylan. In this fitting, f_s for xylan is estimated from the minimization and compared with this reference. The Avicel contains 100% of glucans so that $f_s = 1$.

There are six kinetic parameters to be estimated including the pre-exponent factor (k_0), the exponent of acid concentration (n), and the activation energy (E_a) from Eq. (4.7)

for two consecutive reactions in Figure 4.1 for C5 and C5. The concentration of H_2SO_4 in %w/v is used to fit the kinetic parameters (see Table 4.2).

Table 4.2. Sulfuric acid concentration used to fit the kinetic model.

%wt	10	20	30	40	50
%w/v	10.7	22.8	36.6	52.4	70.0

In addition to the kinetic parameters, the initial concentrations of sugar C_0 in five batch experiments of set 2 (C5) and set 4 (C6) are allowed to vary and estimated from the minimization. This is because the measurement C_0 was very difficult; the reaction vessel may not have been stirred sufficiently at the beginning of the experiments, and the reaction may have proceeded in the time between sampling and HPLC analysis. Additionally, we found that these parameters are sensitive to the fitting procedure. Nevertheless, the initial concentration cannot be significantly different from the nominal value of $C_{prep}^{in} = 30$ g/L which was the intended initial concentration of experiments for both C5 and C6. To allow somewhat minor deviation from the nominal value, Tikhonov regularization is used in the objective function, Eq.(4.8), with a small parameter, ρ [105]. In this optimization problem, there are 12 degrees of freedom in the C5 fitting and 11 degrees of freedom in the C6 fitting.

The optimization is carried out by the fminsearch function in MATLAB where the optimal values of the kinetic parameters as well as other estimated parameters found from the minimization are shown in Table 4.3. From the table, the value C^0 of both C5 and C6 deviates from the nominal value $C_{prep}^{in} = 30$ g/L only slightly for all conditions, and the composition of xylan (f_s) is consistent with the analysis from the reference.[104]

Table 4.3. Estimated kinetic parameters for each reaction path

Parameter	Optimal values		
C_0 (g/L) of xylose in experiment set 2	29.5, 30.2, 29.7, 28.8, 29.6, 28.1		
C_0 (g/L) of glucose in experiment set 4	29.1, 30.5, 30.1, 28.3, 29.3, 28.6		
f_s for xylan	70.6%		
Reactions	k_0 (min^{-1}(%w/v)$^{-n}$)	n	E_a (kJ/mol)
Xylan hydrolysis	1.42×10^{17}	1.96	142.52
Xylose decomposition	3.15×10^{14}	2.88	151.30
Avicel hydrolysis	2.96×10^{10}	2.94	129.98
Glucose decomposition	1.76×10^{10}	3.00	127.32

From the estimated value of the kinetic parameters shown in Table 4.3, the activation energy (*Ea*) of the xylan and xylose is higher than that of Avicel and glucose which indicates that the rates of C5 reaction paths are more sensitive to the temperature. In terms of the acid concentration, the values of the exponent *n* for the Avicel hydrolysis and glucose decomposition are similar. However, the value of *n* for the xylan hydrolysis is lower than the xylose decomposition. This means that the rate of xylose decomposition is more sensitive to the acid concentration compared to the xylan hydrolysis. Therefore, a very high acid concentration may not be favorable for C5 reaction paths due to a higher rate of xylose decomposition.

The fitting of the C5 paths is compared with the experimental results at each reaction condition (see Figure 4.3 and Figure 4.4), and a very good agreement between experimental data and model is observed for all reaction conditions. The parameters are validated by using the estimated valued to predict the kinetics of the xylan hydrolysis at H_{30}-T_{80} in experiment set 1 as well as xylose decomposition at H_{40}-T_{100} in experiment set 2 where a good prediction is observed for both batch experiments. From these results, we can see the first-order kinetic model with two consecutive reaction mechanism is

sufficiently accurate to estimate the xylose concentration from the concentrated acid hydrolysis of xylan.

The comparison between the experiment results with the model fitting of C6 for Avicel hydrolysis and glucose decomposition reaction are illustrated in Figure 4.7 and Figure 4.8. It can be observed that the kinetic parameters gives a good fitting for both sets of experiment for most of the reaction conditions. In Figure 4.7b, the predicted glucose yield slightly under estimate the experimental results of the condition H_{20}-T_{100}. Therefore, caution should be exercised in using the model at low sulfuric acid concentrations. The kinetic parameters are validated in prediction of the glucose concentration from the Avicel hydrolysis and glucose decomposition at the reaction condition of H_{40}-T_{100}. It can be seen from Figure 4.7 that the model gives a good prediction for the glucose concentration compared with the experimental results. The prediction of the glucose concentration from glucose decomposition at H_{40}-T_{100} shown in Figure 4.8 is slightly lower than that from the experiments. It can be concluded that the first-order two consecutive reaction mechanism shown in Figure 4.1 is sufficient to predict the kinetics of the concentrated acid hydrolysis for Avicel and glucose decomposition reaction.

The kinetic model used in the work for all reaction paths of C5 and C6 does not consider the effect of mass transfer resistance. A study from Brennan and Wyman [106] showed that the mass transfer model could explain many features of the biomass hydrolysis for the continuous flowthrough system. Mass transfer is an important phenomenon in the processing of biomass particles, but it is good modeling practice to try to separate the intrinsic kinetics from mass transfer where possible. Additionally, the initial value of CrI of the Avicel is not included in this kinetic model which is discussed in the next section.

4.3.4 Cellulose crystallinity index and its effect on hydrolysis reaction

Figure 4.12 shows the CrI of the pretreated Avicel at different phosphoric acid concentration. It is confirmed that there is a strong correlation between the acid concentration and the CrI which decreases with acid concentration. The CrI of the non-pretreated Avicel is around 56.7 % while there is a steep change in CrI over a very narrow range of phosphoric acid concentration between around 77 – 80 wt% but relatively small change when the acid concentration is greater than 80 wt%. A very similar trend is also observed in previous work.[90]

During the pretreatment experiment, we observed significant swelling of the Avicel samples. The swelling was most significant at the H_3PO_4 concentration of approximately 80 wt%, while it was much less pronounced at a higher or lower concentration.
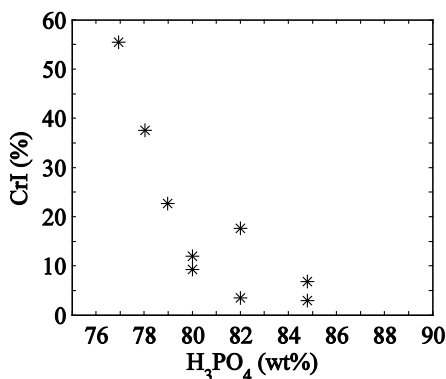
Figure 4.12. Effect of phosphoric acid concentration on the crystallinity index.

The initial CrI of the Avicel strongly influences the rate of the hydrolysis reaction. Figure 4.13 illustrates the glucose yield from the concentrated sulfuric hydrolysis reaction over seven hours reaction length of the partial decrystallized Avicel with different initial CrI. From the figure, the final glucose yield ($t = 420$ mins) is around 8.4 % for the non-pretreated sample where CrI = 56.7 %. The final yield increases to 22 % when the initial

CrI is around 37 %, and further increases to 35 % when initial CrI is around 12 %. When the initial CrI becomes smaller than 10 %, the samples becomes almost completely amorphous and more accessible, which enables the acid to penetrate and hydrolyze the cellulose where the final glucose yield increase to around 45 %. From these results, the initial CrI has a strong impact on the hydrolysis rate where the cellulose with the more amorphous forms increases the ability of acid to penetrate and extract glucose. A more complicated kinetic model for the cellulose hydrolysis which include the effect of CrI should be further investigated and validated in future work.
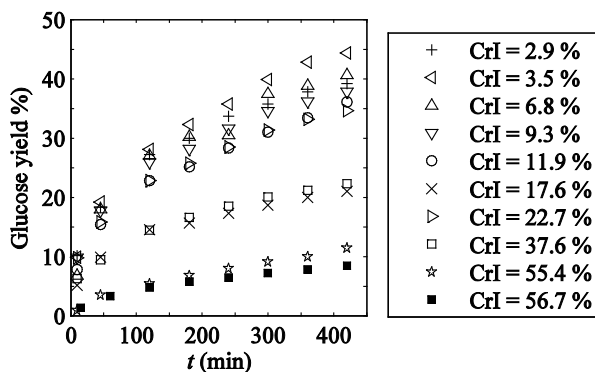
Figure 4.13. Glucose yield as a function of hydrolysis reaction time for different initial crystallinity index.

4.4   Conclusions

Batch experiments for the concentrated acid hydrolysis of microcrystalline cellulose (Avicel) and xylan from beechwood as well as the decomposition of glucose and xylose are performed to investigate the reaction kinetics in the temperature range of 80 – 100 °C and the sulfuric acid concentration of 10 – 50 wt%. The kinetic parameters are estimated to fit and predict the concentration of sugars using a reaction mechanism that

consists of two consecutive reactions where the good agreement between the experimental results and the kinetic model are found. The kinetic parameters estimated from the batch experiment in this chapter could be used to investigate the performance of the reactor system or the reactive separation process such as solid phase reactive separation system[92] for the biomass hydrolysis via concentrated acid hydrolysis which is discussed in the following chapter.

The effect of the initial CrI of the cellulose Avicel are investigated where the Avicel is pretreated with phosphoric acid at different concentration to generate samples with different CrI. It is observed that the initial CrI of the Avicel strongly affect the kinetic of the hydrolysis reaction. Further experiments should be performed to determine the reaction mechanisms and the reaction kinetics of the Avicel hydrolysis with a different portions of the crystalline and amorphous forms in future work.

CHAPTER 5

SOLID PHASE REACTIVE CHROMATOGRAPHIC SEPARATION SYSTEM FOR SACCHARIFICATION FROM BIOMASS VIA ACID HYDROLYSIS

5.1   Motivation

The cost of producing sugars from cellulosic materials is a significant barrier to the widespread use of processing routes such as fermentation. The hydrolysis process using acid is one of the main well-known process which has been investigated by several past studies for both dilute[107-108] and concentrated acid[97, 109] where the main benefit of acid hydrolysis is a fast reaction rate.[108]
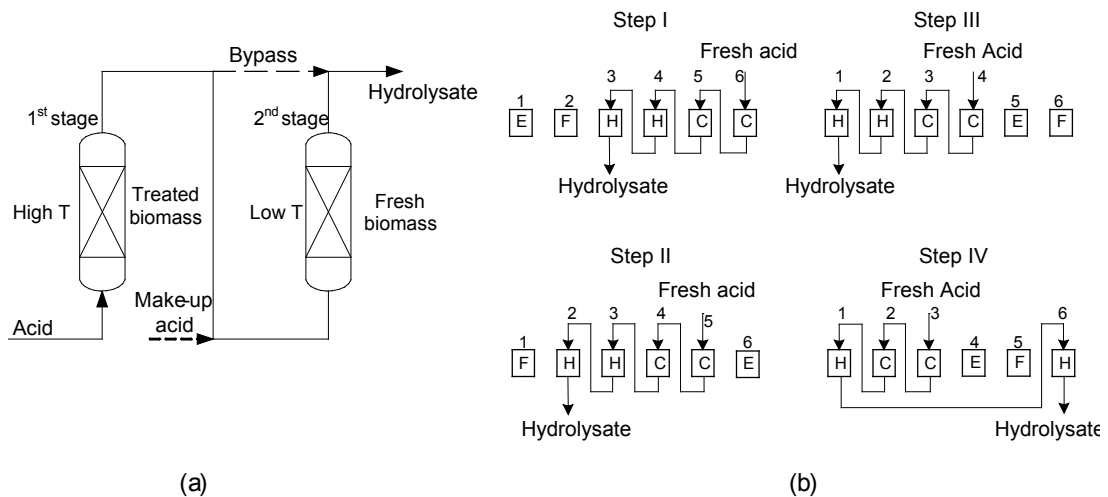
Figure 5.1. Reactor systems (a) two-stage reverse flow with step change in reactor conditions, lower temperature is applied to the fresh biomass, and higher temperature to the treated biomass (b) progressing batch reactor (F = biomass filling, E = biomass emptying, C = cellulose hydrolysis, H = hemicellulose hydrolysis).

The main drawback of the acid hydrolysis process is the byproduct formation such as furfural and hydroxymethylfurfural (HMF) which strongly inhibit the subsequent fermentation process for bioethanol production. Several reactor operation and configurations have been considered to improve the sugar yield from biomass hydrolysis. Torget et al[110] investigated a step-change in reaction temperature and acid flow rate where the biomass was first treated with a lower temperature and then followed by a higher temperature step. An improvement of sugar yield is observed owing to the different optimal reaction condition to hydrolyze different extent of cellulose and hemicellulose as well as the biphasic behavior of hemicellulose hydrolysis. Furthermore, two-stage reverse flow percolation reactor shown in Figure 5.1a, which resembles a countercurrent flow between the biomass and the acid, is also developed where the sugar concentration and yield are better than those from the step-change operation.[110] A similar idea has been previously proposed by Wright et al[111] named the progressing batch reactor (PBR). The key operation of this reactor configuration is the movement of the feed location of the acid stream to a different percolation reactor[112] arranged in series (see Figure 5.1b). This is to mimic the countercurrent movement between the biomass and the acid where a significant improvement of sugar yield was observed due to the shorter time of sugar decomposition.[102, 113] In addition, it avoids the complexity of moving solids through the reactor. The main advantage of PBR is the realization of countercurrent flow scheme while maintaining its simplicity of percolation reactor operation. Kim et al[114] proposed another reactor operation to improve the sugar yield from hydrolysis reaction using a step-change in acid concentration.
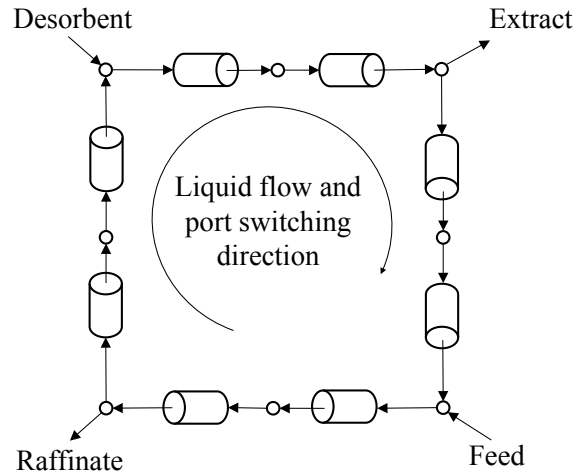
Figure 5.2. Simulated moving bed chromatography

There are several decisions from past studies that can be further optimized. From previous work,[110, 114] temperature, acid concentration, and acid flow rate are three operating parameters that can be adjusted using a step-change operation to hydrolyze different composition of biomass, and the most efficient scheme is countercurrent which can achieve high sugar concentration. A temperature gradient can be applied to each of the percolation reactor independently in PBR; however, to create the gradient in acid concentration and the acid flow rate simultaneously while maintaining a high sugar concentration is not straightforward. From Figure 5.1a, to change the acid concentration in the second reactor, a make-up acid stream with different concentrations may be mixed in to the second reactor. However, this would dilute the concentration of sugar components, and the liquid flow rate passing through the second reactor cannot also be adjusted to the optimal value independently from the first reactor. These considerations motivate the creation of a new process configuration in order to adjust all reaction conditions to their optimal values for each percolation reactor and to enable more flexible and robust operation.

After the hydrolysis has been performed by a reactor, the acid must be separated from the sugar hydrolysates. Several acid recovery technologies[11, 115] such as simulated moving-bed (SMB) chromatographic separation for sugar and acid separation[24, 26] have been considered. The concentrated acid hydrolysis with chromatographic separation technology from Arkenol[5,116] has been developed and successfully scaled up for bench-scale[117], and commercial implementation is being performed by BlueFire Renewables.[88, 97] The underlying principle of SMB is that the fluid is in contact with the solid phase where the feed and outlet streams switch to simulate the movement of solid phase to achieve a countercurrent flow.[118-120] In the applications of SMB chromatography to sugar-acid separation, multiple chromatographic columns, which are packed with ion exchange resin, are connected to column train, as shown in Figure 5.2. A mixture of acid and hydrolysates is supplied continuously to the recycle loop as the feed stream. To elute the component from the resin, water is supplied as desorbent. If cation exchange resin, such as in H^+ form, is employed as the packing material, then acid has lower affinity to the resin and is recovered as the raffinate stream, while purified sugar solution is recovered as the extract stream. The two feeding locations and two product withdrawal locations are switched periodically, which mimics the counter-current operation between the adsorbent phase and liquid phase. This pseudo counter-current operation can be approximated to a true counter-current process, true-moving bed chromatography, as discussed in the next section.

This work proposes a new reactive chromatographic separation process which integrates SMB and PBR in a single reactive separation process. Such integration allows variations of reaction parameters including temperature, acid concentration, and flow rate inside reactor system, as well as recovers fermentable sugar from the biomass hydrolysates.

The biomass feedstocks can contain both cellulose and hemicellulose which have different rates of hydrolysis reaction. Previous studies have explored the reactive separation principle using the SMB chromatography[121-126], or reactive SMB, for both liquid gas phase reactions for equilibrium-limited reactions,[127-129] but no previous work has considered a combination of SMB and reactor where the reactants are in the solid phase. We propose the solid-phase reactive separation system (SPRSS) combining the PBR and SMB units which have similar principles of the movement of the liquid feed to imitate the countercurrent movement of solid and liquid phase. The reaction and separation occur in the reactors and adsorption columns separately inside the process similar to the reactive separation proposed by Hashimoto et al[129] which has been applied for several process such as the production of high-fructose syrup from glucose isomerization[130-132] and p-xylene production.[133] This new process creates different reactor operating conditions, including acid concentrations and flow rates, by means of the SMB separation to hydrolyze different compositions of biomass in the PBR and recovers fermentable sugar from the hydrolysates. The ultimate goal is to improve the sugar yield and sugar product concentration while minimizing the sugar decomposition reaction and undesired product formation. Moreover, the acid from the separation can be directly recycled; therefore, the cost of acid consumption is reduced especially for concentrated acid hydrolysis.

In this chapter, we first evaluate the potential of this new process, SPRSS, by constructing a model with continuous movement of solid biomass and adsorbent using the kinetic parameters of dilute acid hydrolysis reactions from the literature. Although we explore an application of SPRSS to sugar production from biomass in this study, the

principle of SPRSS may be applied to other separation problems that involve solid reactants.

This chapter organized as follows: section 5.2 introduces two alternatives designs of the reactor and chromatographic separator systems including the proposed SPRSS for saccharification from biomass. The model development of the approximate continuous SPRSS including the countercurrent reactor and true-moving-bed chromatography and the superstructure formulation for the optimization problem are discussed in section 5.3. The multi-objective optimization problem formulation is presented in section 5.4. The optimization results for two cases as well as the analysis on the advantages of the SPRSS at different kinetic parameters are presented in section 5.5.
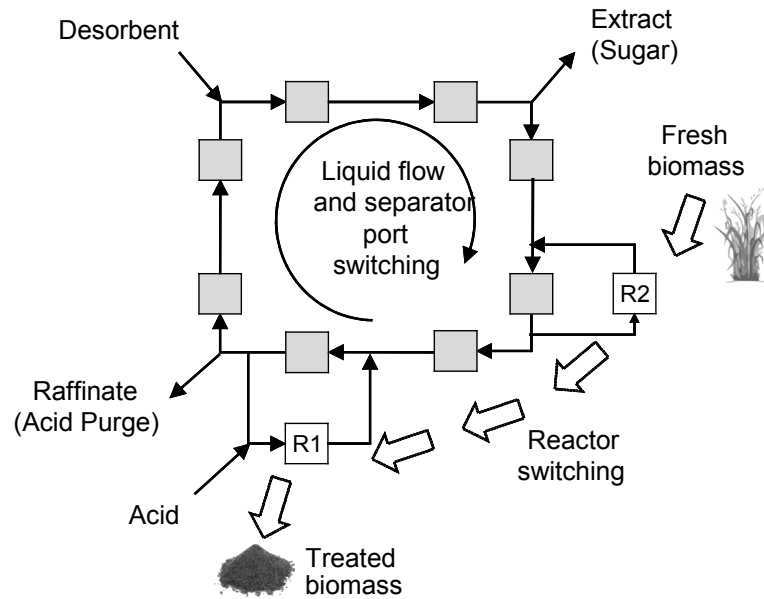
Figure 5.3. A realization of solid phase reactive separation system (SPRSS)
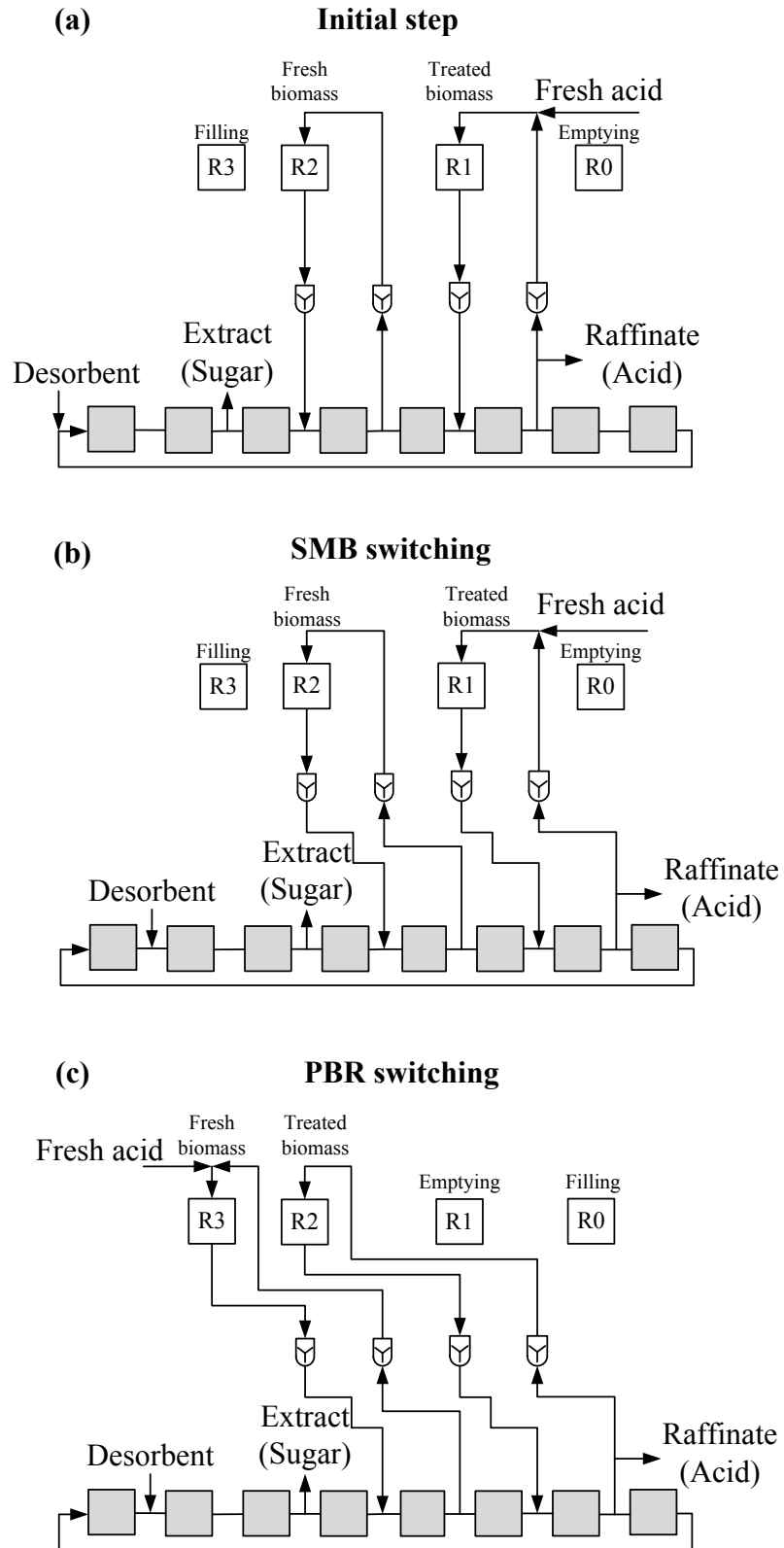
Figure 5.4. PBR and SMB operations in SPRSS (a) initial step (b) after SMB switching (c) after SMB and PBR switching.

5.3 Solid phase reactive separation system

SPRSS can be realized by integrating SMB chromatography and PBR in a single loop of liquid recycle. One potential design of SPRSS is shown in Figure 5.3, which consists of eight chromatographic columns and two reactors. As discussed in Section 1, the pseudo counter-current operation of SMB is realized by periodically shifting the locations of the feed, desorbent, extract and raffinate streams (separator port switching). Similarly, the pseudo counter-current operation of PBR is realized by periodically shifting the two reactors, R1 and R2 (reactor switching). These two independent switching operations are performed in a single SPRSS unit as illustrated in Figure 5.4. Figure 5.4a shows the initial SPRSS configuration where there are buffer tanks between PBR and SMB systems to maintain constant concentrations of all interconnecting streams. The liquid from one of the chromatographic columns is supplied to R1 and R2, and the outlets from R1 and R2 are recycled back to the SMB loop. Figure 5.4b shows the configuration after SMB switching and Figure 5.4c shows the configuration after switching of SMB and PBR. The order of the switching between PBR and SMB systems can change depends on the SPRSS design.

It should be noted that there are many possible SPRSS designs. Design decisions include the number of chromatographic columns, the number of reactors, and configurations of the chromatographic columns and reactors. These decisions can be optimized to improve the performance of SPRSS, as discussed more in detail in the next section. For example, a strategy to prevent byproduct formation is not to expose the hemicellulose in the fresh biomass in R2 to concentrated acid. On the other hand, to improve the overall conversion, the partially converted biomass in R1 must be treated with

a more concentrated acid solution. Such arrangements are realized in the design shown in Figure 5.3 and Figure 5.4, where R2 is located away from the acid inlet while R1 is located next to the acid feeding point.
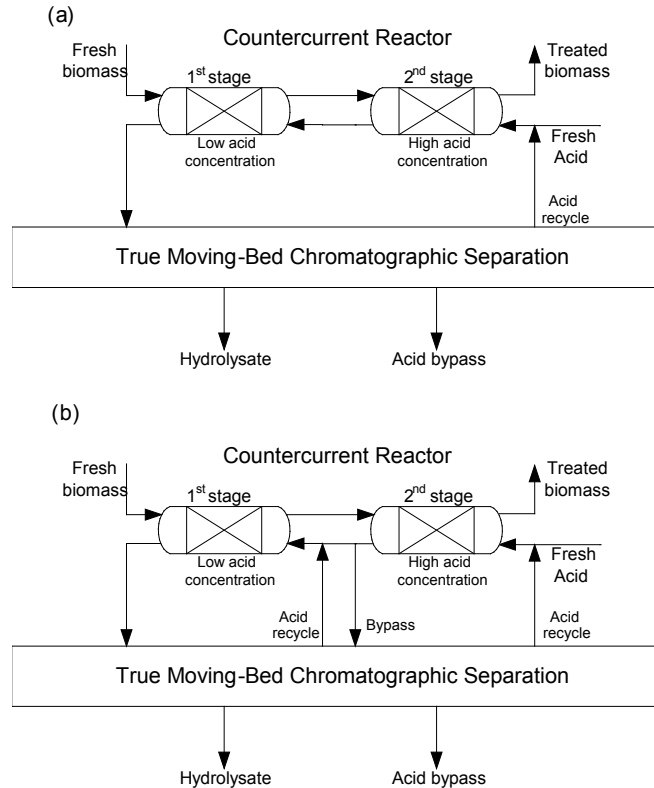
Figure 5.5. Comparison of two alternative designs for saccharification from biomass via acid hydrolysis (a) sequential design (b) SPRSS design.

The principle of the SPRSS operation can be approximated as the countercurrent flow between the solid and liquid phase by switching the liquid inlets and outlet ports for both PBR and SMB. The PBR component of SPRSS is approximated as a countercurrent reactor[102] (CCR) to capture the hypothetical movement of the solid biomass. Similarly, the SMB is approximated by the true moving-bed chromatographic separation (TMB) model.[134] By this simplification, SPRSS can be preliminarily designed on a steady state basis as the first step to investigate potential benefits of this new process.

In this study, we consider two specific configurations that combine a CCR and TMB, which are shown in Figure 5.5. Both designs, the sequential configuration (Figure 5.5a) and SPRSS (Figure 5.5b) contain two stages of CCR where each reactor can have different reaction temperature. In Figure 5.5a, the countercurrent reactor is connected with the TMB separation in a straightforward manner where the acid from hydrolysate from CCR is separated from sugar in TMB columns and recycled back to CCR and mixed with fresh acid stream. There is no intermediate recycle and bypass streams, and the acid feed with similar acid concentration therefore goes to both reactors. In contrast, Figure 5.5b shows the proposed SPRSS configuration which fully integrates countercurrent reactor with TMB separation with intermediate recycled and bypass streams. Therefore, the acid concentration of each reactor can be manipulated by the chromatographic separation which removes the acid from the hydrolysate. Figure 5.6 shows the sample concentration profile inside the TMB for the sugar (xylose)-acid separation using a cation exchange resin (CS16GC in acid form[135]). As the liquid stream in the TMB chromatographic separation has variation in acid concentration, the streams could consequently be recycled to different reactors containing different biomass composition with a different acid concentration as well as flow rate. These degrees of freedom create a significant advantage over a standard countercurrent reactor, especially for the concentrated acid hydrolysis process which operates at mild temperatures without any pressurization, and the acid concentration strongly affects the reaction rate.
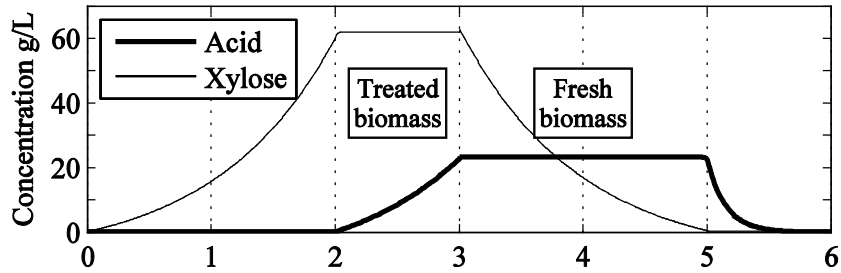
Figure 5.6. Concentration profile inside TMB chromatography for sugar-acid separation.

5.4 Model development

5.4.1 Kinetics of biomass hydrolysis

A widely used kinetic model of cellulose hydrolysis was first proposed by Saeman[101] consisting of two homogeneous consecutive first order reactions as previously illustrated in chapter 4 and shown in Figure 5.7a.[136] There are several modifications of the Saeman kinetic model where intermediate water-soluble oligosaccharides are formed before being further hydrolyzed to sugar. However, this heterogeneous behavior can be neglected when the conversion of oligosaccharides to glucose is relatively fast compared to cellulose to oligomers reaction at high temperature.[137] In the case of hemicellulose hydrolysis, a biphasic behavior is often observed where a part of hemicellulose is hydrolyzed faster as illustrated in Figure 5.7b.[138-139] The kinetic constants of all first order reactions have been modeled using an Arrhenius expression for temperature and the acid concentration C_A as previously presented in chapter 4 and shown in Eq. (5.1).[102]

$$k = k_0 \left(C^A \right)^n e^{-\left(\frac{E_a}{\Gamma T} \right)}$$
(4.1)

74
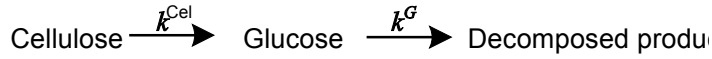
a. Kinetic scheme of lignocellulose hydrolysis by Saeman[101]
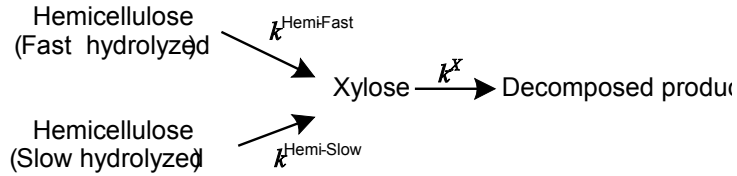
b. Hydrolysis of hemicellulose

Figure 5.7. Kinetics pattern for lignocellulose hydrolysis

Different biomass has a different composition and physical form, and the kinetics of hydrolysis may vary significantly because these are macroscopic models that do not distinguish between mass transfer and kinetics for these heterogeneous materials. This work considers using sulfuric acid catalyst where the summary of the kinetics parameters in Eq. (5.1) for the hydrolysis reaction of different biomass is shown in Table 5.1.

The purpose of our investigation is to understand the benefit of the acid concentration variation inside the reactor system. We assume the reaction temperature in all reactors is fixed, which would avoid the difficult operation of changing the temperature of the solid phase. Under this assumption, the reaction kinetics depend only on the concentrations of the acid and other components. The pre-exponent and the exponential terms of the reaction rate constant in Eq. (5.1) can be combined to become a pre-factor $P = k_0 \, e^{\frac{-E_a}{\Gamma T}}$ so that

$$k = P\left(C^A\right)^n \tag{4.2}$$

Table 5.1: Kinetic parameters for biomass hydrolysis with dilute sulfuric acid

k_0 $(min^{-1}(\%w/v)^{-n})$	n	E_a (kJ/mol.K)	Temperature (C°)	Acid concentration (%w/v)	Reference
Fast-hydrolyzed hemicellulose to xylose					
1.46×10^{15}	1	129.2	160–190	0.49–1.95	[102]
1.22×10^{14}	0.66	118.7	150–190	0.05–0.2	[114]
6.17×10^{13}	1.4	117.0	140–185	0.5	[140]
Slow-hydrolyzed hemicellulose to xylose					
1.30×10^{14}	0.5	125.4	160–190	0.49–1.95	[102]
6.03×10^{13}	1.18	117.0	150–190	0.05–0.2	[114]
1.88×10^{14}	1.2	129.6	140–185	0.5	[140]
Xylose to decomposed product					
1.62×10^{12}	0.8	115.0	160–190	0.49–1.95	[102]
4.82×10^{13}	0.71	128.3	150–190	0.05–0.2	[114]
1.01×10^{11}	0.48	105.9	140–185	0.5	[140]
Cellulose to glucose					
5.23×10^{17}	1.11	172.6	180–220	0.07–0.28	[137]
2.80×10^{20}	1.78	188.7	180–240	0.20–1.00	[141]
1.16×10^{19}	1	171.7	200–240	1.3–4.4	[141]
Glucose to decomposed product					
4.85×10^{10}	0.44	105.8	180–220	0.07–0.28	[137]
4.90×10^{14}	0.55	137.2	180–240	0.20–1.00	[141]
4.13×10^{15}	0.67	142.4	200–240	1.3–4.4	[141]

[a]All oligosaccharides is assumed to converted to monosaccharides very fast for simplicity

The variations of the value of P are estimated from the parameters in Table 5.1 at several temperatures between 100 – 180 °C and are presented as the approximate ranges in Table 5.2. From the table, the kinetic parameter P of the fast-hydrolyzed hemicellulose hydrolysis reaction is up to approximately 20 times faster than that of slow-hydrolyzed hemicellulose and can be up to 8,000 times faster than that of the cellulose. The uncertainty in kinetics parameters of hydrolysis reactions may significantly affect the performance of

the designed process. In this work, the effect of the variation of these kinetic parameters to the performance of the proposed SPRSS is investigated.

Table 5.2. Range of the kinetic parameter ratios of hydrolysis reactions at $100 - 180$ °C

Parameter	Range of values
Acid concentration (g/L)	0.5–50
n	0.5–1.8
$P^{\text{Hemi-fast}}$ (h^{-1}(%w/v)$^{-n}$)	0.05–150
$P^{\text{Hemi-fast}} / P^{\text{Hemi-slow}}$	1–20
$P^{\text{Hemi-Fast}} / P^{X}$	1–60
$P^{\text{Hemi-Fast}} / P^{\text{Cel}}$	1–8000
P^{Cel} / P^{G}	0.005–6

5.4.2 Countercurrent reactor and true-moving bed chromatography models

A mathematical model of CCR used in this work was developed by Lee et al.[102] We let the liquid flow in the positive direction for both systems. We define a set of component $NC = \{A, S, B\}$ to denote the acid, sugar (glucose, G, and xylose, X), and all byproduct, respectively. C_{CCR}^{j} is the concentration of component j inside the CCR while B^{fast} and B^{slow} are the concentration of fast and slow hydrolyzed biomass inside the CCR. Figure 5.8a shows a single stage of CCR at where the mass balances of all components in the hydrolysis reaction are given in Eq. (5.3) – (5.6).

Mass balance of fast-hydrolyzed biomass:

$$\frac{d\left((-v_B)B^{\text{fast}}\right)}{dx} = -k^{\text{fast}}B^{\text{fast}} \qquad (4.3)$$

Mass balance of slow-hydrolyzed biomass:

$$\frac{d\left((-v_B)B^{\text{slow}}\right)}{dx} = -k^{\text{slow}}B^{\text{slow}} \qquad (4.4)$$

Mass balance of sugars:

$$b_v u_{CCR} \frac{dC^S_{CCR}}{dx} = k^{\text{fast}} B^{\text{fast}} + k^{\text{slow}} B^{\text{slow}} - b_v k^S C^S_{CCR} \qquad (4.5)$$

Mass balance of byproducts:

$$u_{CCR} \frac{dC^B_{CCR}}{dx} = k^S C^S_{CCR} \qquad (4.6)$$

Boundary conditions:

$$x = 0, \quad C^j_{CCR} = C^j_{CCR}(0) \quad j \in NC$$

$$x = L, \quad B = \begin{cases} B^{\text{fast}}_0 & \text{(fast portion)} \\ B^{\text{slow}}_0 & \text{(slow portion)} \end{cases}$$
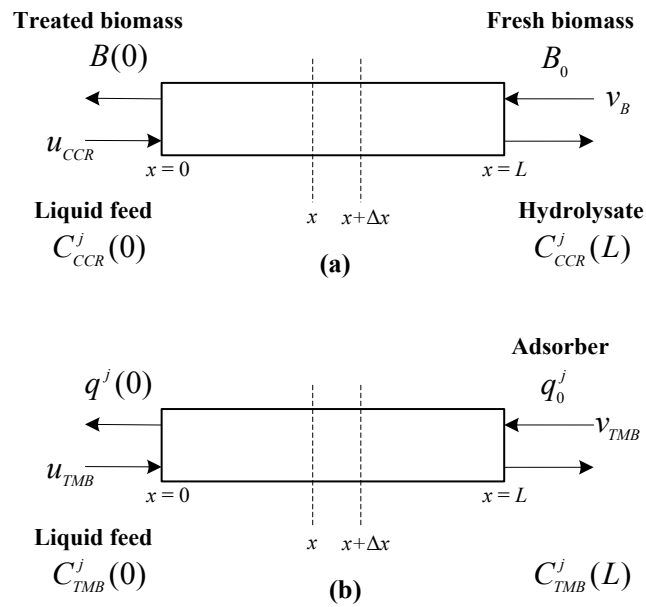
Figure 5.8. The single stage models of (a) countercurrent reactor and (b) true-moving-bed chromatographic separation

where u_{CCR} is the interstitial velocity while b_v is the biomass void fraction. In this study, we assume the effect of shrinking-bed is negligible so that the biomass velocity (v_B) is

constant. The acid concentration is also constant throughout the reactor. These sets of equations can be applied to both cellulose and hemicellulose. In this work, it is assumed for simplicity that glucose is produced only from cellulose and the decomposed product is only HMF, while xylose is produced from hemicellulose and the decomposed product is only furfural. Eq. (5.3) – (5.5) also describe the monophasic behavior by setting a kinetic constant of the fast and slow hydrolyzed biomass hydrolysis reaction to be equal $k^{fast} = k^{slow}$.[102] The boundary condition of the biomass is applied to both fast and slow hydrolyzed biomass where B_0 is the inlet biomass concentration. These simplifications make the model easier to solve, but are unlikely to have a significant impact on the conclusions of the relative performance of the systems we examine.

The mathematical model for TMB chromatographic separation has been reported in past studies.[142-145] This work uses the linear driving force mass transfer resistance model described as follows in Eq. (5.7) – Eq. (5.9) (see Figure 5.8b).[134]

Liquid phase mass balance:

$$\varepsilon u_{TMB} \frac{dC_{TMB}^j}{dx} = -\bar{k}_f^j \left(C_{TMB}^j - C_{TMB}^{eq,j} \right) \quad j \in NC \tag{4.7}$$

Adsorbent phase mass balance:

$$-(1-\varepsilon) v_{TMB} \frac{dq^j}{dx} = \bar{k}_f^j \left(C_{TMB}^j - C_{TMB}^{eq,j} \right) \quad j \in NC \tag{4.8}$$

Adsorption isotherm:

$$q^j = H^j C_{TMB}^{eq,j} \quad j \in NC \tag{4.9}$$

Boundary conditions:

$$x = 0, \quad C_{TMB}^j = C_{TMB}^j(0) \quad j \in NC$$
$$x = L, \quad q^j = q_0^j \quad j \in NC$$

79

where $\bar{k}_f^j$ is the component mass transfer coefficient, u_{TMB} and v_{TMB} are the interstitial liquid and adsorbent velocity, respectively, ε is the total bed porosity, C_{TMB}^j and q^j are the concentrations of liquid and solid phase, respectively, and $C_{TMB}^{eq,j}$ is the equilibrium concentration at the liquid film. These equations describe the mass transfer between the solid phase and liquid phase where a linear equilibrium adsorption isotherm is used. The effect of axial dispersion is lumped into the mass transfer resistance coefficient.[142] The cation exchange resin CS16GC in acid form is used in this work where $\varepsilon = 0.391$ and the Henry's constants (H^j) are dependent on the acid concentration.[18, 135] Our investigation reveals that the Henry's constants of all components vary insignificantly within the acid concentration range of $0 - 5$ %w/v assumed in this work which has negligible effect on the optimal design of the process; therefore, we used the values at the average sulfuric acid concentration of 2.5 %w/v. The mass transfer coefficient of the same column is estimated from the correlation in Heinonen and Sainio[24] and all values are shown in Table 5.3.

Table 5.3. Henry's law and mass transfer coefficients for adsorption column

Components	Linear Henry's law constant	Mass transfer coefficient (s^{-1})
Sulfuric acid	0.02	0.02
Glucose	0.18	0.03
Xylose	0.23	0.03
HMF	1.60	0.15
Furfural	2.25	0.15

5.4.3 Superstructure of solid phase reactive separation system

There are numerous alternative designs that integrate the reactors and chromatographic columns into one process. To find the best design from the many

alternatives, we consider a superstructure of SPRSS to include all possible process configurations.

Several assumptions have been made to construct the SPRSS superstructure in this work that are based on the practical issues in PBR and SMB processes. First, we consider the reactor system with a large number of columns while the SMB separation system contains M columns. This is to limit the number of adsorption columns; each column requires careful packing of the ion exchange resin which can be significantly more expensive than a reactor chamber. In addition, we divide the reactor system into N sections of variable lengths to limit the number of connecting streams between reactor and separation system. Under these assumptions, we approximate the PBR and SMB into CCR and TMB and construct the superstructure of SPRSS shown in Figure 5.9.
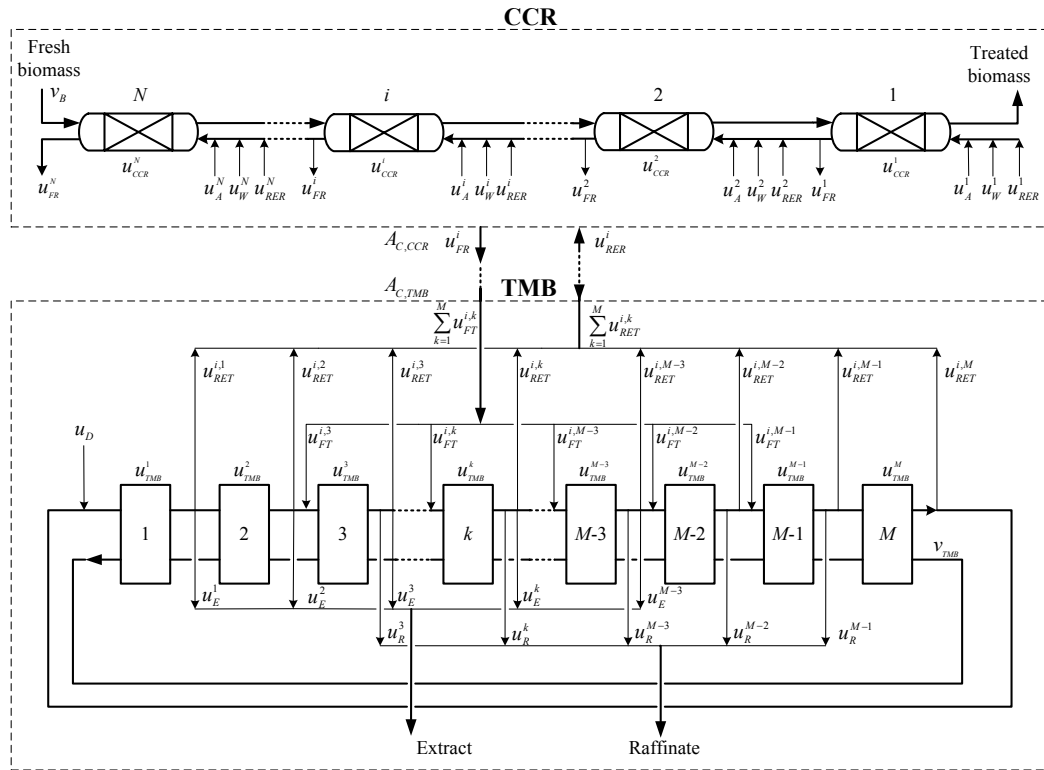
Figure 5.9. Superstructure of SPRSS

This superstructure comprises of the N number of CCR between biomass and acid stream arranged in series and M number of TMB separation columns. Each CCR reactor represents each section in PBR and may have different length. We define L^T as the total length of overall reactor system.

$$\sum_{i=1}^{N} L^i = L^T \qquad (4.10)$$

The lengths of all TMB columns are equal where each TMB column represents a single SMB column. We define $NR = \{1,2,..,i,..,N\}$ to be a set of the number of reactors, and $NT = \{1,2,..,k,..,M\}$ to be a set of TMB separation columns. The flow and component balances of each reactor feed are shown as follows.

CCR flow rate balances:

$$u_{CCR}^1 = u_A^1 + u_W^1 + u_{RER}^1 \qquad (4.11)$$

$$u_{CCR}^i = u_A^i + u_W^i + u_{RER}^i + u_{CCR}^{i-1} - u_{FR}^{i-1} \quad i \in NR - \{1\} \qquad (4.12)$$

CCR mass balances:

$$u_{CCR}^1 C_{CCR}^{j,1}(0) = u_A^1 C^A + u_{RER}^1 C_{RER}^{j,1} \qquad (4.13)$$

$$u_{CCR}^i C_{CCR}^{j,i}(0) = u_A^i C^A + u_{RER}^i C_{RER}^{j,i} + \left(u_{CCR}^{i-1} - u_{FR}^{i-1}\right) C_{CCR}^{j,i-1}(L)$$

$$j \in NC, i \in NR - \{1\} \qquad (4.14)$$

We must also avoid draining of the feed and recycle stream without passing through the reactor.

$$u_{CCR}^i - u_A^i - u_W^i - u_{RER}^i \geq 0 \qquad (4.15)$$

In this superstructure, the fresh acid (u_A^i), water stream (u_W^i), and the recycle stream from TMB (u_{RER}^i) are allowed to feed to any of the reactors where C^A and $C_{RER}^{j,i}$ are the

fresh acid feed concentration and the concentration of the recycle stream, respectively. The product streams from reactor i can go to the next reactor or bypass to the TMB systems (u_{FR}^i).

The bypass streams from any of the reactors can be chosen to feed any TMB separation columns. Furthermore, the recycle stream from any of the TMB separation columns can be recycled to any of the reactors. However, the size of the reactors and the columns can be different. Therefore, the interstitial velocities of the liquid streams connected between the reactors and TMB columns are related by the mass balances

Mass balances between CCR and TMB:

$$u_{FR}^N = u_{CCR}^N \tag{4.16}$$

$$b_v A_{C,CCR} u_{FR}^i = \varepsilon A_{C,TMB} \sum_{k=1}^{M} u_{FT}^{i,k} \quad i \in NR \tag{4.17}$$

$$b_v A_{C,CCR} u_{RER}^i = \varepsilon A_{C,TMB} \sum_{k=1}^{M} u_{RET}^{i,k} \quad i \in NR \tag{4.18}$$

$$b_v A_{C,CCR} u_{RER}^i C_{RER}^{j,i} = \varepsilon A_{C,TMB} \sum_{k=1}^{M} u_{RET}^{i,k} C_{TMB}^{j,k}(L) \quad j \in NC, i \in NR \tag{4.19}$$

where $u_{FT}^{i,k}$ is the liquid velocity of the feed from reactor i to the TMB column k and $u_{RET}^{i,k}$ is that from TMB column k to reactor i. The bypass stream from the final stage of reactor is simply the liquid flow inside the reactor (Eq. (5.16)). $A_{C,CCR}$ and $A_{C,TMB}$ are the cross-sectional area of the reactors and TMB separation columns, respectively.

The standard superstructure of the TMB columns[146] is employed in this superstructure. The velocity of the liquid phase inside kth TMB column (u_{TMB}^k) with the feed concentration $C_{TMB}^{j,k}(0)$ can be found from the flow and component balance.

TMB flow rate balances:

$$u_{TMB}^1 = u_{TMB}^M - u_E^M - u_R^M - \sum_{i=1}^N u_{RET}^{i,M} + u_D^1 + \sum_{i=1}^N u_{FT}^{i,1} \tag{4.20}$$

$$u_{TMB}^k = u_{TMB}^{k-1} - u_E^{k-1} - u_R^{k-1} - \sum_{i=1}^N u_{RET}^{i,k-1} + u_D^k + \sum_{i=1}^N u_{FT}^{i,k} \quad k \in NT - \{1\} \tag{4.21}$$

TMB mass balances:

$$u_{TMB}^1 C_{TMB}^{j,1}(0) = \left(u_{TMB}^M - u_E^M - u_R^M - \sum_{i=1}^N u_{RET}^{i,M} \right) C_{TMB}^{j,M}(L) + \sum_{i=1}^N u_{FT}^{i,1} C_{CCR}^{j,i}(L) \tag{4.22}$$

$$j \in NC$$

$$u_{TMB}^k C_{TMB}^{j,k}(0) = \left(u_{TMB}^{k-1} - u_E^{k-1} - u_R^{k-1} - \sum_{i=1}^N u_{RET}^{i,k-1} \right) C_{TMB}^{j,k-1}(L) + \sum_{i=1}^N u_{FT}^{i,k} C_{CCR}^{j,i}(L) \tag{4.23}$$

$$j \in NC, k \in NT - \{1\}$$

u_E^k and u_R^k are the velocity of extract and raffinate stream withdrawn from column k, and u_D^k is the velocity of the desorbent fed to column k. We define the set $NTR = \{3, 4,\ldots, M-1\}$ for the possible locations of the raffinate and feed stream and set $NTE = \{1, 2,\ldots, M-3\}$ for the possible locations of extract stream, and we avoid non-unique solutions due to the symmetry by fixing the specific flow rate.

$$u_D^k = 0 \quad k \in NT - \{1\} \tag{4.24}$$
$$u_{FT}^{i,k} = 0 \quad i \in NR, k \in NT - NTR \tag{4.25}$$
$$u_R^k = 0 \quad k \in NT - NTR \tag{4.26}$$
$$u_E^k = 0 \quad k \in NT - NTE \tag{4.27}$$

The solution of the SPRSS optimization problem with the superstructure formulation may contain many sub-optimal solutions. From our investigation, we make several assumptions and avoid some local solutions by introduce the binary variables (δ) to constrain the locations of several streams with logic constraints as follow.

1. The outlet stream from each reactor is allowed to be fed to only one TMB column (i.e. splitting the feed stream is not allowed). Similarly, the outlet from only one TMB column can be recycled to each reactor (i.e. recycle from multiple TMB column is not allowed). In addition, we consider a binary separation system between sugars and acid where all sugars (both glucose and xylose) are withdrawn together from one chromatographic column as a product, while the acid is allowed to remove out of the process from another column. From these assumptions, only one location of the feed, the raffinate, the extract, and the recycle streams are allowed.

$$u_{FT}^{i,k} \le u_{TMB\max} \delta_{FT}^{i,k} \quad i \in NR, k \in NTR \tag{4.28}$$

$$\sum_{k \in NTR} \delta_{FT}^{i,k} = 1 \quad i \in NR \tag{4.29}$$

$$u_R^k \le u_{TMB\max} \delta_R^k \quad k \in NTR \tag{4.30}$$

$$\sum_{k \in NTR} \delta_R^k = 1 \tag{4.31}$$

$$u_E^k \le u_{TMB\max} \delta_E^k \quad k \in NTE \tag{4.32}$$

$$\sum_{k \in NTE} \delta_E^k = 1 \tag{4.33}$$

$$u_{RET}^{i,k} \le u_{TMB\max} \delta_{RET}^{i,k} \quad i \in NR, k \in NT \tag{4.34}$$

$$\sum_{k \in NT} \delta_{RET}^{i,k} = 1 \quad i \in NR \tag{4.35}$$

$u_{TMB\max}$ is the maximum velocity inside TMB column which will be chosen based on the maximum allowable pressure drop.

2. There must be at least one separation column between the location of the feed streams and the raffinate, extract, and recycle streams.

$$\delta_{FT}^{i,k} + \delta_R^{k-1} \le 1 \quad i \in NR, k \in NTR \tag{4.36}$$

$$\delta_{FT}^{i,k} + \delta_E^{k-1} \le 1 \quad i \in NR, k \in NTR \tag{4.37}$$

$$\delta_{FT}^{i,k} + \delta_{RET}^{i,k-1} \le 1 \quad i \in NR, k \in NTR \tag{4.38}$$

3. The columns between the desorbent feed and the extract stream are mainly for desorbing the sugars from the adsorbent. Therefore, the feed, the extract, and the raffinate stream are not allowed to enter in this zone.

$$\delta_{FT}^{i,k} \leq \sum_{\bar{k}<k} \delta_E^{\bar{k}} \quad i \in NR, k \in NTR \tag{4.39}$$

$$\delta_{RET}^{i,k} \leq \sum_{\bar{k}<k} \delta_E^{\bar{k}} \quad i \in NR, k \in NT \tag{4.40}$$

$$\delta_R^k \leq \sum_{\bar{k}<k} \delta_E^{\bar{k}} \quad k \in NTR \tag{4.41}$$

In this study, we use two CCR ($N = 2$) and 12 TMB columns ($M = 12$). The optimal SPRSS can be found by optimizing this superstructure where the optimizer can choose the locations of all connecting streams between the CCR and TMB, and the design complexity must be justified carefully. It should be noted that the sequential configuration shown in Figure 5.5a can also be found from this superstructure by requiring the flow rates all intermediate streams between each reactor to be zero.

5.5   Multi-objective optimization problem formulations

The ultimate goal for this work is to maximize the sugar productivity as well as minimize the production cost which includes capital and operating costs. Table 5.4 lists the objectives which should be considered for designing SPRSS. In this work, we simplify and make several assumptions for the optimization problem as follows. First, we fix the temperature in the reactor system where the kinetic model shown in Eq. (5.2) is used, since this work mainly focuses on the effect of acid concentration on the reactions as previously discussed. Therefore, the heat consumption of the process is fixed. Second, the diameters

of the two reactors are fixed to one meter allowing the reactor capital cost depends only on the length while the TMB columns length is fixed to one meter allowing the TMB capital cost depends only on the diameter. Third, the cost of fresh water consumption (diluent in reactor system and desorbent in TMB separation) is assumed negligible, while water evaporation cost is represented by the sugar concentration. Under these assumptions, we consider the single-objective optimization problem with constraints presented in Table 5.5 where the decision variables and all model assumptions used in this study are summarized in Table 5.6.

Table 5.4. Objectives for designing SPRSS

Objectives	
maximize	Total yield of sugars
	Sugar concentration in extract
	Biomass throughput
	Selectivity of sugars
minimize	Capital cost - Size of Reactor and TMB columns (length and diameter)
	Operating cost - Acid consumption - Water consumption - Energy consumption (reaction temperature)

Table 5.5. Optimization problem formulation

max Y^S_{SPRSS}	Yield of sugars
Subject to:	
1. $C^S \geq C^S_{min}$	minimum sugar concentration (g/L)
2. $M^B \geq M^B_{min}$	minimum biomass throughput (kg/h)
3. $S^S_{SPRSS} \geq S^S_{min}$	minimum selectivity of sugars (%)
4. $D_{TMB} \leq D_{TMB\,max}$	maximum TMB column diameter (m)
5. $L^T \leq L^T_{max}$	maximum CCR length (m)
6. $F^A \leq F^A_{max}$	maximum fresh acid consumption (kg/h)

Table 5.6. Decision variables and model assumptions

Decision variables	Model Assumptions	
Biomass velocity	Reactor diameter	1 m
The lengths of two reactors	Number of reactors	2
Acid and water feed rates to each of two reactors	TMB column length	1 m
Two outlet flow rates from each of the two reactors and its feed location to TMB	Number of TMB columns	12
Two recycle flow rates to each of the two reactors and its location from TMB	$D_{TMB\,max}$	2 m
One extract stream flow rate and its location in TMB	$u_{CCR,max}, u_{TMB,max}$	10 m/h
One desorbent stream flow rate at the first TMB column	Fresh acid concentration, C^A	900 g/L
One raffinate stream flow rate and its location in TMB	biomass void fraction, b_v	0.8
Adsorbent velocity		

In addition to the constraints in Table 5.5, we have additional constraints on the acid purity at the product stream and the maximum liquid flow rate of all reactors and TMB columns to avoid excessive pressure drop.

$$\text{PUR}^A \leq \text{PUR}^A_{max} \tag{4.42}$$

$$u^i_{CCR} \leq u_{CCR\,max} \tag{4.43}$$

$$u^k_{TMB} \leq u_{TMB\,max} \tag{4.44}$$

The overall sugars' yield, Y^S, containing glucose from cellulose and xylose from fast and slow hydrolyzed hemicellulose can be found from Eq. (5.45).[110]

$$Y^S = f^G Y^G + f^X Y^X \tag{4.45}$$

where each coefficient f is the fraction of the corresponding biomass. The calculations of the sugar yield and all constraints are shown in Table 5.7.

Table 5.7. Definition of objective funtion and model constraints

Xylose yield[a]

$$Y^X = \frac{\varepsilon A_{C,TMB} \sum\limits_{k=1}^{M} u_E^k C_{TMB}^{X,k}(L)}{B_0^{\text{Hemi}} A_{C,CCR} v_B}$$

$$= \left(\frac{b_v A_{C,CCR} \sum\limits_{i=1}^{N} \left(u_{FR}^i C_{CCR}^{X,i}(L) - u_{RER}^i C_{RER}^{X,i} \right)}{B_0^{\text{Hemi}} A_{C,CCR} v_B} \right) \left(\frac{\varepsilon A_{C,TMB} \sum\limits_{k=1}^{M} u_E^k C_{TMB}^{X,k}(L)}{b_v A_{C,CCR} \sum\limits_{i=1}^{N} \left(u_{FR}^i C_{CCR}^{X,i}(L) - u_{RER}^i C_{RER}^{X,i} \right)} \right)$$

$$= Y_{CCR}^X Y_{TMB}^X$$

Sugar concentration (g/L)	$C^S = \dfrac{\sum\limits_{k=1}^{M} u_E^k C_{TMB}^{S,k}(L)}{\sum\limits_{k=1}^{M} u_E^k}$
Biomass throughput (kg/h)	$M^B = A_{C,CCR} v_B \left(\sum B_0 \right)$
Selectivity of sugars (%)	$S^S = \dfrac{\sum\limits_{k=1}^{M} u_E^k C_{TMB}^{S,k}(L)}{\sum\limits_{k=1}^{M} u_E^k \left(C_{TMB}^{S,k}(L) + C_{TMB}^{B,k}(L) \right)}$
Fresh acid consumption (kg/h)	$F^A = b_v A_{C,CCR} \sum\limits_{i=1}^{N} u_A^i C_A$
Acid purity at extract stream	$PUR^A = \dfrac{\sum\limits_{k=1}^{M} u_E^k C_{TMB}^{A,k}(L)}{\sum\limits_{k=1}^{M} \sum\limits_{j \in NC} u_E^k C_{TMB}^{j,k}(L)}$

[a] Xylose yield is defined as the ratio of the mass of xylose from both fast and slow hydrolyzed hemicellulose produced at the extract stream over the biomass throughput. The overall sugars' yield can also be expressed in terms of the multiplication of the yield from the reaction in CCR and the yield from the recovery of sugar in TMB separation. The glucose yield can be calculated similar to the xylose yield.

5.6 Results and discussions

The superstructure of SPRSS mathematical model is formulated as an MINLP problem and solved in GAMS 23.8.1 environment using CONOPT 3.15A solver, and the optimizations are run on six-Core 2.4 GHz AMD Opteron(tm) Processor with 8 GB of RAM. The analytical solutions of the ordinary differential equations of reactor systems are used while the TMB columns are discretized into 50 elements using the first order backward difference for liquid phase and forward difference for solid phase. The superstructure model consists of approximately 9500 variables with 72 integer variables, and the computation times is up to 15 minutes.

5.6.1 Optimal configuration of SPRSS

In this study, we consider two different cases to analyze the optimal process structure of SPRSS. In Case 1, we consider only hemicelluloses which produces xylose and further decomposes into furfural. We consider a biphasic system, where the biomass consists of two fractions: fast decomposing and slow decomposing. In Case 2, we consider a more extensive case study where both hemicelluloses and cellulose exist. In both cases, we compare the sequential configuration with SPRSS design (Figure 5.5) in order to see the benefits of the variation of acid concentration. In the case of sequential configuration, all inlets and outlet streams between two reactors are switched off. Only one recycled stream from TMB column is allowed which is mixed with the fresh acid feed stream. The length of each reactor has no effect on the optimal solutions and is fixed to be equal. For the SPRSS configuration, there is no restriction on the inlets and outlets streams between

two reactors, and each reactor length are allowed to vary with the same L_{max}^T. In both cases,

the constraints on selectivity of sugars (S_{min}^S) and fresh acid consumption (F_{max}^A) are chosen

to be their minimum and maximum values, respectively, that make both constraints 3 and

6 in Table 5.5 active for the sequential configuration design.

Table 5.8. Model parameters

	Case 1	Case 2
Design parameters	$M_B = 400$ kg/h $L_{max}^T = 3$ m $F_{max}^A = 0.74$ kg/h $C_{min}^S = 60$ g/L $PUR_{max}^A = 0.1$ (wt%) $S_{min}^S = 76.9$ %	$M_B = 500$ kg/h $L_{max}^T = 5$ m $F_{max}^A = 0.44$ kg//h $C_{min}^S = 80$ g/L $PUR_{max}^A = 0.1$ (wt%) $S_{min}^S = 73.3$ %
Kinetic parameters	$B_0^{\text{Hemi-Fast}} = 65$ kg/m^3 $B_0^{\text{Hemi-Slow}} = 35$ kg/m^3 $P^{\text{Hemi-fast}} = 35$ h^{-1} (%w/v)$^{-n}$ $P^{\text{Hemi-slow}} = 1.75$ h^{-1} (%w/v)$^{-n}$ $P_X = 3.5$ h^{-1} (%w/v)$^{-n}$ $n_{\text{Hemi-fast}} = 0.5$ $n_{\text{Hemi-slow}} = 1.5$ $n_X = 1.1$	$B_0^{\text{Hemi-Fast}} = 39$ kg/m^3 $B_0^{\text{Hemi-slow}} = 21$ kg/m^3 $B_0^{\text{Cel}} = 40$ kg/m^3 $P^{\text{Hemi-fast}} = 8$ h^{-1} (%w/v)$^{-n}$ $P^{\text{Hemi-slow}} = 4$ h^{-1} (%w/v)$^{-n}$ $P^X = 4$ h^{-1} (%w/v)$^{-n}$ $P^{Cel} = 2.67$ h^{-1} (%w/v)$^{-n}$ $P^G = 0.53$ h^{-1} (%w/v)$^{-n}$ $n_{\text{Hemi-fast}} = 0.5$ $n_{\text{Hemi-slow}} = 0.5$ $n_X = 1.0$ $n_{Cel} = 0.8$ $n_G = 0.9$

Case 1: Biphasic hemicellulose

We first apply the SPRSS model to the system where biomass contains only hemicellulose with the biphasic behavior (see Figure 5.7b), or equivalently where the conditions are too mild for the cellulose to react. In this case, the system contains only three components including acid, xylose, and furfural as a decomposed product. The model parameters are assumed and presented in Table 5.8 where the values of the kinetic parameters are chosen based on Table 5.2.

Figure 5.10 shows the optimal solution and concentration profile inside CCR and TMB separation of the sequential configuration. In Figure 5.10a, it can be seen that the conversion of the fast-hydrolyzed hemicellulose increase sharply at the solid inlet ($x = 3$) and reach the final conversion of nearly 100% at the solid outlet ($x = 0$) while that of slow-hydrolyzed hemicellulose increase at a slower rate and reach the final conversion of around 98% at $x = 0$. This makes the xylose concentration increase rapidly at $x = 2.5$ to 3 as presented in Figure 5.10b. In a trade-off between the biomass conversion and the sugar decomposition, the optimizer found the acid concentration at 24.6 g/L inside CCR with the maximum total reactor length $L^T = L^T_{max}$ give the highest xylose yield. The liquid stream from the TMB column 10 has relatively low xylose concentration as well as high acid concentration which is therefore chosen to be recycled to the CCR with a negligible amount of purge as raffinate stream (see Figure 5.10c). The fresh acid consumption is therefore small at 0.74 kg/h. This small amount can be further reduced by tightening the constraints on the fresh acid consumption (F^A_{max}) which sacrifices the xylose yield slightly.
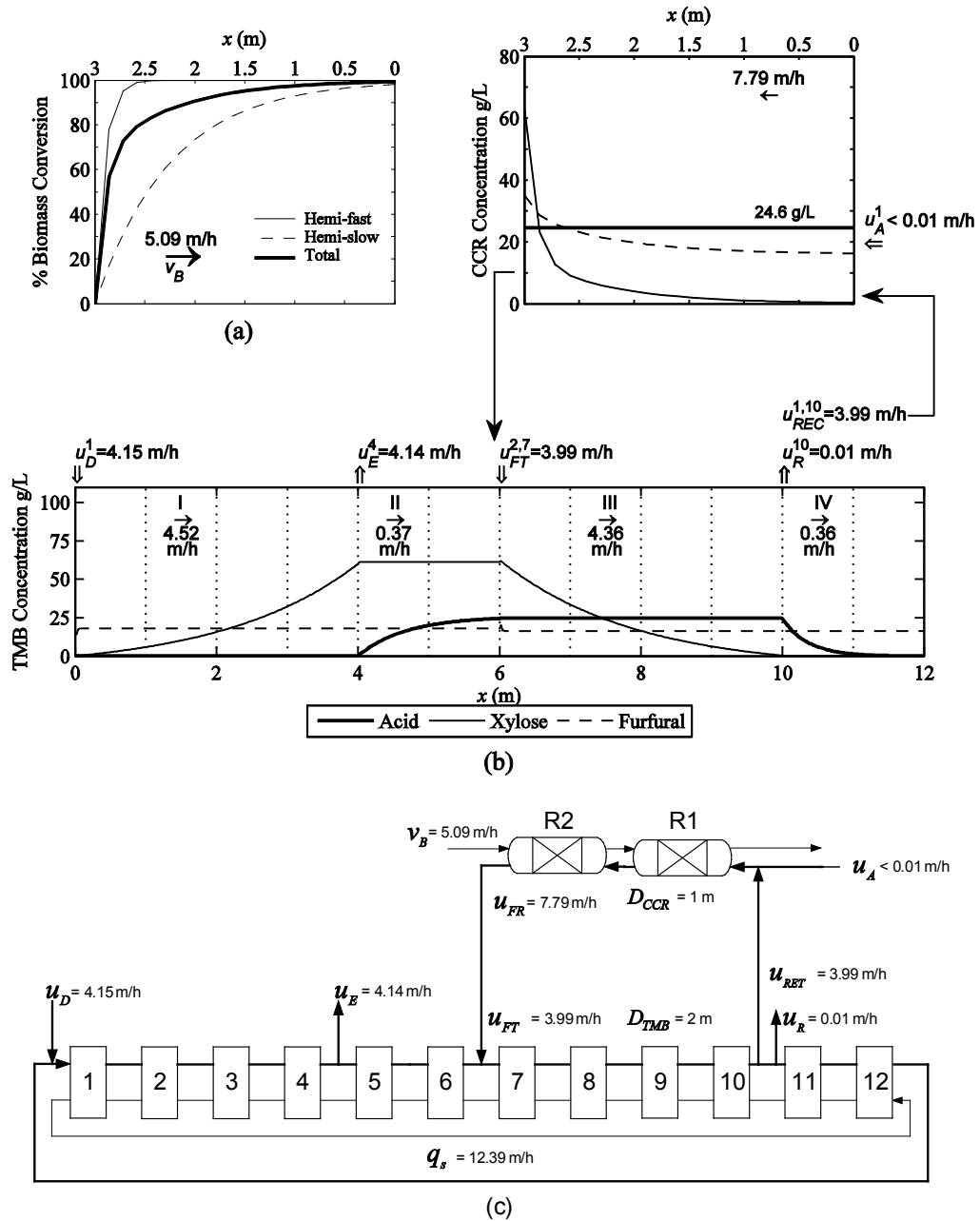
Figure 5.10. Optimal solution of the sequential configuration for biphasic hemicellulose hydrolysis (a) biomass conversion of fast-hydrolyzed, slow-hydrolyzed, and total hemicellulose (b) concentration profile inside CCR and TMB columns (c) optimal process configuration.
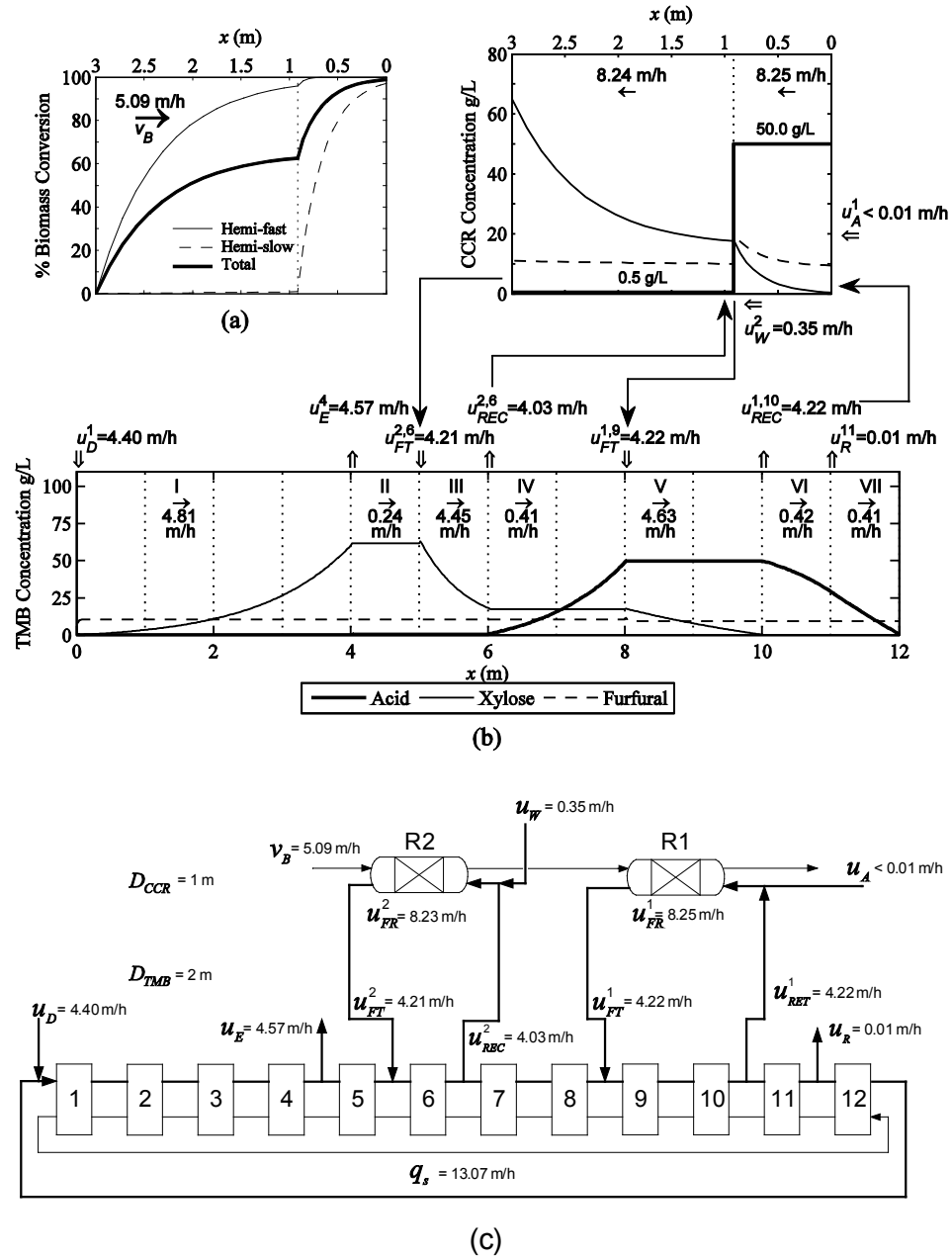
Figure 5.11. Optimal solution of the SPRSS design for biphasic hemicellulose hydrolysis (a) biomass conversion of fast-hydrolyzed, slow-hydrolyzed, and total hemicellulose (b) concentration profile inside CCR and TMB columns (c) optimal process configuration.

Figure 5.11 shows the optimal solution and concentration profiles inside the CCR and TMB of the SPRSS configuration. The initial guess for this optimization is the optimal solution for the sequential design. From Figure 5.11a, it can be seen that the fast-hydrolyzed hemicellulose is mainly hydrolyzed in R2 which contacts a low acid concentration of 0.5 g/L while the slow-hydrolyzed hemicellulose is only converted in R1 by a higher acid concentration at 50 g/L (see Figure 5.11b). The reactor length of the R2 is approximately twice that of R1 which means the reaction time of the hydrolysis reaction with the high acid concentration is around one-third of the total reaction time.

The optimal solution of the SPRSS shown in Figure 5.11c has two interconnecting loops between the CCR and TMB which have different internal acid concentrations. One loop is between R1 in the CCR and Columns 9 and 10 in the TMB. In this loop, the outlet of R1 is fed to the Column 9 where the xylose, a higher affinity component, is adsorbed into the solid phase. The liquid flows to Column 10 with a reduction in xylose concentration, and the outlet is recycled to R1. Similarly, there is another loop between R2 in the CCR and Column 6 in the TMB. In this loop, the outlet of R2 is fed to Column 6 in the TMB where the xylose is adsorbed, and the liquid from the same column is recycled to R2. These create two separate closed recycle loops with different acid concentrations where the xylose is produced inside the CCR and then partially recovered by TMB separation. It is noteworthy that the optimizer chooses to feed the xylose of a moderately high concentration from Column 6 back to R2. This is to increase the sugar concentration to meet the constraint for the minimum sugar concentration (Constraint 1 in Table 5.5). Furthermore, a small amount of fresh water is fed to the second reactor to further dilute the acid which has a small effect on the xylose concentration. The key observation is that the

SPRSS design can change the acid concentration inside the reactor system independently from the sugar concentration, which is enabled by the separation of the TMB.

The TMB separation can be divided into seven zones as shown in Figure 5.11b. In Zone I, all xylose from the adsorbent is desorbed into the liquid phase and the product is removed at the extract stream. In Zone II and Zone IV, the acid is desorbed from the adsorbent and the acid concentration in the liquid stream rises to the optimal acid concentration which is recycled back to the reactor. The xylose from the reactor outlet is adsorbed in Zone III and Zone V so the sugar concentration reduces while the acid concentration remains the same. Zone VI and Zone VII of the TMB separation are used to adsorb the acid before being recycled back to Zone I. The acid is recycled from column 6 to R2 and from column 10 to R1 while the remaining amount, which is negligible, is purged as the raffinate stream at column 11. Our investigation reveals that the acid purging stream may increase at different model parameters to allow a higher acid concentration to be recycled to the first reactor.

The optimal results of the sequential and SPRSS designs are compared in Table 5.9. It can be seen in this table that the SPRSS configuration increases the total yield of xylose by 7.9%. In addition, less furfural formation is observed and the selectivity of xylose improves by 8.2%. It is noteworthy that the total sugar yield consists of two parts: the reaction yield and the recovery of sugar from TMB separation (see Table S3 in the Supporting Information). Our investigation shows that in both designs, there is negligible amount of xylose lost to the raffinate stream, which indicates that the recovery of sugar from the TMB separation is nearly complete. Thus, the total xylose yield at the extract product stream is equivalent to the sugar yield from the reaction.

The constraints on the sugar concentration, biomass throughput, TMB column diameter, reactor length, and fresh acid consumption are all active in the optimal solutions for both configurations. There is no constraint on the fresh water consumption; however, the values for both configurations are similar. These results demonstrate the potential improvement of sugar yield using the SPRSS configuration.

Table 5.9. Comparison of sequential and SPRSS optimal configuration

Parameters	Case 1		Case 2	
	Sequential configuration	SPRSS configuration	Sequential configuration	SPRSS configuration
Y^S	76.3 %	84.2 %	65.0 % $Y^X = 65.3$ % $Y^G = 64.7$ %	73.2 % $Y^X = 72.0$ % $Y^G = 73.4$ %
S^S	76.9 %	85.1 %	73.3 %	77.6 %
Water usage	5.1 m^3/h	5.6 m^3/h	4.0 m^3/h	4.6 m^3/h
F^A	0.74 kg/h		0.44 kg/h	
C^S	60 g/L		80 g/L	
M^B	400 kg/h		500 kg/h	
D_{TMB}	2 m		2 m	
L^T	3 m		5 m	

Case 2: Mixture of cellulose and hemicellulose

We now consider the system where both cellulose and hemicellulose exist in the biomass (see Figure 5.7). The system now contains five component including acid, glucose, xylose, HMF, and furfural, and the separation becomes more complex. In this case study, we assume the biomass has a total concentration of 100 kg/m^3 consisting of 60% hemicellulose ($f^X = 0.6$) with 65% fast-hydrolyzed and 35% slow-hydrolyzed, and 40% cellulose ($f^G = 0.4$). The initial concentration of each biomass portion and the model parameters are assumed based on Table 5.2 and shown in Table 5.8.

Figure 5.12 shows the optimal solution of the sequential configuration. In Figure 5.12a, it can be seen that final conversion of the fast-hydrolyzed hemicellulose, slow-hydrolyzed hemicellulose, and cellulose at the solid outlet from the reactor ($x = 0$) are 99.3%, 91.9%, and 76.8%, respectively, while the optimal acid concentration inside the reactor is 6.4 g/L (see Figure 5.12b). The model chooses a slightly low acid concentration to lessen the amount of byproduct formation with an expense of lower conversion of slow-hydrolyzed hemicellulose and cellulose. The concentration profiles inside the TMB and the optimal process configuration (Figure 5.12c) are similar to Case 1. The acid from Column 11 is recycled completely to R1 without any purge stream, and the flow rate of fresh acid feeding to the first reactor is therefore very small.

The optimal solution of the SPRSS configuration is shown in Figure 5.13 where we use the optimal solution of the sequential configuration as an initial guess. In Figure 5.13a, the final conversion of the fast, slow-hydrolyzed hemicellulose, and cellulose at $x = 0$ increase to 99.7%, 94.8%, and 88.9%, respectively, which was enabled by the two-level acid concentration in the CCR (Figure 5.13b). The optimal configuration also contains two loops (Figure 5.13c) where the first loop is connected to reactor R1 with a high acid concentration of 25.3 g/L while the second loop is connected to reactor R2 with a lower acid concentration of 2.4 g/L. There is no raffinate stream and the acid from TMB column 8 and 11 is recycled to the CCR, thus there are six separation zones in this case as shown in Figure 5.13b.
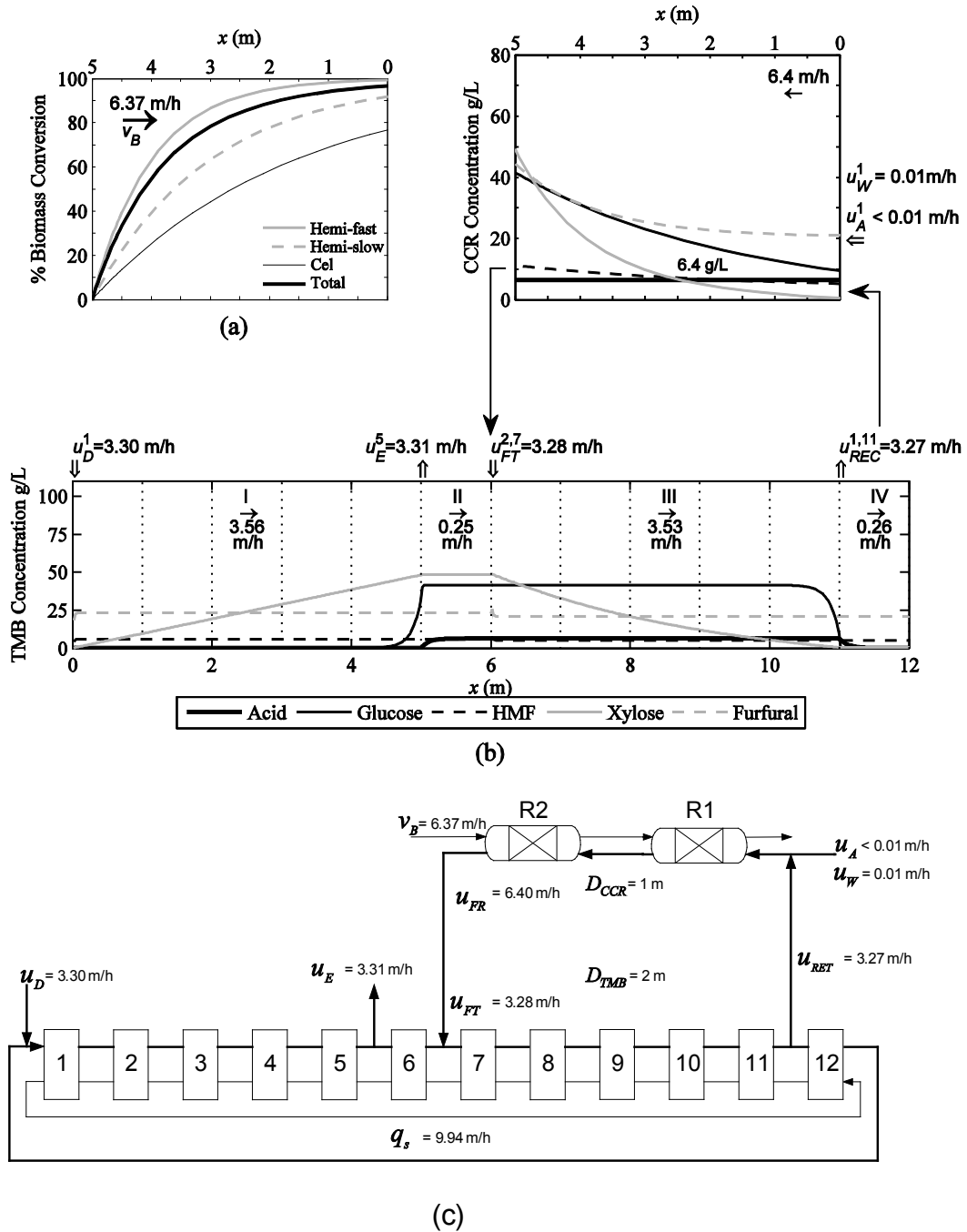
Figure 5.12. Optimal solution of the sequential configuration for cellulose and biphasic hemicellulose hydrolysis (a) biomass conversion of fast and slow hydrolyzed hemicellulose, cellulose, and total biomass conversion (b) concentration profile inside CCR and TMB columns (c) optimal process configuration.
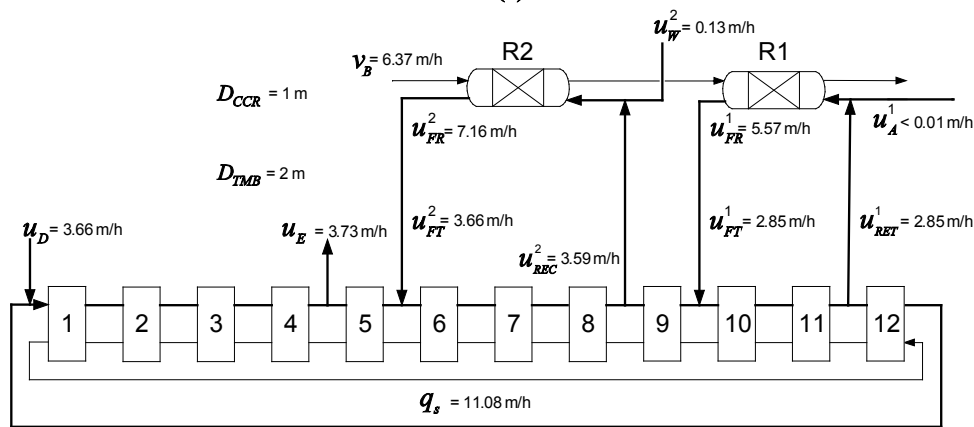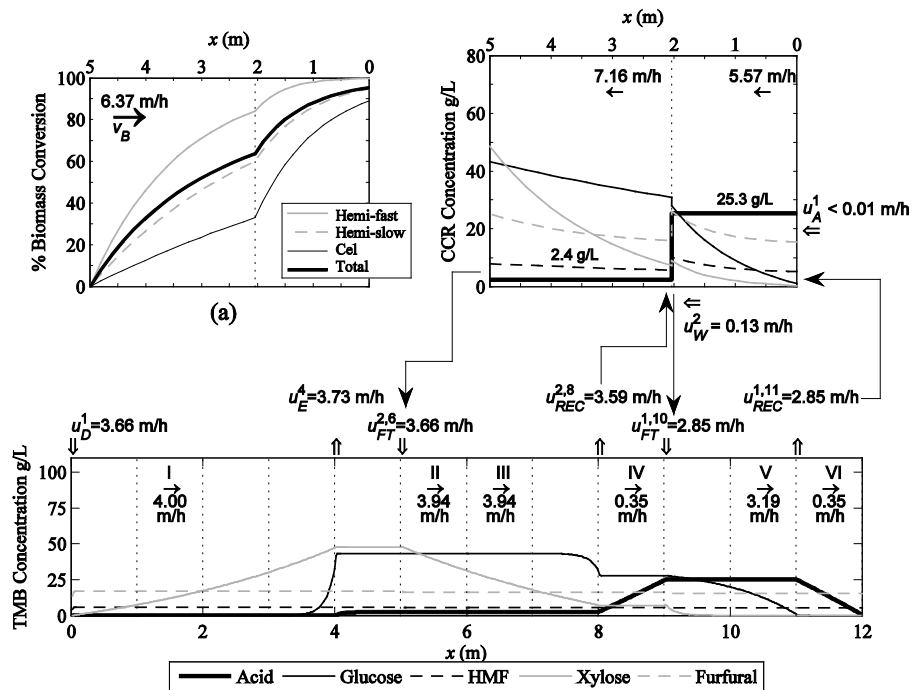
Figure 5.13. Optimal solution of SPRSS design for cellulose and biphasic hemicellulose hydrolysis (a) biomass conversion of fast and slow hydrolyzed hemicellulose, cellulose, and total biomass conversion (b) concentration profile inside CCR and TMB columns (c) optimal process configuration.

The comparison of the sequential and SPRSS configurations is presented in Table 5.9 where an improvement in total sugar yield is 8.2 % while the selectivity increases by 4.3 %. The optimal solutions can vary significantly depending on the constraints and model assumptions. The effect of kinetic parameters is examined in the next section.

5.6.2 Effect of kinetic parameters to the SPRSS design

The results presented in the previous section shows the benefits of the SPRSS configuration over the sequential configuration. However, the optimal solutions can vary significantly depending on many model parameters including the size of equipment, the value of the constraints on the problem formulation such as the biomass throughput and biomass initial concentration, and all of kinetic parameters of the hydrolysis reactions. Our investigation reveals that the kinetic parameters have the most significant impact on the sugar yield improvement of the SPRSS over that of sequential design. The improvement from SPRSS in this work mainly comes from the ability to change the acid concentration without interfering with the sugar concentration. Consequently, SPRSS design is favorable when changing acid concentration significantly influences the reaction kinetics.

In the investigation below, we always avoid trivial solutions by assuming that when the acid concentration increases, the reaction rate of the byproduct formation increases more significantly than that of the sugar formation. This condition can be expressed in the reaction model considered in Figure 5.7 and Eq. (5.2) as the following conditions:

$$\left(n_{\text{Hemi-Fast}} \le n_X\right) \quad \vee \quad \left(n_{\text{Hemi-Slow}} \le n_X\right) \quad \vee \quad \left(n_{\text{Cel}} \le n_G\right) \tag{4.46}$$

Without this condition, the optimizer would always find a trivial solution of increasing the acid concentration to the highest value.

There are many reaction paths that occur during biomass hydrolysis where each kinetic parameter of each reaction could have an interaction effect on the objective function. It is not straightforward to determine at which values of these kinetics parameters would justify the more complex SPRSS design than that of the sequential design.

Our investigation below reveals two main observations of the kinetic parameters' values that could further enhance the advantage of using SPRSS configuration over sequential design. In these two observations, the sequential and SPRSS configuration designs are compared at several different kinetic parameters based on model parameters from Case 1 in Table 5.8 where the value of S_{min}^{S} and F_{max}^{A} are chosen to be the minimum and maximum values, respectively, so that the constraints 3 and 6 in Table 5.5 are active for the sequential configuration design. We always assume that Eq. (5.46) is satisfied in this investigation. In addition, each reactor length, TMB column diameter, and all integer variables are fixed at the optimal solution of Case 1 for both sequential and SPRSS configurations. This is to investigate the flexibility of both designs at different kinetic parameters.

5.6.2.1 Effect of reaction kinetic parameters for byproduct formation

The SPRSS design can be more favorable at a higher rate of byproduct formation. In the reaction model considered in Eq. (5.2), this corresponds to a large value of P^{X} and n_{X} in the reaction path shown in Figure 5.7b. Figure 5.14 shows an improvement of xylose yield of the SPRSS over sequential configuration design at different $P^{X} / P^{\text{Hemi-fast}}$ and n_{X}.

From the figure, the xylose yield improvement increases with increasing the ratio $P^X / P^{\text{Hemi-fast}}$ at $n_X = 0.7$ and 0.8. This indicates that when the rate of byproduct formation increases relative to sugar generation so that suppressing decomposition of sugars is more difficult, the SPRSS configuration has greater advantages over the sequential design. However, when the order of acid concentration of xylose decomposition reaction increases to $n_X = 1.1$, the increase is less significant, while the yield improvement decrease when $n_X = 1.5$ at a high $P^X / P^{\text{Hemi-fast}}$. This is because the byproduct formation rate is extremely fast and highly sensitive to the acid concentration, and consequently the optimizer decides to lower the acid concentration. Figure 5.15 illustrates the acid concentration inside the reactors R1 and R2 of the SPRSS design. From the figure, the acid concentration inside R2 is almost constant in all cases, while that of R1 decreases when increasing the ratio $P^X / P^{\text{Hemi-fast}}$ at $n_X = 1.1$ and 1.5. Due to a very high byproduct formation rate, even the SPRSS design cannot avoid the sugar decomposition and thus it is necessary to reduce the acid concentration to avoid the decomposition reaction. In addition, it can be seen from the figure that this causes a smaller difference in acid concentration between R1 and R2. Due to a smaller variation of acid concentration inside the reactor system, the benefit of changing the acid concentration accordingly becomes smaller resulting in a smaller advantage of the SPRSS design over the sequential configuration. In summary, at a high rate of byproduct formation relatively to sugar generation, SPRSS could suppress byproduct formation better than the sequential design leading to an improvement of sugar yield, but a too fast byproduct formation cannot be suppressed even by SPRSS.
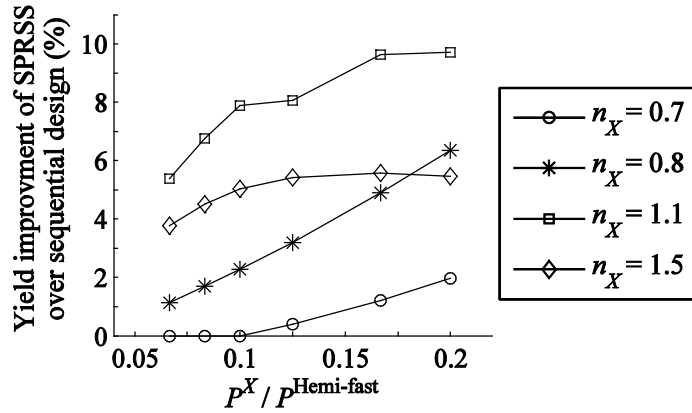
Figure 5.14. Effect of the ratio $P^X / P^{\text{Hemi-fast}}$ and n_X on an improvement of xylose yield of the SPRSS configuration over sequential design.
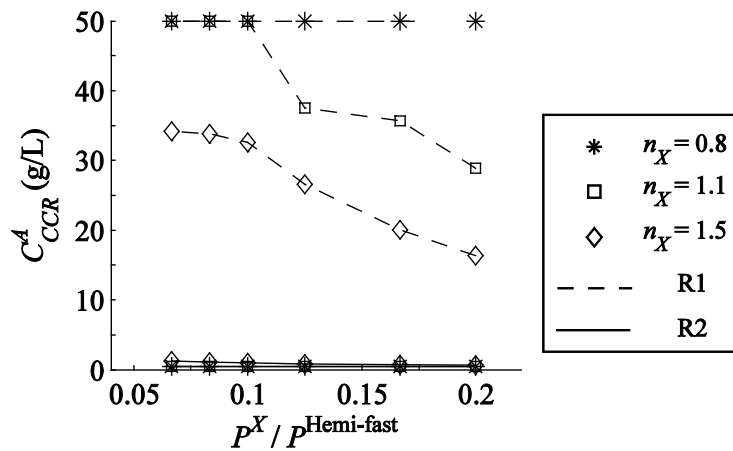
Figure 5.15. Effect of the ratio $P^X / P^{\text{Hemi-fast}}$ and n_X on acid concentration inside R1 and R2 of SPRSS.

5.6.2.2 Effect of the different sensitivities of the sugar production rates to the acid

concentration for different biomass portions

The improvement of SPRSS design over the sequential configuration is more

significant if there is a substantial difference in the sensitivity of sugar formation rate from

different biomass portions to the acid concentration. This is corresponding to a large difference between the values of $n_{\text{Hemi-slow}}$ and $n_{\text{Hemi-fast}}$ in the model in Eq. (5.2) for the reaction paths presented in Figure 5.7b. In this investigation, the parameter $n_{\text{Hemi-slow}}$ is varied while $n_{\text{Hemi-fast}}$, n_X, and the other model parameters from Case 1 are used and fixed.
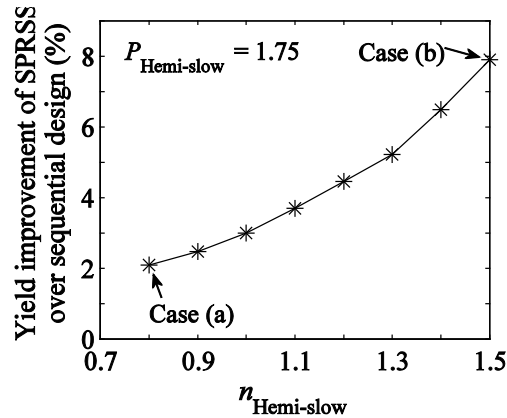
Figure 5.16. Effect of $n_{\text{Hemi-slow}}$ on an improvement of xylose yield of SPRSS over sequential configuration design.

Figure 5.16 shows an improvement of xylose yield of the SPRSS over the sequential configuration design at different values of $n_{\text{Hemi-slow}}$. As can be seen in this figure, the improvement in the yield of the SPRSS is greater at a high value of $n_{\text{Hemi-slow}}$. The reason for this can be explained by a higher degree of conflict in choosing the acid concentration for the two hemicellulose portions in the biomass, as discussed in Section 5.6.1, which is examined more in detail below.

The improvement of the SPRSS over the sequential configuration can be illustrated further by comparing the ratio of the kinetic constant, which is described in Equation 2, between fast-hydrolyzed and slow-hydrolyzed hemicellulose to that of byproduct formation at different acid concentration demonstrated in Figure 5.17. We consider two

cases (see Figure 5.16); Case (a) is for a small difference in the sensitivities of the sugar-forming reaction rates to the acid concentration ($n_{\text{Hemi-fast}} / n_X = 0.45$ and $n_{\text{Hemi-slow}} / n_X = 0.73$), while Case (b) is for a large difference ($n_{\text{Hemi-fast}} / n_X = 0.45$ and $n_{\text{Hemi-slow}} / n_X = 1.36$).
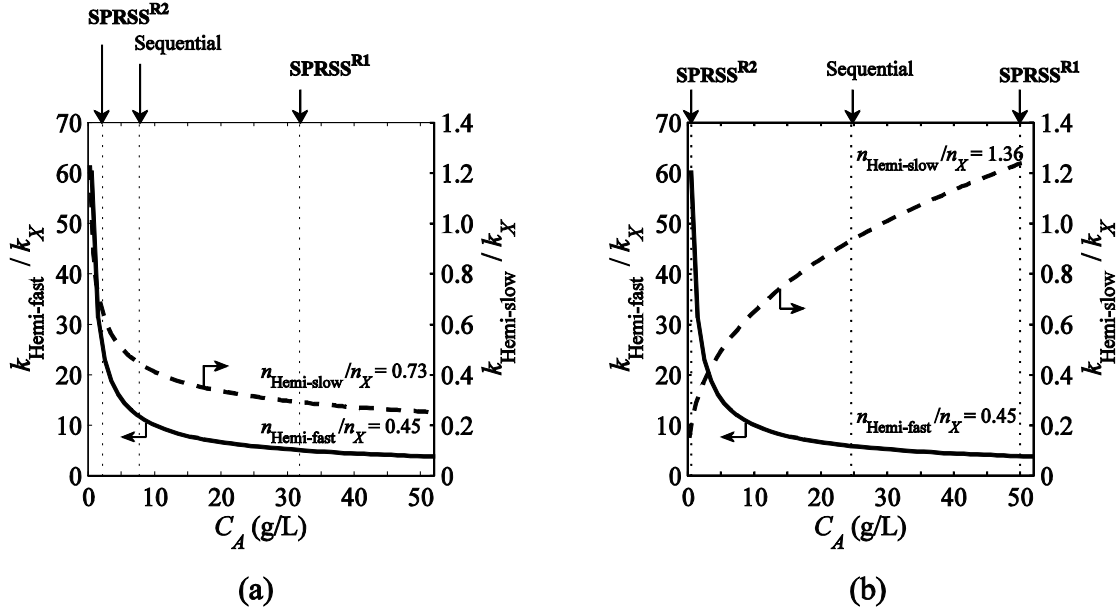
Figure 5.17. The ratio of the kinetic constant between fast-hydrolyzed and slow-hydrolyzed hemicellulose to that of byproduct formation reaction at different acid concentration, $P^{\text{Hemi-fast}} = 35 \text{ h}^{-1}(\%\text{w/v})^{-n}$, $P^{\text{Hemi-slow}} = 1.75 \text{ h}^{-1}(\%\text{w/v})^{-n}$, $P^X = 3.5 \text{ h}^{-1}(\%\text{w/v})^{-n}$, and $n_X = 1.1$, (a) $n_{\text{Hemi-slow}} = 0.8$ (b) $n_{\text{Hemi-slow}} = 1.5$.

Case (a) is illustrated in Figure 5.17a where the difference in the sensitivities of the sugar-forming reaction rates to the acid concentration is small. It can be seen that when the acid concentration increases, both $k_{\text{Hemi-fast}} / k_X$ and $k_{\text{Hemi-slow}} / k_X$ reduce because the values of both $n_{\text{Hemi-fast}} / n_X$ and $n_{\text{Hemi-slow}} / n_X$ are less than one. As the fast and slow hydrolyzed hemicellulose in this case behave quite similarly, the optimal acid concentration between the sequential and SPRSS designs for both R1 and R2 are not significantly different

compared to Case (b). Consequently, the improvement of the sugar's yield of the SPRSS over sequential design is small.

In contrast, Case (b) shown in Figure 5.17b where the difference in the sensitivities of the sugar-forming reaction rates to the acid concentration is large, the two ratios of the reaction rate constants behave differently to the change of acid concentration; the ratio $k_{\text{Hemi-slow}} / k_X$ rises when the acid concentration is increased since $n_{\text{Hemi-slow}} / n_X$ is greater than one, while $k_{\text{Hemi-fast}} / k_X$ decreases. Due to this difference in the behavior of $k_{\text{Hemi-fast}} / k_X$ and $k_{\text{Hemi-slow}} / k_X$, it can be seen that the optimal acid concentrations of SPRSS for R1 and R2 diverge to the two values: one at the maximum value of 50 g/L in R1 to hydrolyze slow biomass portion, and another at the minimum value at 0.5 g/L to hydrolyze fast biomass portion. Such a large difference in the optimal acid concentration of SPRSS between R1 and R2 in Figure 5.17b compared to that in Figure 5.17a indicates that there is a higher degree of conflict in choosing the acid concentration to hydrolyze different biomass composition when increasing the value of $n_{\text{Hemi-slow}}$. From this investigation, it can be concluded that the advantage of SPRSS could be further enhanced when there is a significant difference in the sensitivity of the rates of sugar generation from different biomass compositions to the acid concentration.

There are other biomass properties that could affect the advantage of SPRSS. For instance, the different initial biomass concentration of each portion could substantially affect the rate of sugar generation. Additionally, a real biomass could contain different kinds of biomass with different portions as well as various kinetic parameters, which have more complex reaction paths than those shown in Figure 5.7. The analysis above indicates that the SPRSS design has the potential of achieving a higher yield while suppressing

107

byproduct formations by manipulating the acid concentrations. The justification of the optimal complex design of SPRSS must be more carefully examined.

In this study, we examined SPRSS only in an application of sugar production from biomass. The principle of SPRSS may be applied to other separation problems that involve solid-phase reactants. In particular, if there is a sequential reaction that decomposes the desired product, the SPRSS process may produce the desired product more effectively by selectively separating components.

5.7   Conclusions

A new reactive separation process that handles solid reactants, SPRSS, is proposed. This process combines the PBR and SMB together where both have similar principles of the counter-current movement between the solid and liquid phase, and the process is applied to the saccharification of biomass via acid hydrolysis in this work. The principle of SPRSS may be applied to other reactive separation problems related to solid reactants.

The continuous moving-bed model at steady state for the sequential configuration and the new SPRSS design are optimized and compared using the superstructure formulation to investigate the potential advantages of SPRSS. The optimal designs for two cases are demonstrated where one contains only biphasic hemicellulose and the other contains a mixture of cellulose and biphasic hemicellulose in the biomass. Each component of the biomass has a different rate of decomposition during hydrolysis reaction, and the optimal condition for each reaction path is different.

The results show a potential improvement in the sugar yield as well as lower byproduct formation for both cases using the SPRSS design. The key reason for this improvement is mainly from a higher degree of freedom in changing the liquid flow rate as well as acid concentration inside the reactor system without diluting the sugar concentration. The process enables the fresh biomass to contact a low acid concentration to convert a fast-hydrolyzed biomass portion in the first stage and the treated biomass is treated with a high acid concentration in the second stage to decompose the remaining slower-hydrolyzed biomass portion.

The kinetic parameters of the hydrolysis reactions strongly affect the optimal process configuration design of sugar production. When there is a high byproduct formation rate, as well as a large difference in the kinetic behavior of the sugar generation reactions from different biomass portions, the more complex SPRSS design improves the sugar yield and selectivity.

A potential improvement of the SPRSS design for saccharification via acid hydrolysis has been demonstrated within a dilute acid concentration range. An improvement in sugar yield from acid hydrolysis reaction using this new SPRSS process is expected to increase in the concentrated acid hydrolysis process where the acid concentration play an important role in the reaction kinetics, which is discussed in the next chapter.

CHAPTER 6

APPLICATION OF SOLID-PHASE REACTIVE

CHROMATOGRAPHIC SEPARATION SYSTEM FOR BIOMASS

SACCHARIFICATION VIA CONCENTRATED ACID HYDROLYSIS

6.1   Motivation

The solid phase reactive separation system (SRPSS) for biomass saccharification is proposed in the previous chapter where the kinetic parameters in the dilute-acid-hydrolysis region is explored. The benefits of SPRSS comes from the variation in acid concentration inside the reactor system without any dilution or interfering the sugar concentration. The benefits of the SPRSS is expected to be higher for the concentrated acid hydrolysis process where the acid concentration plays an important role in the reaction kinetics.

Due to the different and complex composition of the biomass, there is a high uncertainty in the kinetic parameters of the hydrolysis reactions. The previous chapter explored the effect of these kinetic parameters to the benefits of the SPRSS over the sequential design. It was found that the rate of byproduct formation must be sufficiently fast and more sensitive to the acid concentration compared to the sugar generation to see the benefits of SPRSS. In addition, a higher difference in sensitivities of the rate of sugar production to the acid concentration from the different biomass composition could increase the benefits of SPRSS. These observation can be used to preliminary investigate the benefits of SPRSS for different biomass with different hydrolysis kinetic parameters.

In this chapter, the benefit of SPRSS is investigated for the concentrated acid hydrolysis process where the real kinetic parameters from the batch experiment presented in Chapter 4 is used with the simplified continuous model of SPRSS including countercurrent reactor (CCR) and true moving bed chromatography (TMB) discussed in Chapter 5. The optimization problem formulation follows the same method as presented in previous chapter where two alternative designs including the sequential and SPRSS are compared.

This chapter is organized as follow: section 6.2 presents the investigation on the kinetic parameters of the concentrated acid hydrolysis reaction for the potential benefits of the SPRSS process. The model parameters for the optimization problem is shown in section 6.3 and the comparison between the optimal results two alternative designs are presented in section 6.4.

6.2 Analysis of the kinetics parameters of the concentrated acid hydrolysis

The kinetic parameters for the concentrated acid hydrolysis of the xylose (C5) reaction paths and glucose (C6) reaction paths estimated from the experimental work in Chapter 4 are summarized in Table 6.1 where the reaction mechanism is shown in Figure 4.1 with the Arrhenius expression as follows.

$$k = k_0 \left(C^A \right)^n e^{-\left(\frac{E_a}{\Gamma T} \right)} \tag{5.1}$$

These parameters are applicable for the range of sulphuric acid concentration between 10wt% (around 100g/L) and 50wt% (around 700 g/L) and temperature between

111

80 – 100 °C. From the table, it can be seen that the xylose decomposition reaction is more sensitive to the acid concentration with the exponent $n = 2.88$ compared to the xylan hydrolysis reaction where $n = 1.96$. In contrast, the sensitiveness of the rate of glucose decomposition and Avicel hydrolysis to the acid concentration is quite similar where $n = 2.94$ and 3.00, respectively. These kinetics parameters satisfies the condition shown in Eq. (5.46) which enables the benefits of changing the acid concentration. Furthermore, the kinetic behaviour of the xylan and Avicel hydrolysis is very different where Avicel is more sensitive to the acid concentration ($n_{cel} > n_{xylan}$) but the pre-exponent of the rate constant (see Eq. (5.2) and Table 6.1) is around 10^5 times lower than that of xylan hydrolysis. These observation can preliminary justify that the SPRSS design can be favourable over the sequential design.

Table 6.1. Kinetic parameters of concentrated acid hydrolysis reaction.

Reactions	k_0 (min^{-1}(%w/v)$^{-n}$)	n	E_a (kJ/mol)
Xylan hydrolysis	1.42×10^{17}	1.96	142.52
Xylose decomposition	3.15×10^{14}	2.88	151.30
Avicel hydrolysis	2.96×10^{10}	2.94	129.98
Glucose decomposition	1.76×10^{10}	3.00	127.32
Temperature (°C)	80	90	100
Xylan pre-exponent (min^{-1}(%w/v)$^{-n}$)	1.18×10^{-4}	4.49×10^{-4}	1.59×10^{-3}
Avicel pre-exponent(min^{-1}(%w/v)$^{-n}$)	1.76×10^{-9}	5.95×10^{-9}	1.89×10^{-8}

6.3   Model parameters

The column CS16GC[18, 24] is used in TMB system where the Henry's coefficient is varied at different sulfuric acid concentration. In this work, the sulfuric acid concentration is set to vary between 10 wt% and 50 wt%. Therefore, the Henry's coefficients are estimated at the average sulfuric concentration of 30 wt%. The Henry's coefficients and mass transfer resistance are estimated and summarized in Table 6.2.

Table 6.2. Henry's law and mass transfer coefficients for adsorption column

Components	Linear Henry's law constant	Mass transfer coefficient (s^{-1})
Sulfuric acid	0.23	0.02
Glucose	0.36	0.03
Xylose	0.42	0.03
HMF	3.00	0.15
Furfural	3.13	0.15

The optimization problem is simplified to be a single-objective optimization problem with three main assumptions as presented in section 5.4. It is found that the constraints on the optimization problem significantly affect the benefits of the SPRSS. This investigation additionally assume that the size of the CCR is fixed for both length and diameter so that the capital cost of the reactor system is fixed. The single-objective optimization problem considered in this study is shown in Table 6.3. It should be noted that the selectivity constraint (constraint 3 in Table 5.5) is ignored and replaced with the constraint on the furfural concentration (decomposed product of xylose) of the extract sugar product stream. The design and model parameters are shown in Table 6.4 and the decision variables are presented in Table 6.5.

Table 6.3. Optimization problem formulation

max Y_{SPRSS}^S	Yield of sugars
Subject to:	
1. $C^S \geq C_{min}^S$	minimum sugar concentration (g/L)
2. $M^B \geq M_{min}^B$	minimum biomass throughput (kg/h)
3. $C^{Furfural} \leq C_{max}^{Furfural}$	maximum furfural concentration (g/L)
4. $D_{TMB} \leq D_{TMB\,max}$	maximum TMB column diameter (m)
5. $F^A \leq F_{max}^A$	maximum fresh acid consumption (kg/h)
6. $PUR^A \leq PUR_{max}^A$	maximum purity of acid in extract
7. $u_{TMB} \leq u_{TMB,max}$	maximum flow rate in TMB (m/h)
8. $u_{CCR} \leq u_{CCR,max}$	maximum flow rate in CCR (m/h)

Table 6.4. Design and model parameters

M_B^{min}	1000 kg/h
F_{max}^A	400 kg/h
C_{min}^S	80 g/L
PUR_{max}^A	1 wt%
$C_{max}^{furfural}$	0.1 g/L
B_0^{Hemi}	48 kg/m³
B_0^{Cel}	64 kg/m³
Reactor diameter	1.5 m
Total Reactor length	20 m
SPRSS Reactor section length	Section 1 = 15 m Section 2 = 5 m
Number of reactors	2
TMB column length	1 m
Number of TMB columns	12
$D_{TMB\,max}$	3 m
$u_{CCR,max}, u_{TMB,max}$	10 m/h
Fresh acid concentration	900 g/L
biomass void fraction (b_v)	0.8
Reaction temperature	90 °C
Range of acid concentration	100 – 700 g/L

Table 6.5. Decision variables

Acid and water feed rates to each of two reactors, u_A, u_W
Two outlet flow rates from each of the two reactors and its feed location to TMB, u_{FT}
Two recycle flow rates to each of the two reactors and its location from TMB, u_{RET}
One extract stream flow rate and its location in TMB, u_E
One desorbent stream flow rate at the first TMB column, u_D
One raffinate stream flow rate and its location in TMB, u_R
Adsorbent velocity, v_{TMB}

6.4   Optimal designs of the SPRSS for concentrated acid hydrolysis process

Figure 6.1 illustrates the CCR and TMB profile from the optimal results of the sequential configuration. From the result, the acid concentration is chosen to be relatively low at 210.4 g/L which could hydrolyze all hemicellulose portion. However, the cellulose portion is unable to convert at this low acid concentration. This is because the optimizer avoids the formation of the byproduct to meet the constraint on the furfural concentration (constraint 3 in Table 6.3), and therefore choose not to have high acid concentration and convert only the easily hydrolyzed hemicellulose. It can be seen from Figure 6.1a that the conversion of hemicellulose occurs only around one-fourth of the total reactor length. This indicates that the reactor system with this fixed size is not optimal for this sequential configuration.

Figure 6.2 shows the CCR and TMB profile from the optimal results of the SPRSS design. From the figure, it can be seen that the optimizer choose to have two acid concentration where one is at its maximum at 700 g/L in section 1 and the other one is at its almost minimum at 102.7 g/L in section 2. This variation in the acid concentration is enabled by the interconnecting stream between CCR and TMB. The high acid

concentration in section 1 is able to convert the cellulose around 25 % which occurs for three-fourth of the total reactor length. On the other hand, hemicellulose is mainly converted in section 2 with a lower acid concentration where the reaction happens for one-fourth of the total reactor length. This is to avoid the byproduct formation to meet the constraint on the furfural concentration. It can be seen from Figure 6.2a that the reactor with this size is fully utilized to convert two portions of the biomass.

Table 6.6 compares optimal results between the sequential and SRPSS design. It can be seen that the SPRSS could improve the sugar yield by around 7.7 % from the sequential design while maintaining the same concentration of furfural at 0.1 g/L. The optimal acid purity in the product extract stream of the sequential design is chosen to be lower than that of the SPRSS design. Both configurations have the acid purging stream through the raffinate stream where the acid concentration is relatively low: 33.2 g/L in sequential design and 61.9 g/L in SPRSS design. The acid in the raffinate stream can be concentrated by evaporation and recycled to the reactor system. A slightly higher acid concentration in the purging raffinate stream in SPRSS design could reduce the evaporation cost of the acid compared to the sequential design. It should be noted that there is no constraint on the byproduct of glucose (HMF) on the extract sugar product stream from this optimization problem. Therefore, the SPRSS produces more HMF at around 5 g/L in the product stream compared to the sequential designs which has almost no byproduct from glucose since there is almost no cellulose conversion.

It is found that the benefits of the SPRSS is significantly sensitive to these constraints. Table 6.7 shows the sensitivity of two constraints including the furfural concentration at the product stream and the fresh acid consumption. From the table,

increase the maximum allowable furfural concentration increases the sugar yield of the sequential design. However, this constraint is not active for the SPRSS design and therefore the sugar yield and the furfural concentration remain the same. Moreover, tightening the constraint on fresh acid consumption reduce the sugar yield of the sequential slightly but significantly decrease the yield from the SPRSS design. There are some other parameters such as the initial biomass concentration and the reactor length that could also affect the benefit of SPRSS. The justification on choosing the optimal design between the SPRSS and sequential design must be performed carefully.

Table 6.6. Comparison of sequential and SPRSS optimal configuration

Parameters	Sequential configuration	SPRSS configuration
Y^S	43.3 % $Y^G = 1.0$ % $Y^X = 99.5$ %	51.0 % $Y^G = 14.4$ % $Y^X = 99.7$ %
C^{HMF}	0.01 g/L	5.0 g/L
Acid concentration in raffinate	33.2 g/L	61.9 g/L
PUR^A	0.07 %	1 %
$C^{Furfural}$	0.1 g/L	
C^S	80 g/L	
M^B	1000 kg/h	
D_{TMB}	3 m	
F^A	400 kg/h	

Table 6.7. Sensitivity of the model constraints

Constraints	Y^S	
	Sequential design	SRPSS design
$C_{max}^{furfural}$		
0.1 g/L	43.3 %	51.0 %
0.3 g/L	45.9 %	51.1 % (inactive)
0.5 g/L	46.7 %	51.1 % (inactive)
F_{max}^A		
400 kg/h	43.3 %	51.0 %
200 kg/h	43.1 %	47.7 %
50 kg/h	42.9 %	43.2 %
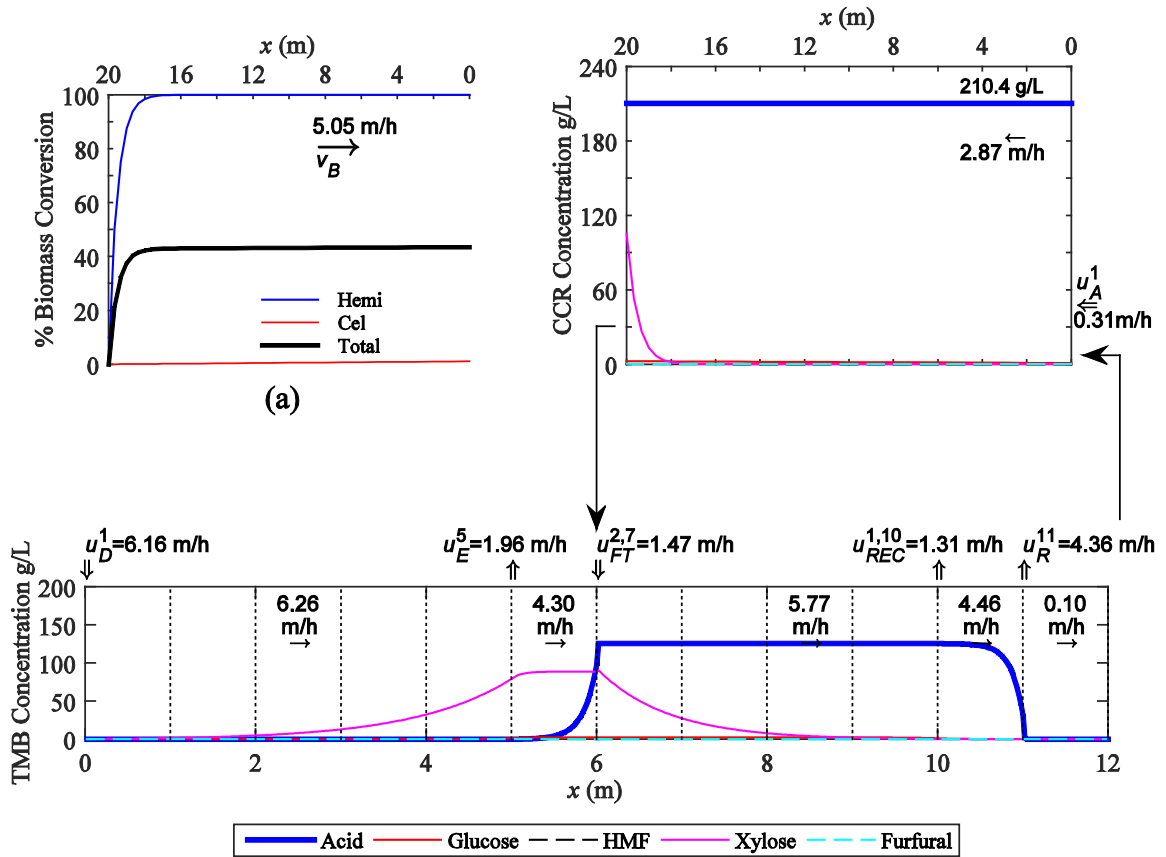
Figure 6.1. Optimal solution of the sequential design (a) biomass conversion of different portions, (b) CCR and TMB concentration profiles.
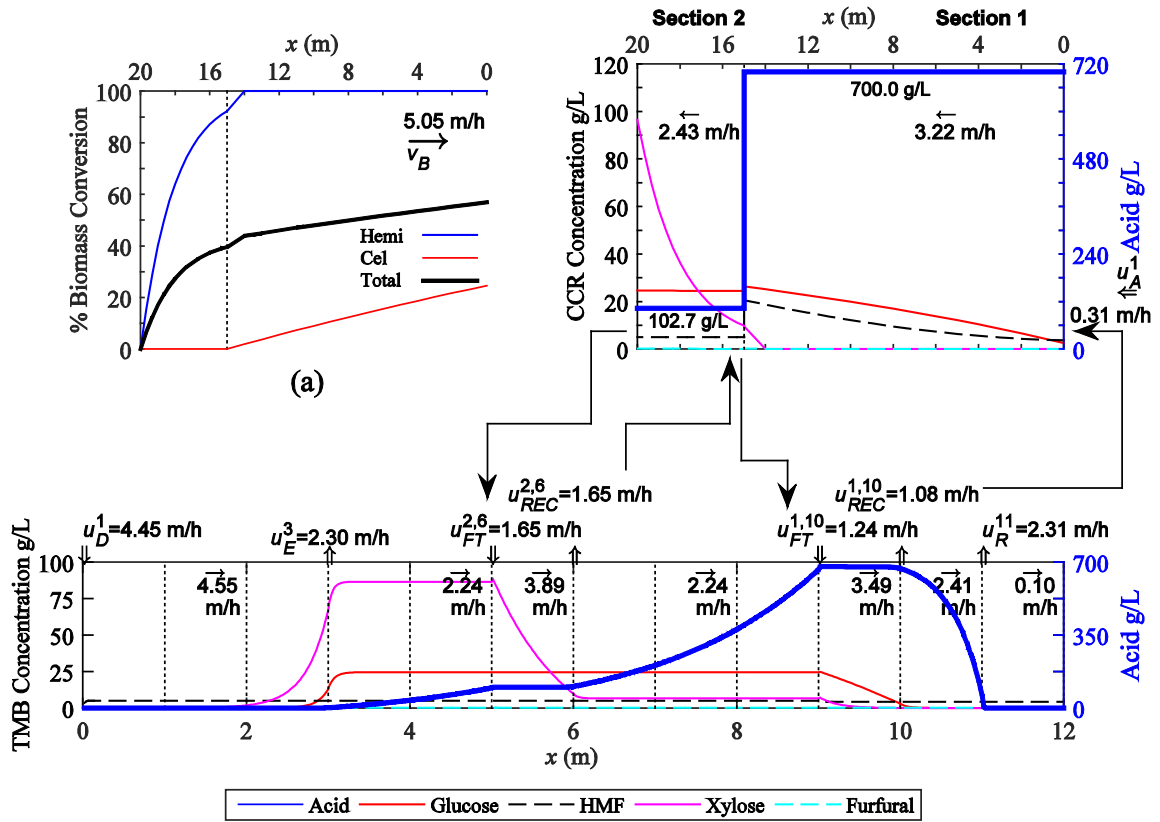
Figure 6.2. Optimal solution of the SPRSS design (a) biomass conversion of different portions, (b) CCR and TMB concentration profiles.

6.5   Conclusions

The benefits of the SPRSS is investigated for the biomass saccharification via concentrated acid hydrolysis. It is found that kinetic parameters of the biomass saccharification via concentrated acid hydrolysis are in the range where using the SPRSS design to vary the acid concentration in the reactor system could be advantageous on an improvement in sugar yield as well as the reduction of the byproduct formation.

Two alternative designs including the sequential and SPRSS designs are optimized and compared using the continuous moving-bed model of the countercurrent reactor and the true-moving-bed chromatography at steady state with the superstructure formulation. With appropriate constraints, it is observed that the SPRSS could increase the sugar yield by allowing the high acid concentration to hydrolyze the slow-hydrolyzed cellulose part and the low acid concentration to hydrolyze the fast-hydrolyzed hemicellulose part. In contrast, the sequential design can only hydrolyze the hemicellulose part with a single acid concentration due to the constraint on the byproduct formation. The results reveal that SPRSS could maintain the same level of byproduct formation from the xylose decomposition reaction and the same amount of fresh acid consumption compared to the sequential design. In addition, the concentration of the acid in the purging raffinate stream from TMB of the SPRSS design is higher than that of the sequential design which could reduce the cost of acid recycle through evaporation. Sensitivity analysis on the model constraints reveals that the benefits of SPRSS could change significantly at different values of the model constraints. Therefore, choosing the optimal design for biomass saccharifcation via acid hydrolysis must be carefully justified.

CHAPTER 7

DYNAMIC MODELLING OF THE PROGRESSING BATCH REACTOR IN SOLID-PHASE REACTIVE CHROMATOGRAPHIC SEPARATION SYSTEM FOR BIOMASS SACCHARIFICATION VIA ACID HYDROLYSIS

7.1   Motivation

The solid-phase reactive chromatographic separation system (SPRSS) has been proposed as a new reactive separation process for the system involving the solid reactants. This process integrates the progressing batch reactor (PBR) and simulated moving bed chromatography (SMB) where both processes have similar principles of the switching of all liquid inlet and outlet ports to imitate the solid phase movement. This work has applied the new SPRSS to the biomass saccharification process via acid hydrolysis. The ultimate goal is to seek an opportunity to increase the sugar yield as well as to minimize the byproduct formation generated from the sugar decomposition such as furfural and hydroxymethylfurfural (HMF) which are the main inhibitors for the fermentation process for bioethanol production.[17]

In the previous chapter, the advantages of the SPRSS has been investigated using the simplified model for sugar production where the countercurrent reactor (CCR) and the true-moving bed chromatography (TMB) are used as the approximation of the PBR and SMB system. The benefit of SPRSS is compared with the sequential design which connects the CCR and TMB in a straightforward manner without any interconnecting stream. It has

been found that the SPRSS can potentially increase the sugar yield and reduce byproduct formation where the key benefit comes from the higher flexibility to vary the acid concentration as well as the liquid flow rate inside the reactor system without interfering high sugar concentration enabled by the chromatographic separation system. These advantages allow the acid with different concentration to hydrolyze different compositions of biomass which has different hydrolysis reaction kinetics.[92]

This chapter presents dynamic modelling of the PBR system as part of the PBR-SMB process for two designs including the sequential design and SPRSS design. The dynamic models of the SMB chromatography have been developed and validated with numerous operating schemes such as VARICOL, POWERFEED[147], and ternary separation configurations.[148] A good approximation of the concentration profile between the SMB and true moving bed model have been previously demonstrated.[149] In contrast, dynamic modelling of the PBR operation is not well-established. Several steps in cyclic operations for PBR such as emptying and loading the solid biomass require several assumptions that need to be carefully analyzed as these steps are not captured in the steady state countercurrent reactor model. In this work, the biomass filling and dumping operation for the two alternative designs are proposed where the operating parameters from the steady state countercurrent reactor model are used to estimate that of PBR. The simulation results from the PBR model is compared with that from the CCR.

This chapter is organized as follows. The dynamic modelling of PBR as well as the proposed filling and emptying step of biomass are presented in section 7.2. The PBR simulation problem formulation is discussed in section 7.3 and the simulation results of the PBR model in a comparison of CCR is discussed in section 7.4.

7.2   Progressing batch reactor

The operation of PBR proposed by Wright et al.[111] has been discussed in previous chapter and are re-illustrated in Figure 7.1. From the figure, each step of the PBR operation follows the same pattern where the acid feeding stream are switched in the direction of the liquid flow. Likewise, the reaction temperature are switched to hydrolyse different composition of the biomass where a high temperature are applied to hydrolyse cellulose and low temperature are applied to hydrolyse hemicellulose. The operation in each step proceed similarly, and thus the operation becomes a cycle which is similar to the SMB process.

Despite these similarities, the operation of the solid biomass in PBR requires the filling and emptying process, and cannot be recycled like the adsorbent in the SMB process. From the PBR operation in Figure 7.1, the liquid inside the reactor E for all steps are dumped, and thus the sugars as well as acid are left out of the reactor system. Therefore, the sugar concentration in the product stream and the sugar recovery reduces. In addition to this, during the biomass filling step in reactor F, an assumption must be made for the initial condition whether there is a liquid acid or nothing inside the reactor filled with the fresh biomass. These steps are not present in the SMB chromatography operation and requires unique mathematical modelling as well as assumptions to model the PBR system. This work proposes the filling and emptying of the biomass for both sequential and SPRSS designs which could partially recover the sugars and acid to the reactor system. The detailed discussion of these are given in the following section.
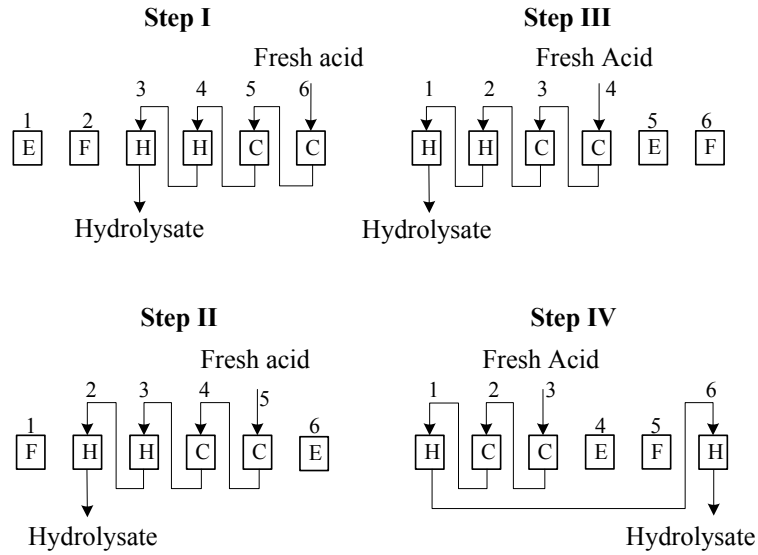
Figure 7.1. Operation of the progressing batch reactor (F = biomass filling, E = biomass emptying, C = cellulose hydrolysis, H = hemicellulose hydrolysis).

7.2.1 Dynamic model of progressing batch reactor

In this chapter, the biomass is assumed to contain both cellulose and hemicellulose where the reaction mechanism follows the same pattern presented in Figure 5.6. The two consecutive first-order reactions is applied for cellulose hydrolysis and the biphasic behaviour is assumed for the hemicellulose hydrolysis. The kinetic model proposed by Saeman[101] is implemented for all reaction paths which depends on temperature and acid concentration shown in Eq.(5.1).

The mathematical model of a single percolation reactor has been present by Kim et al.[110] In this work, the PBR contain a series of percolation reactors where the mass balances of each component in the solid and liquid phases shown in Eq. (7.1) - (7.4) are applied.

124

$$\frac{\partial B^{k,i}(x,t)}{\partial t} = -k^B B^{k,i}(x,t) \quad k = \text{fast, slow} \tag{6.1}$$

$$\frac{\partial C^{A,i}(x,t)}{\partial t} + u_{PBR}\frac{\partial C^{A,i}(x,t)}{\partial x} = D_{ax}\frac{\partial^2 C^{A,i}(x,t)}{\partial x^2} \tag{6.2}$$

$$\frac{\partial C^{S,i}(x,t)}{\partial t} + u_{PBR}\frac{\partial C^{S,i}(x,t)}{\partial x} = D_{ax}\frac{\partial^2 C^{S,i}(x,t)}{\partial x^2} + \frac{1}{b_v}\sum_k k^{B_k} B^{k,i}(x,t) - k^S C^{S,i}(x,t)$$
$$\tag{6.3}$$

$$\frac{\partial C^{B,i}(x,t)}{\partial t} + u_{PBR}\frac{\partial C^{B,i}(x,t)}{\partial x} = D_{ax}\frac{\partial^2 C^{B,i}(x,t)}{\partial x^2} + k^S C^{S,i}(x,t) \tag{6.4}$$

where u_{PBR} is the liquid flow rate in the PBR, $B^{k,i}, C^{A,i}\ C^{S,i}$, and $C^{B,i}$ are the concentrations of solid biomass of the fast and slow hydrolysed portions, acid, sugar, and byproducts at reactor i, respectively, b_v is the biomass porosity, and u_{PBR} is the liquid interstitial velocity. This model also considers the axial dispersion in the liquid phase with Danckwerts boundary conditions[149] shown below.

$$\left[uC - D_{ax}\frac{\partial C}{\partial x}\right]_0 = uC_0 \tag{6.5}$$

$$\left.\frac{\partial C}{\partial x}\right|_0 = 0 \tag{6.6}$$

In this work, an identical operation in each step is repeated while performing the liquid port switching in the downstream direction, resulting in a cyclic steady state (CSS) and symmetric operation. In such an operation, the concentration profiles at the end of each step are identical to those at the beginning of the same step where the entire profiles are shifted in the downstream direction for the length of a one reactor chamber, which is similar to the cyclic operation with step symmetric in SMB process.[146] The following constraints

are enforced to ensure that the concentration profiles of liquid phase in PBR at the end of the next step is identical to those at the beginning of the current step.

$$C^{j,i}(x,0) = C^{j,i+1}(x,t_{step}^{SMB}) \quad i = 1,...,N-1 \tag{6.7}$$

$$C^{j,N}(x,0) = 0 \tag{6.8}$$

$$B^{k,i}(x,0) = B^{k,i+1}(x,t_{step}^{SMB}) \quad i = 1,...,N-1 \tag{6.9}$$

$$B^{k,N}(x,0) = B_0^{k,N} \tag{6.10}$$

The liquid concentration of component j in Reactor i is denoted by $C^{j,i}$. In the PBR system with N reactor chambers, we assume that the fresh biomass is loaded in Reactor N at a given initial biomass concentration, Eq. (7.10), and is filled with fresh water, and thus the initial liquid concentration of all components are zero as shown in Eq. (7.8).

7.2.2 Biomass filling and emptying

Two optimal designs including the sequential and SPRSS designs from the case 2 presented in Chapter 5 are generalized to the PBR and SMB and shown in Figure 7.2a and Figure 7.2b, respectively. Both designs from the figures consist of five PBRs and twelve SMB columns where it is assumed that the system has small buffer tanks to connect all streams between these two processes and no reaction occurs in this tank due to the sufficiently small residence time. These tanks are to ensure that the component concentration of the feed streams from the PBR to SMB and that of the recycle streams from the SMB to PBR are constant.
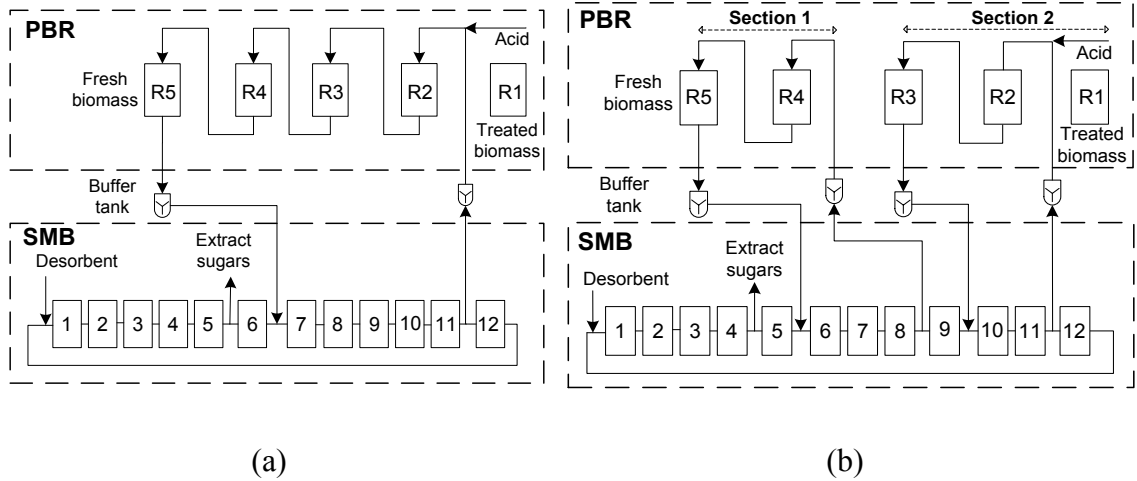
Figure 7.2. Optimal configurations found from the superstructure of SPRSS continuous model (a) Sequential design (b) SPRSS design.
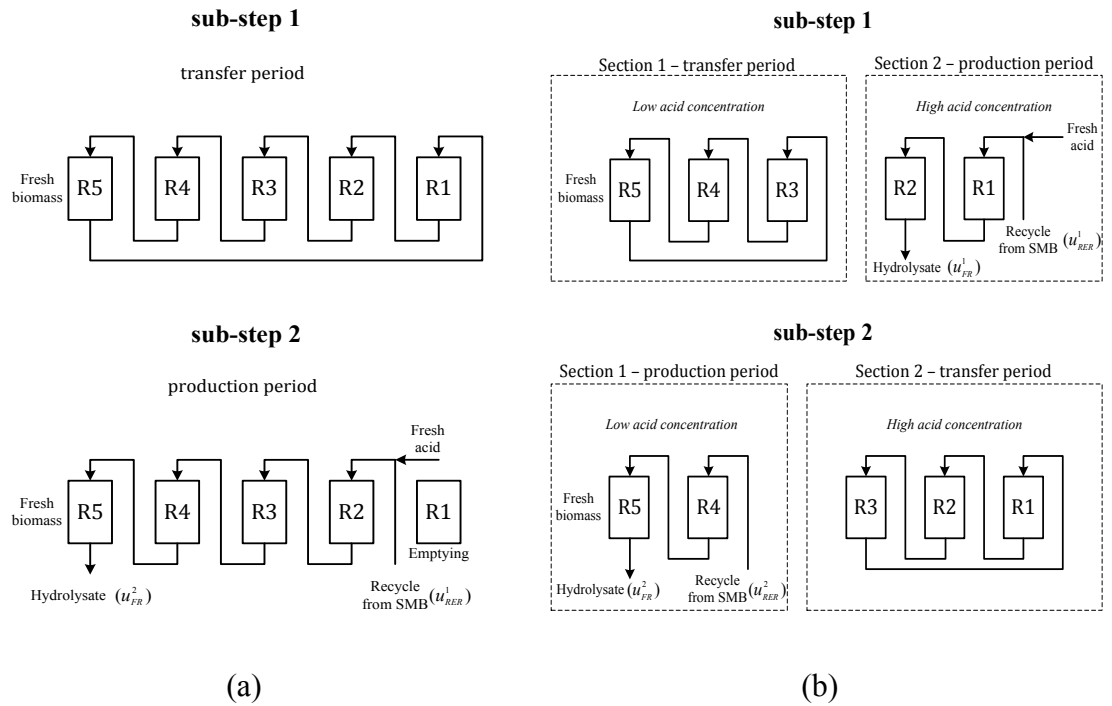
Figure 7.3. Progressing batch reactor with proposed filling and emptying steps as part of the (a) sequential design (b) SPRSS design.

The operations of the biomass filling and emptying steps could significantly affect the sugar concentration and yield from the hydrolysis reaction. In this study, we include the biomass filling and empting step by dividing the PBR operation in each step into two sub-steps consisting of the production period (t_{prod}) and the transfer period (t_{tran}) which are illustrated in Figure 7.3 for both sequential and SPRSS designs for $N = 5$. The PBR in the sequential design (Figure 7.3a) has the same liquid residence time inside all reactors since there is no interconnecting stream. On the other hand, for the PBR in the SPRSS design illustrated in Figure 7.3b, the process is divided into two sections which have two and three percolation reactors. By having the interconnecting streams between PBR and SMB, the reactor system can have different liquid residence time as well as acid concentration in each section. At the beginning of a step in these two designs, the fresh biomass is filled in R5, which is filled with fresh water while the treated biomass stays inside R1.

The first sub-step of the PBR operation in the sequential design illustrated in Figure 7.3a corresponds to the transfer period where the acid in R4 flows to hydrolyze the fresh biomass in R5, while the water in R5 goes to R1 which contains the treated biomass. The second sub-step corresponds to the production period where the external fresh acid and the recycle stream from SMB is fed to R2 and the hydrolysate is produced at R5. The treated biomass filled with water inside R1 is also dumped at this step.

For the PBR system in the SPRSS design which has two sections shown in Figure 7.3b, the transfer and production periods occur simultaneously at different sections. In the first sub-step, the transfer process occurs in section 1 (R3-R4-R5) while production process happens in section 2 (R1-R2). In section 1, the liquid with low acid concentration is

transferred to hydrolyze the fresh biomass in R5 while the water in R5 goes to the R3. Meanwhile, in section 2, the liquid with higher acid concentration from the fresh acid stream and the recycle stream from SMB are fed to R1 to hydrolyze the treated biomass and the hydrolysate is produced at R2. In the second sub-step, the transfer process is switched to occur in section 2 (R1-R2-R3), while the production process takes place in section 1 (R4-R5). In section 1, the recycle stream from SMB is fed to R4 and the hydrolysate is produced at R5. For section 2, the water in R3 is moved to the R1 before being dumped with the treated biomass. It can be seen that a different number of reactor chamber is allocated in each section. In this operation, the hydrolysis condition of the partially treated biomass in R3 is switched from a low to a high acid concentration and is exposed to a different liquid residence time.

In this proposed filling and dumping the biomass, the operating parameters from the steady state countercurrent reactor model including the liquid interstitial velocity (u_{CCR}) and the biomass interstitial velocity (v_b) can be directly converted to the operating parameters of PBR including the overall switching time (t_{step}^{PBR}), transfer period (t_{tran}), production period t_{prod}, and the interstitial velocity of liquid phase (u_{PBR}) from the following equations:

$$L_R = \frac{\text{Total TMB reactor length}}{(N_R - 1)} \tag{6.11}$$

$$t_{step}^{PBR} = \frac{L_R}{v_b} \tag{6.12}$$

$$u_{PBR} = u_{CCR} + v_b \tag{6.13}$$

$$t_{prod} u_{PBR} = t_{step}^{PBR} u_{CCR} \tag{6.14}$$

$$t_{tran} + t_{prod} = t_{step}^{PBR} \qquad (6.15)$$

The proposed emptying and filling steps require one additional percolation reactor to the PBR system because there is no hydrolysate produced during the transfer period, and so Eq. (7.11) must be applied. Eq. (7.14) is to ensure the average outlet stream from the reactor system between PBR and CCR are equivalent. It should be noted that in the two sub-step process where Eq. (7.15) is applied, the following constraint are required for the CCR model in order to convert CCR parameters into those for PBR

$$v_b = \sqrt{u_{CCR}^1 u_{CCR}^2} \qquad (6.16)$$

where u_{CCR}^1 and u_{CCR}^2 are the liquid velocity inside CCR in section 1 and section 2, respectively.

7.3   Problem formulation and numerical approaches

The dynamic models of the PBR with the biomass filling and emptying sub-step for both designs are formulated in the GAMS modeling environment discretizing the time domain with six finite elements by the Radau collocation, and spatial domain with 60 elements by the centered finite difference method. The simulation problems of these two designs are solved where the flow rates and the concentration of all feed streams including the fresh acid and the recycle streams from SMB are fixed at the values in the optimal solutions obtained from the steady state countercurrent reactor and true moving bed chromatography model.

7.4   Results and discussion

The reactor length, the switching time, and the time period of the PBR for the transfer and production period are estimated from CCR using Eq. (7.11) – Eq. (7.15) and the values are shown in Table 7.1. The optimal concentration and flow rate of the inlet and outlet streams of the continuous CCR model as part of the sequential and SPRSS design are presented in Table 7.2 and Figure 7.4, respectively. These results are achieved from the optimization problem discussed in Case 2 of the section 5.5.1 where where the axial dispersion coefficient D_{ax} is set to 1.4×10^{-4} m^2/s for all components. In addition, the constraint in Eq. (7.16) is also applied for the SPRSS design. The concentration and flow rate of these recycle streams and the feed streams to the PBR system for both designs are fixed at the optimal values from the CCR.

Table 7.1. PBR parameters

Parameters	Sequential design	SPRSS design
Number of Reactor	5	
The length of each reactor (m)	1.25	
Switching time (s)	706.85	
Transfer period	362.23	344.04 (section 2)
Production period	344.63	362.81 (section 2)

Table 7.2. Concentration of each streams

Configuration	Stream	Concentration (g/L)				
		Acid	Glucose	HMF	Xylose	Furfural
CCR Sequential	u_{RER}^1	5.03	13.70	5.30	0.89	24.25
	u_{FR}^2	5.03	41.49	10.08	49.61	45.12
PBR Sequential	u_{FR}^2	4.04	38.31	7.77	48.97	36.65
CCR SPRSS	u_{RER}^1	20.27	5.86	7.68	0.33	19.97
	u_{FR}^1	20.38	30.68	15.31	9.96	33.69
	u_{RER}^2	2.22	34.68	8.63	9.40	21.18
	u_{FR}^2	2.22	45.37	10.73	48.18	31.13
PBR SPRSS	u_{FR}^1	17.29	28.42	9.88	9.62	25.21
	u_{FR}^2	1.83	42.25	9.62	46.01	26.86
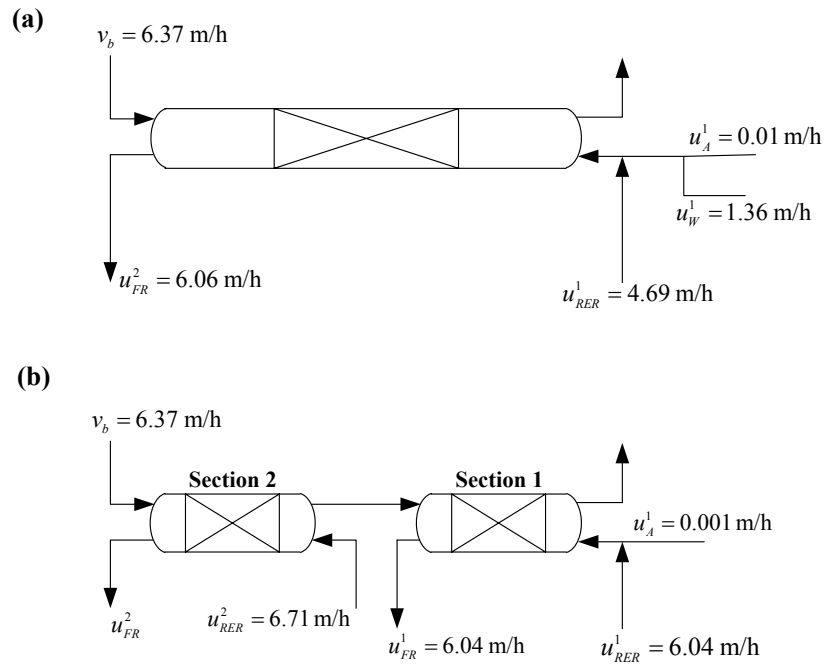
Figure 7.4. Optimal countercurrent reactor as part of (a) sequential design (b) SPRSS design.

The concentrations of the outlets of all interconnecting streams of the PBR and SMB from the simulation results is shown in Table 7.2. By comparing the concentration of the similar stream from CCR, it can be seen that the concentration of all components reduce slightly from the CCR model for both designs. This is mainly because a small amount of these components remains inside the treated biomass and are lost during the biomass emptying step. This phenomenon is illustrated in Figure 7.5 which shows the concentration profile of the liquid phase for SPRSS design at the $t = t_{step}^{PBR}$ before emptying the biomass in R1. From the figure, it can be seen that there are some amount of sugars, acid, and other components remaining inside R1 which are lost when emptying the biomass. Our investigation shows that these losses are caused by the axial dispersion. During the transfer periods of SPRSS (see Figure 7.3b) where the fresh water is transferred from R5 to R3 in sub-step 1 and then from R3 to R1 in sub-step 2, all components diffuse into this portion of water. Consequently, the loss of these components during dumping the treated biomass with the liquid in R1 is inevitable. This phenomenon is not captured in the CCR model.
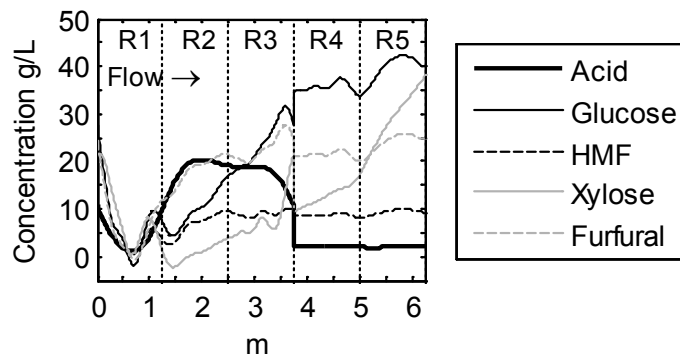
Figure 7.5. PBR concentration profile in the SPRSS design at $t = t_{swt}$ before biomass emptying.

The comparison of the reactor performance in the sequential and SPRSS designs between the CCR and PBR are shown in and Table 7.3. From the table, the conversion of the biomass in both designs between the CCR and PBR are very close to each other. However, the sugar yield at the outlets of the PBR is lower than that from the CCR due to the sugar lost during the biomass emptying step. The sugar and acid lost are calculated based on the percentage of the outlet stream shown below.

$$\% \text{ Lost} = \frac{\text{component mass lost}}{\text{outlet mass (at } u_{FR}) + \text{component mass lost}} \times 100 \qquad (6.17)$$

From Table 7.3, the sugar lost is at 9.7 % for the sequential design and 11.0 % for the SPRSS design while the acid lost for both designs are almost similar at around 19%.

The sugar lost during biomass emptying can be recovered later by the SMB system or another separation process. By assuming these sugars can be fully recovered, the total reaction sugar yield shown in Table 7.3 for both designs are higher than that predicted from the CCR. The reason for this is that there is a dynamic variation in acid concentration resulting from the axial dispersion in PBR which causes different reaction kinetics compared to that in CCR. From the results, the byproduct formation in PBR is observed to be lower than that in CCR. The performance of PBR with the proposed biomass filling and emptying steps can be partially predicted using the CCR model with sufficient accuracy.

It should be noted that the overall performance of the dynamic SPRSS model with these PBR designs may be significantly different from the continuous model. Due to components lost in emptying steps which causes the lower sugar and acid concentration at the outlet stream of the PBR, the feed concentration to the SMB is different from the

134

continuous model. Therefore, the optimal operating parameters of the SMB is different from the TMB model. In addition, this causes the acid concentration as well as other components and the flow rate of the recycle stream from SMB to PBR be different from the continuous model which finally affect the reaction kinetics inside the PBR system. Due to the acid lost during biomass emptying step, it is believed that the fresh acid consumption for the dynamic SPRSS model is higher than what is predicted from the continuous model. Therefore, the optimal design of the dynamic SPRSS model may be significantly different from the continuous SPRSS model.

Table 7.3. Performance comparisons between CCR and PBR

	Sequential Design		SPRSS Design	
	Countercurrent	PBR	Countercurrent	PBR
Biomass conversion	85.3 %	84.1 %	94.3 %	94.2 %
Sugar yield at outlet	60.7 %	57.8 %	67.9 %	61.5 %
Sugar lost in emptying step	-	9.7 %	-	11.0 %
Acid lost in emptying step	-	19.5 %	-	19.0 %
Total reaction sugar yield	60.7 %	64.9 %	67.9 %	74.3 %

7.5   Conclusions

Dynamic models of PBR in SPRSS are formulated and the biomass filling and emptying processes are proposed for sequential and integrated designs by diving each step operation into two sub-steps including the transfer and production period. The operating parameters of the PBR with the proposed configuration can be obtained from the proper conversion of the CCR operating parameters. The results show that the performance of the PBR process can be partially predicted from that of CCR where the difference comes from the dynamics that are not accounted for in the CCR model. The proposed filling and emptying steps result in a lower outlet concentration of the outlet streams for all components owing to the lost amount during emptying the biomass which is not captured in the CCR model. Due to these discrepancies, the optimal design of the full dynamic SPRSS model with PBR and SMB may be significantly different from the continuous SPRSS model with CCR and TMB.

CHAPTER 8

CONCLUSION AND FUTURE WORK

8.1   Conclusions

The results presented in this thesis have met the three main objectives stated in Chapter 2:

1. To identify the optimal separation process configuration with feed pretreatment via reverse osmosis for dilute bioethanol purification processes.

2. To model the kinetics of concentrated acid hydrolysis reactions of cellulose and hemicellulose.

3. To conceptualize and design a novel optimal solid phase reactive chromatographic separation system for biomass saccharification using a rigorous optimization strategy.

The first objective is discussed in Chapter 3, where separation processes with reverse osmosis membrane pretreatment are investigated for fuel-grade bioethanol production from dilute ethanol-water mixtures. The superstructure of the hybrid distillation column – membrane pervaporation with the reverse osmosis membrane pretreatment is formulated and optimized to find the best separation scheme at minimal unit separation cost. It was found that reverse osmosis membrane pretreatment could reduce the separation costs for the dilute ethanol feeds at less than 3 wt% where the optimal process configuration of the reverse osmosis membrane system is observed to be different at different ethanol feed concentrations. In addition, the pretreatment is found to be necessary at a high feed throughput to meet the constraint on the size of the distillation column. The key benefit of reverse osmosis membrane pretreatment is the significant saving in the energy

137

consumption of the reboiler duty of the distillation column when the ethanol feed purity is very low. The results for this research objective provides a useful guideline for choosing the optimal separation technology at different ethanol feed concentrations.

The second research objective is satisfied by the experimental work on concentrated acid hydrolysis of cellulose and hemicellulose which is discussed in Chapter 4. The batch experiments for xylan and pure cellulose (Avicel) hydrolysis as well as xylose and glucose decomposition have been performed at different sulfuric acid concentrations between 10 – 50 wt% and temperatures between 80 – 100 °C. From the experiments, increasing the temperature and acid concentration increases the hydrolysis reaction rate as well as the rate of sugar decomposition. It has been found that rate of cellulose (Avicel) hydrolysis is much slower than that of xylan, and this is hypothesized to be due to the cellulose crystallinity. The effect of initial crystallinity of the cellulose to the rate of acid hydrolysis is also investigated in a separate series of batch experiments where the pure cellulose is treated with phosphoric acid at different concentrations. A dramatic reduction in cellulose crystalline index is observed when the phosphoric acid concentration is increased at a very narrow range between 77 – 80 wt%. The initial crystallinity of the Avicel significantly affects the hydrolysis rate where the rate increases with a lower initial crystallinity index.

The kinetic parameters for concentrated acid hydrolysis have been estimated from the batch experiments for the glucose and xylose reaction paths where, for the sugar concentration evolution over time, good agreement between the model predictions and the batch experiments is observed. These kinetic parameters were used to predict the performance of the reactive separation system for the concentrated acid hydrolysis of biomass.

The research work for the final objective of the research thesis is discussed in Chapter 5, Chapter 6, and Chapter 7 where a new solid-phase reactive chromatographic separation (SPRSS) process is proposed and the benefits of this new process are investigated. In this new process, the progressing batch reactor (PBR) and simulated moving bed chromatography (SMB) are combined. Both systems have similar principles for the imitation of the solid phase movement by liquid port switching in the direction of the liquid flow. This new process can be applied to systems involving solid reactants like biomass.

The integration of PBR and SMB has been compared for two alternative designs. The first one is the sequential design where the PBR and SMB are integrated in a straightforward manner, in series, where PBR and SMB have no interconnecting stream. The second one is the proposed SPRSS design where the interconnecting streams between PBR and SMB are allowed so that the PBR is fully integrated into SMB. The simplified continuous moving-bed model including the countercurrent reactor (CCR) and true-moving-bed chromatography (TMB) at the steady state for the two designs are optimized and compared using the superstructure formulation to investigate the potential advantages of SPRSS for biomass saccharification. The SPRSS with the kinetic parameters from the dilute acid hydrolysis reaction are investigated in Chapter 5 while that of the concentrated acid hydrolysis fitted from experiments are addressed in Chapter 6. It has been found that there is a potential improvement in sugar yield and less byproduct formation for the SPRSS design compared to the sequential design where the key benefit comes from the flexibility in varying the acid concentration and flow rate in the reactor system without interfering with the sugar concentration and dilution. The proposed SPRSS allows different acid

concentrations to hydrolyze different compositions of biomass which have different hydrolysis rates where the high acid concentration hydrolyzes the slow-hydrolyzed biomass portion like cellulose, and the low acid concentration hydrolyzes the fast hydrolyzed biomass portion like hemicellulose. These advantages enhance the saccharification process with less byproduct formation and thus reduce the subsequent separation cost of byproducts from sugars, which are strong inhibitors for the fermentation process.

The dynamic model of the progressing batch reactor as part of the full SPRSS system is formulated for two alternative designs. The filling and emptying step of the biomass in PBR system is proposed to recover the sugars lost during the emptying step. Each step of PBR operation is divided into two sub-steps including the transfer period and production period. The operating parameters of this proposed process can be estimated from the CCR model with appropriate reformulation. The simulation results from the PBR model is compared with that from CCR where a slight mismatch is observed which comes from the loss of the component during the emptying step as well as the dynamic behavior of the PBR system. The results from the CCR can be used to approximate the PBR system with sufficient accuracy for design purposes.

Overall, this work has developed novel pretreatment processes for bioethanol production from the biomass where an optimization strategy is successfully applied to systematically determine the optimal process design. These processes could reduce the bioethanol cost from the conversion of the lignocellulosic material and make the process more economically attractive. Furthermore, the separation process with pretreatment could be applied for the separation of other components when the feed is dilute. Likewise, the

propose solid-phase reactive separation system can be applied to other process which involves solid reactants.

8.2   Future work

There are some open questions that must be further investigated and some recommendations for future research projects.

8.2.1   Model refinement

8.2.1.1   Kinetic model refinement

A more rigorous kinetic model for the biomass hydrolysis should be investigated and implemented in the reactor model to investigate its performance. In the current study, Saeman's model[101] is assumed in the reactor model which consists of two consecutive reactions where the biomass is hydrolyzed into monosaccharides and decomposed into byproducts which are assumed to be HMF and furfural. However, oligosaccharides can also present in the system as well as other byproducts such as humins, formic acid, and levulinic acid. These components could affect the reactor performance as well as the separation in the SMB system. There are several studies that consider a more rigorous kinetic model for the cellulose and hemicellulose for the pretreatment process using dilute acid hydrolysis. Figure 8.1a illustrates the reaction path from the pretreatment using stream explosion where there is reversible reaction between the crystalline and amorphous cellulose where both may yield oligomers at a different rates before being further hydrolyzed into glucose and decomposed products.[150] A more complex reaction scheme

for the xylose reaction path from hemicellulose is illustrated in Figure 8.1b for dilute acid pre-hydrolysis.[151] These reaction schemes may happen in the concentrated acid hydrolysis process and should be further investigated the experiments.

(a)

(b)
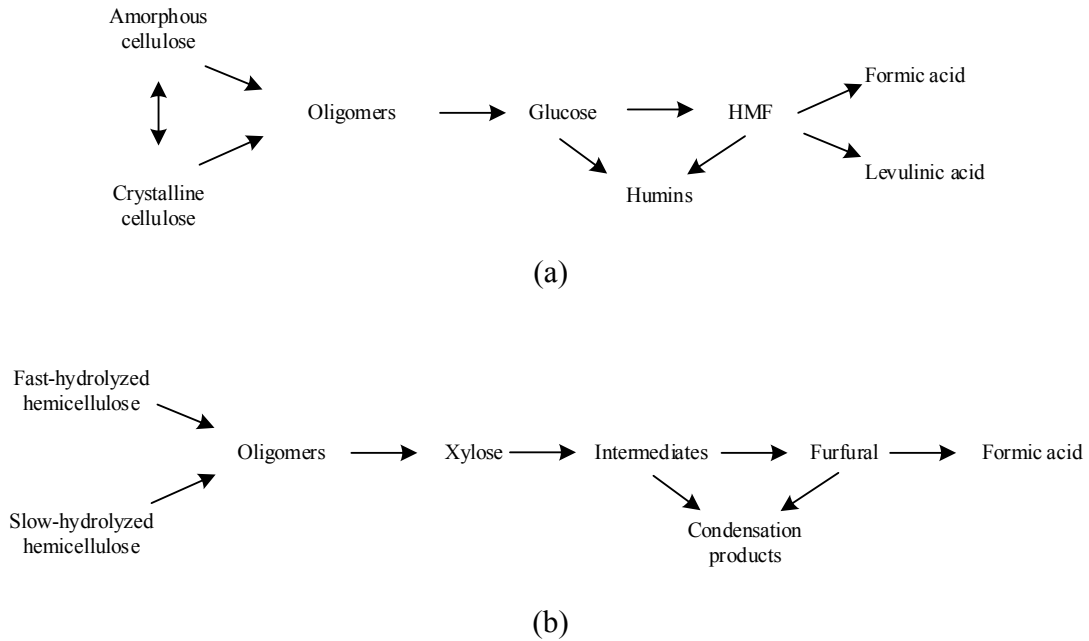
Figure 8.1. A more rigorous kinetic model for hydrolysis reaction (a) glucose reaction path[150] (b) xylose reaction path.[151]

In addition, the effect of the mass transfer resistance could be added into the reactor model. The current work has neglected the effect of mass transfer resistance from the reactor system because it is assumed the particle size is relatively small. In biomass with larger particles, this effect may have a significant impact on the reaction kinetics. Several past studies have investigated the effect mass transfer resistance. Mittal et al. [152] has assumed the kinetic model of xylan autohydrolysis reaction in hot water with three mechanisms including xylan solubilization, reaction in the pore liquor, and reaction in the bulk liquor where the xylose is formed both inside and outside the biomass particles. Dasari and Berson [153] have investigated the effect of the cellulose particle size on the enzymatic

hydrolysis rate where the glucose concentration from the hydrolysis of cellulose from sawdust is shown in Figure 8.2. It can be seen that for the smaller size of particles, the release rate of glucose is higher. It is possible that there is a concentration gradient of acid inside the particle so that the rate of hydrolysis is different. There is only a limited number of studies on the kinetic model with the effect of mass transfer resistance especially on the biomass saccharification via acid hydrolysis. This model should be developed and validated through experiment with different reactor systems.
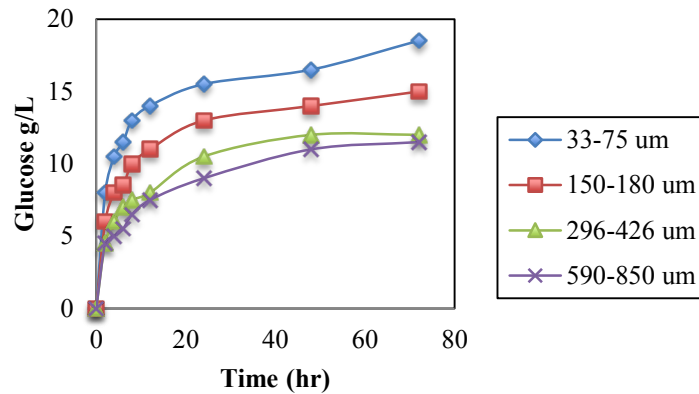
Figure 8.2. Glucose concentration from enzymatic hydrolysis for different initial cellulose particle size, Dasari and Berson [153]

8.2.1.2 Nonlinear adsorption isotherm

This work consider a simple linear isotherm where all Henry's coefficients are approximated at the average acid concentration of the process. However, the Henry's coefficient can change significantly especially for the concentrated acid hydrolysis process where the acid concentration varies significantly. Previous research has modeled the non-linear isotherm with the exponential function for the acid and the competitive anti-

Langmuir isotherms for the sugars.[24] Different adsorption isotherms may significantly affect the performance of the SMB in SPRSS which should be investigated carefully.

8.2.2 Extension of SPRSS to different process schemes

8.2.2.1 Incorporation of biomass pretreatment steps

It has been shown that the reaction rate of the cellulose hydrolysis strongly depends on its initial crystallinity. The pretreatment step is commonly done at a very high acid concentration with a cold temperature to decrystallize the cellulose as well as avoid the hydrolysis reaction to occur. It is possible to incorporate the pretreatment step into the SPRSS system where the SMB could vary the acid concentration inside the reactor to decrystallize as well as hydrolyze the biomass at different percolation reactors without the acid dilution. This could save the cost of acid recovery as well as increase the sugar yield.

8.2.2.2 Multicomponent separation

Multicomponent separation schemes can be applied and explored in the SPRSS system which could bring several advantages. One potential improvement could be from the separation of sugars from the biomass saccharification. For example, hexoses and pentoses require different microorganism for fermentation to achieve the highest bioethanol yield. Hence, the overall ethanol yield could be improved by performing the multicomponent separation between each sugar and acid where the separated sugar is fed to fermentation separately. In addition, multicomponent separation could be performed to separate the byproduct from the acid and sugars. This could create a more favorable condition of the hydrolysate for the fermentation and will subsequently reduce the cost of the detoxification process.

An example of straightforward configurations of SPRSS which separates two sugars from the acid is illustrated in Figure 8.3 which consists of two separated SMB. From the figure, the concentrated acid hydrolyzes the treated biomass in Section 1, which mainly contains cellulose to achieve glucose and goes to the SMB-1 to separate acid from glucose. The acid from SMB-1 becomes dilute and can recycle to the Section 2 to hydrolyze fresh biomass which mainly contain hemicellulose. The hydrolysate from this reactor, which contains mainly pentose such as xylose, goes to the SMB-2 to separate pentoses from acid. From this configurations, the hexoses, pentoses, and acid are separated and each sugar could be fed to the fermentation separately while acid can be concentrated and recycled to the reactor system.
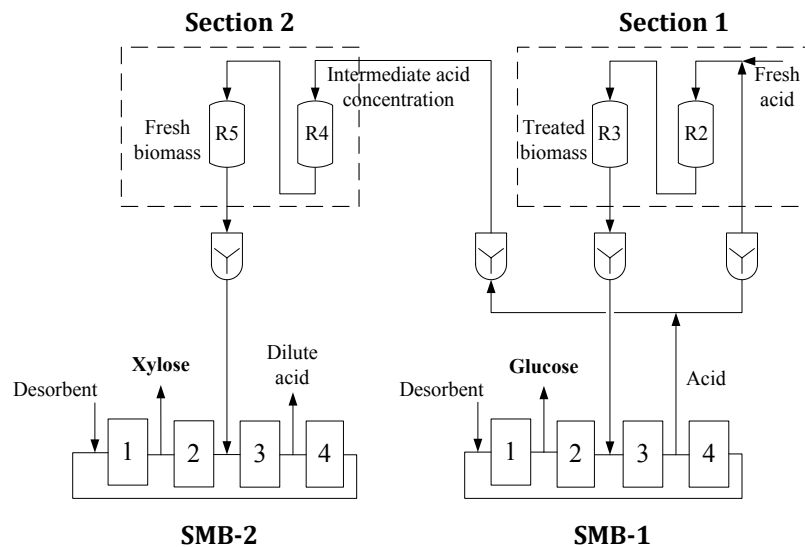

Figure 8.3. The integration of PBR and two SMBs to separate the C5 and C6 sugars from acid.

There are many other configurations for the multicomponent separation using SMB such as eight-zone configuration, JO process, and generalized full cycle configuration which are for ternary separation.[148] These configurations could be incorporated into the superstructure of the SPRSS to seek the potential benefits of multicomponent separation system.

8.2.2.3   Nonstandard configurations

The nonstandard SMB could be employed into the SPRSS process. This includes the PowerFeed where the liquid inlets and outlets velocities are time-variant, and VARICOL process where the system performs asynchronous valve switching.[147, 154-155] In addition, the reactor system can be integrated with the SMB without the intermediate buffer tanks. Therefore, the concentrations as well as the velocities of the feed stream to the SMB and the recycle stream to reactor system are time-variant. A new mathematical model of this process should be constructed where the two cyclic operations of the progressing batch reactor and the SMB chromatography must be optimally designed. These nonstandard configurations provide more flexibility to the process operation which could potentially increase the advantage of the SPRSS.

8.2.3   Dynamic optimization of SPRSS with experimental validation

Optimization of the full dynamic SPRSS model proposed in this thesis should be performed. Moreover, the optimal design of the SPRSS found from the model should be validated by the experiment. This includes the experiment solely on the reactor system as well as the overall SPRSS. There are several points from the mathematical model which need to be compared with the experiment. First, the kinetic model as well as the effect of

mass transfer resistance in the percolation reactor should be validated by experiment. In addition, the impact of the shrinking bed should be investigated carefully from the experiment as the biomass keeps dissolving into the liquid phase during the hydrolysis causing the reduction in the packing bed size.[156] Finally, the overall SPRSS performance from the experiment should be compared with the prediction from the model such as sugar concentration and acid consumption. Additional model refinement may be required based on the results from the experiment.

.

REFERENCES

[1]   THINNES, B., "BP's energy outlook to 2030," Hydrocarb Process, vol. 91, no. 3, pp. 17-19, 2012.

[2]   GALBE, M.,ZACCHI, G., "A review of the production of ethanol from softwood," Appl Microbiol Biot, vol. 59, no. 6, pp. 618-628, 2002.

[3]   EIA, U. S., International Energy Outlook, 2011. U.S. Energy Information Administration: Washington DC, USA, 2011.

[4]   EIA, U. S., International Energy Outlook 2014: World Petroleum and Other Liquid Fuels with projections to 2040. U.S. Energy Information Administration: Washington DC, USA, 2014.

[5]   PATEL, S., "World Energy Outlook Forecasts Great Renewables Growth," Power, vol. 156, no. 1, pp. 8-15, 2012.

[6]   HUANG, H. J.,RAMASWAMY, S.,TSCHIRNER, U. W.,RAMARAO, B. V., "A review of separation technologies in current and future biorefineries," Sep Purif Technol, vol. 62, no. 1, pp. 1-21, 2008.

[7]   GUPTA, A.,VERMA, J. P., "Sustainable bio-ethanol production from agro-residues: A review," Renew Sust Energ Rev, vol. 41, pp. 550-567, 2015.

[8]   KUMAR, P.,BARRETT, D. M.,DELWICHE, M. J.,STROEVE, P., "Methods for Pretreatment of Lignocellulosic Biomass for Efficient Hydrolysis and Biofuel Production," Ind Eng Chem Res, vol. 48, no. 8, pp. 3713-3729, 2009.

[9]   DWIVEDI, P.,ALAVALAPATI, J. R. R.,LAL, P., "Cellulosic ethanol production in the United States: Conversion technologies, current production status, economics, and emerging developments," Energy Sustain Dev, vol. 13, no. 3, pp. 174-182, 2009.

[10]   COLLARD, F. X.,BLIN, J., "A review on pyrolysis of biomass constituents: Mechanisms and composition of the products obtained from the conversion of cellulose, hemicelluloses and lignin," Renew Sust Energ Rev, vol. 38, pp. 594-608, 2014.

[11]   TAHERZADEH, M. J.,KARIMI, K., "Acid-Based Hydrolysis Processes for Ethanol from Lignocellulosic Materials: A Review," Bioresources, vol. 2, no. 3, pp. 472-499, 2007.

[12]   BECK, M. J.,JOHNSON, R. D.,BAKER, C. S., "Ethanol-Production from Glucose Xylose Mixes by Incorporating Microbes in Selected Fermentation Schemes," Appl Biochem Biotech, vol. 24-25, no. 1, pp. 415-424, 1990.

[13]   LAPLACE, J. M.,DELGENES, J. P.,MOLETTA, R.,NAVARRO, J. M., "Ethanol-Production from Glucose and Xylose by Separated and Coculture Processes Using High Cell-Density Systems," Process Biochem, vol. 28, no. 8, pp. 519-525, 1993.

[14]   DEUTSCHMANN, R.,DEKKER, R. F. H., "From plant biomass to bio-based chemicals: Latest developments in xylan research," Biotechnol Adv, vol. 30, no. 6, pp. 1627-1640, 2012.

[15]   DMYTRUK, O. V.,DMYTRUK, K. V.,VORONOVSKY, A. Y.,SIBIRNY, A. A., "Metabolic engineering of the initial stages of xylose catabolism in yeast for the purpose of constructing efficient producers of ethanol from lignocellulosics," Cytol Genet+, vol. 42, no. 2, pp. 127-138, 2008.

[16]   CAO, L. M.,TANG, X. L.,ZHANG, X. Y.,ZHANG, J. T.,TIAN, X. L.,WANG, J. Y.,XIONG, M. Y.,XIAO, W., "Two-stage transcriptional reprogramming in Saccharomyces cerevisiae for optimizing ethanol production from xylose," Metab. Eng., vol. 24, pp. 150-159, 2014.

[17]   GIRISUTA, B.,JANSSEN, L. P. B. M.,HEERES, H. J., "A kinetic study on the conversion of glucose to levulinic acid," Chem Eng Res Des, vol. 84, no. A5, pp. 339-349, 2006.

[18]   SAINIO, T.,TURKU, I.,HEINONEN, J., "Adsorptive removal of fermentation inhibitors from concentrated acid hydrolyzates of lignocellulosic biomass," Bioresour. Technol., vol. 102, no. 10, pp. 6048-6057, 2011.

[19]   RANJAN, R.,THUST, S.,GOUNARIS, C. E.,WOO, M.,FLOUDAS, C. A.,VON KEITZ, M.,VALENTAS, K. J.,WEI, J.,TSAPATSIS, M., "Adsorption of fermentation inhibitors from lignocellulosic biomass hydrolyzates for improved ethanol yield and value-added product recovery," Microporous Mesoporous Mater., vol. 122, no. 1-3, pp. 143-148, 2009.

[20]   HANLY, T. J.,HENSON, M. A., "Dynamic Model-Based Analysis of Furfural and HMF Detoxification by Pure and Mixed Batch Cultures of S. cerevisiae and S. stipitis," Biotechnol Bioeng, vol. 111, no. 2, pp. 272-284, 2014.

[21]   DELGENES, J. P.,MOLETTA, R.,NAVARRO, J. M., "Effects of lignocellulose degradation products on ethanol fermentations of glucose and xylose by Saccharomyces cerevisiae, Zymomonas mobilis, Pichia stipitis, and Candida shehatae," Enzyme Microb. Technol., vol. 19, no. 3, pp. 220-225, 1996.

[22]   MUSSATTO, S. I.,ROBERTO, I. C., "Alternatives for detoxification of diluted-acid lignocellulosic hydrolyzates for use in fermentative processes: a review," Bioresour. Technol., vol. 93, no. 1, pp. 1-10, 2004.

[23]   JANGA, K. K.,OYAAS, K.,HERTZBERG, T.,MOE, S. T., "Application of a Pseudo-Kinetic Generalized Severity Model to the Concentrated Sulfuric Acid Hydrolysis of Pinewood and Aspenwood," Bioresources, vol. 7, no. 3, pp. 2728-2741, 2012.

[24]   HEINONEN, J.,SAINIO, T., "Modelling and performance evaluation of chromatographic monosaccharide recovery from concentrated acid lignocellulosic hydrolysates," J. Chem. Technol. Biotechnol., vol. 87, no. 12, pp. 1676-1686, 2012.

[25]   FARONE, W. A.,CUZENS, J. E., "Method for producing sugars using strong acid hydrolysis of cellulosic and hemicellulosic materials," U.S. Patent 5,562,777, Oct 8, 1996.

[26]   XIE, Y.,CHIN, C. Y.,PHELPS, D. S. C.,LEE, C. H.,LEE, K. B.,MUN, S.,WANG, N. H. L., "A five-zone simulated moving bed for the isolation of six sugars from biomass hydrolyzate," Ind Eng Chem Res, vol. 44, no. 26, pp. 9904-9920, 2005.

[27]   WOOLEY, R.,MA, Z.,WANG, N. H. L., "A nine-zone simulating moving bed for the recovery of glucose and xylose from biomass hydrolyzate," Ind Eng Chem Res, vol. 37, no. 9, pp. 3699-3709, 1998.

[28]   AL-ASHEH, S.,BANAT, F.,AL-LAGTAH, N., "Separation of ethanol-water mixtures using molecular sieves and biobased adsorbents," Chem Eng Res Des, vol. 82, no. A7, pp. 855-864, 2004.

[29]   BEERY, K. E.,LADISCH, M. A., "Chemistry and properties of starch based desiccants," Enzyme Microb. Technol., vol. 28, no. 7-8, pp. 573-581, 2001.

[30]   BEERY, K. E.,LADISCH, M. R., "Adsorption of water from liquid-phase ethanol-water mixtures at room temperature using starch-based adsorbents," Ind Eng Chem Res, vol. 40, no. 9, pp. 2112-2115, 2001.

[31]   SANDER, U.,SOUKUP, P., "Design and Operation of a Pervaporation Plant for Ethanol Dehydration," Journal of Membrane Science, vol. 36, pp. 463-475, 1988.

[32]   WEE, S. L.,TYE, C. T.,BHATIA, S., "Membrane separation process-Pervaporation through zeolite membrane," Sep Purif Technol, vol. 63, no. 3, pp. 500-516, 2008.

[33]   VANE, L. M.,ALVAREZ, F. R., "Membrane-assisted vapor stripping: energy efficient hybrid distillation-vapor permeation process for alcohol-water separation," J. Chem. Technol. Biotechnol., vol. 83, no. 9, pp. 1275-1287, 2008.

[34]   MALIK, R. K.,NAIDU, Y., "A generalized methodology for optimal configurations of hybrid distillation-pervaporation processes," Chem. Eng. Res. Des., vol. 89, no. 8A, pp. 1348-1361, 2011.

[35]   VANE, L. M., "Separation technologies for the recovery and dehydration of alcohols from fermentation broths," Biofuel Bioprod Bior, vol. 2, no. 6, pp. 553-588, 2008.

[36]   KANCHANALAI, P.,REALFF, M. J.,KAWAJIRI, Y., "Optimal Process Configurations of Bioethanol Dehydration for Different Ethanol Inlet Concentrations and Throughputs," Computer Aided Chemical Engineering, Iftekhar, A. K.,Rajagopalan, S., Eds. Elsevier, vol. 31, pp. 425-429, 2012.

[37]   "Chicago Mercantile Exchange, Ethanol Futures Quotes," http://www.cmegroup.com/trading/energy/ethanol/cbot-ethanol.html (accessed February, 2015).

[38]   KAUTTO, J.,REALFF, M. J.,RAGAUSKAS, A. J.,KASSI, T., "Economic Analysis of an Organosolv Process for Bioethanol Production," Bioresources, vol. 9, no. 4, pp. 6041-6072, 2014.

[39]   EGGEMAN, T.,ELANDER, R. T., "Process and economic analysis of pretreatment technologies," Bioresour. Technol., vol. 96, no. 18, pp. 2019-2025, 2005.

[40]   KAZI, F. K.,FORTMAN, J. A.,ANEX, R. P.,HSU, D. D.,ADEN, A.,DUTTA, A.,KOTHANDARAMAN, G., "Techno-economic comparison of process technologies for biochemical ethanol production from corn stover," Fuel, vol. 89, pp. S20-S28, 2010.

[41]   TAO, L.,ADEN, A.,ELANDER, R. T.,PALLAPOLU, V. R.,LEE, Y. Y.,GARLOCK, R. J.,BALAN, V.,DALE, B. E.,KIM, Y.,MOSIER, N. S.,LADISCH, M. R.,FALLS, M.,HOLTZAPPLE, M. T.,SIERRA, R.,SHI, J.,EBRIK, M. A.,REDMOND, T.,YANG, B.,WYMAN, C. E.,HAMES, B.,THOMAS, S.,WARNER, R. E., "Process and technoeconomic analysis of leading pretreatment technologies for lignocellulosic ethanol production using switchgrass," Bioresour. Technol., vol. 102, no. 24, pp. 11105-11114, 2011.

[42]   BALAT, M.,BALAT, H.,OZ, C., "Progress in bioethanol processing," Prog. Energy Combust. Sci., vol. 34, no. 5, pp. 551-573, 2008.

[43]   JOHN, R. P.,ANISHA, G. S.,NAMPOOTHIRI, K. M.,PANDEY, A., "Micro and macroalgal biomass: A renewable source for bioethanol," Bioresour. Technol., vol. 102, no. 1, pp. 186-193, 2011.

[44]   NIGAM, P. S.,SINGH, A., "Production of liquid biofuels from renewable resources," Prog. Energy Combust. Sci., vol. 37, no. 1, pp. 52-68, 2011.

[45]   FROLKOVA, A. K.,RAEVA, V. M., "Bioethanol dehydration: State of the art," Theor. Found. Chem. Eng., vol. 44, no. 4, pp. 545-556, 2010.

[46]   WRIGHT, M.,BROWN, R. C., "Establishing the optimal sizes of different kinds of biorefineries," Biofuel Bioprod Bior, vol. 1, no. 3, pp. 191-200, 2007.

[47]   JEFFRIES, T. W.,JIN, Y. S., "Ethanol and thermotolerance in the bioconversion of xylose by yeasts," Adv. Appl. Microbiol., vol. 47, pp. 221-268, 2000.

[48]   LUO, D. X.,HU, Z. S.,CHOI, D. G.,THOMAS, V. M.,REALFF, M. J.,CHANCE, R. R., "Life Cycle Energy and Greenhouse Gas Emissions for an Ethanol Production Process Based on Blue-Green Algae," Environmental Science & Technology, vol. 44, no. 22, pp. 8670-8677, 2010.

[49]   MOGANTI, S.,NOBLE, R. D.,KOVAL, C. A., "Analysis of a Membrane Distillation Column Hybrid Process," Journal of Membrane Science, vol. 93, no. 1, pp. 31-44, 1994.

[50]   STEPHAN, W.,NOBLE, R. D.,KOVAL, C. A., "Design Methodology for a Membrane Distillation Column Hybrid Process," Journal of Membrane Science, vol. 99, no. 3, pp. 259-272, 1995.

[51]   PETTERSEN, T.,ARGO, A.,NOBLE, R. D.,KOVAL, C. A., "Design of combined membrane and distillation processes," Separ Technol, vol. 6, no. 3, pp. 175-187, 1996.

[52]   FONTALVO, J.,CUELLAR, P.,TIMMER, J. M. K.,VORSTMAN, M. A. G.,WIJERS, J. G.,KEURENTJES, J. T. F., "Comparing pervaporation and vapor permeation hybrid distillation processes," Ind. Eng. Chem. Res., vol. 44, no. 14, pp. 5259-5266, 2005.

[53]   LIPNIZKI, F.,FIELD, R. W.,TEN, P. K., "Pervaporation-based hybrid process: a review of process design, applications and economics," Journal of Membrane Science, vol. 153, no. 2, pp. 183-210, 1999.

[54]   KOCZKA, K.,MIZSEY, P.,FONYO, Z., "Rigorous modelling and optimization of hybrid separation processes based on pervaporation," Cent Eur J Chem, vol. 5, no. 4, pp. 1124-1147, 2007.

[55] HUANG, Y.,BAKER, R. W.,VANE, L. M., "Low-Energy Distillation-Membrane Separation Process," Ind. Eng. Chem. Res., vol. 49, no. 8, pp. 3760-3768, 2010.

[56] HUANG, Y.,LY, J.,NGUYEN, D.,BAKER, R. W., "Ethanol Dehydration Using Hydrophobic and Hydrophilic Polymer Membranes," Ind. Eng. Chem. Res., vol. 49, no. 23, pp. 12067-12073, 2010.

[57] VANE, L. M.,ALVAREZ, F. R.,HUANG, Y.,BAKER, R. W., "Experimental validation of hybrid distillation-vapor permeation process for energy efficient ethanol-water separation," J. Chem. Technol. Biotechnol., vol. 85, no. 4, pp. 502-511, 2010.

[58] SZITKAI, Z.,LELKES, Z.,REV, E.,FONYO, Z., "Optimization of hybrid ethanol dehydration systems," Chem Eng Process, vol. 41, no. 7, pp. 631-646, 2002.

[59] KOOKOS, I. K., "Optimal design of membrane/distillation column hybrid processes," Ind. Eng. Chem. Res., vol. 42, no. 8, pp. 1731-1738, 2003.

[60] CABALLERO, J. A.,GROSSMANN, I. E.,KEYVANI, M.,LENZ, E. S., "Design of Hybrid Distillation-Vapor Membrane Separation Systems," Ind. Eng. Chem. Res., vol. 48, no. 20, pp. 9151-9162, 2009.

[61] VISWANATHAN, J.,GROSSMANN, I. E., "A Combined Penalty-Function and Outer-Approximation Method for Minlp Optimization," Comput Chem Eng, vol. 14, no. 7, pp. 769-782, 1990.

[62] VISWANATHAN, J.,GROSSMANN, I. E., "Optimal Feed Locations and Number of Trays for Distillation-Columns with Multiple Feeds," Ind. Eng. Chem. Res., vol. 32, no. 11, pp. 2942-2949, 1993.

[63] LUYBEN, W. L., "Control of a Column/Pervaporation Process for Separating the Ethanol/Water Azeotrope," Ind. Eng. Chem. Res., vol. 48, no. 7, pp. 3484-3495, 2009.

[64] WIJMANS, J. G.,BAKER, R. W., "A Simple Predictive Treatment of the Permeation Process in Pervaporation," Journal of Membrane Science, vol. 79, no. 1, pp. 101-113, 1993.

[65] WIJMANS, J. G.,BAKER, R. W., "The Solution-Diffusion Model - a Review," Journal of Membrane Science, vol. 107, no. 1-2, pp. 1-21, 1995.

[66] DAVIS, R. A., "Simple gas permeation and pervaporation membrane unit operation models for process simulators," Chem. Eng. Technol., vol. 25, no. 7, pp. 717-722, 2002.

[67]   WESSLEIN, M.,HEINTZ, A.,LICHTENTHALER, R. N., "Pervaporation of Liquid-Mixtures through Poly(Vinyl Alcohol) (Pva) Membranes .1. Study of Water Containing Binary-Systems with Complete and Partial Miscibility," Journal of Membrane Science, vol. 51, no. 1-2, pp. 169-179, 1990.

[68]   CHEN, J. J. J., "Comments on Improvements on a Replacement for the Logarithmic Mean," Chem Eng Sci, vol. 42, no. 10, pp. 2488-2489, 1987.

[69]   PEREZ-GONZALEZ, A.,URTIAGA, A. M.,IBANEZ, R.,ORTIZ, I., "State of the art and review on the treatment technologies of water reverse osmosis concentrates," Water Res., vol. 46, no. 2, pp. 267-283, 2012.

[70]   GUDE, V. G., "Energy consumption and recovery in reverse osmosis," Desalin Water Treat, vol. 36, no. 1-3, pp. 239-260, 2011.

[71]   HSU, J. H.,TAN, C. S., "Separation of Ethanol from Aqueous-Solution by a Method Incorporating Supercritical Co2 with Reverse-Osmosis," Journal of Membrane Science, vol. 81, no. 3, pp. 273-285, 1993.

[72]   CHOUDHURY, J. P.,GHOSH, P.,GUHA, B. K., "Separation of Ethanol from Ethanol-Water Mixture by Reverse-Osmosis," Biotechnol Bioeng, vol. 27, no. 7, pp. 1081-1084, 1985.

[73]   KARUPPIAH, R.,BURY, S. J.,VAZQUEZ, A.,POPPE, G., "Optimal design of reverse osmosis-based water treatment systems," Aiche J, vol. 58, no. 9, pp. 2758-2769, 2012.

[74]   QI, R. H.,HENSON, M. A., "Membrane system design for multicomponent gas mixtures via mixed-integer nonlinear programming," Comput Chem Eng, vol. 24, no. 12, pp. 2719-2737, 2000.

[75]   MASKAN, F.,WILEY, D. E.,JOHNSTON, L. P. M.,CLEMENTS, D. J., "Optimal design of reverse osmosis module networks," Aiche J, vol. 46, no. 5, pp. 946-954, 2000.

[76]   EL-HALWAGI, M. M., "Synthesis of Reverse-Osmosis Networks for Waste Reduction," Aiche J, vol. 38, no. 8, pp. 1185-1198, 1992.

[77]   DU, Y.,XIE, L.,WANG, Y.,XU, Y.,WANG, S., "Optimization of Reverse Osmosis Networks with Spiral-Wound Modules," Ind. Eng. Chem. Res., vol. 51, no. 36, pp. 11764-11777, 2012.

[78]   LU, Y.-Y.,HU, Y.-D.,ZHANG, X.-L.,WU, L.-Y.,LIU, Q.-Z., "Optimum design of reverse osmosis system under different feed concentration and product specification," Journal of Membrane Science, vol. 287, no. 2, pp. 219-229, 2007.

[79]   VOROS, N.,MAROULIS, Z. B.,MARINOSKOURIS, D., "Optimization of reverse osmosis networks for seawater desalination," Comput Chem Eng, vol. 20, pp. S345-S350, 1996.

[80]   SEADER, J. D.,HENLEY, E. J., "Separation Process Principles," 2nd ed., Wiley, New York, 2006.

[81]   KEURENTJES, J. T. F.,LINDERS, L. J. M.,BEVERLOO, W. A.,VANTRIET, K., "Membrane Cascades for the Separation of Binary-Mixtures," Chem Eng Sci, vol. 47, no. 7, pp. 1561-1568, 1992.

[82]   ABEJÓN, R.,GAREA, A.,IRABIEN, A., "Optimum design of reverse osmosis systems for hydrogen peroxide ultrapurification," Aiche J, vol. 58, no. 12, pp. 3718-3730, 2012.

[83]   STOVER, R. L., "Seawater reverse osmosis with isobaric energy recovery devices," Desalination, vol. 203, no. 1-3, pp. 168-175, 2007.

[84]   LEEPER, S. A.,TSAO, G. T., "Membrane Separations in Ethanol Recovery - an Analysis of 2 Applications of Hyperfiltration," Journal of Membrane Science, vol. 30, no. 3, pp. 289-312, 1987.

[85]   SEIDER, W. D.,SEADER, J. D.,LEWIN, D. R.,WIDAGDO, S., "Product and process design principles: synthesis, analysis and evaluation," 3rd ed., Wiley, Hoboken, 2009.

[86]   BAKER, R. W.,LOKHANDWALA, K., "Natural gas processing with membranes: An overview," Ind. Eng. Chem. Res., vol. 47, no. 7, pp. 2109-2121, 2008.

[87]   JOHANNSEN, M., "Modeling of Simulated Moving-bed Chromatography," Modeling of Process Intensification, Wiley-VCH Verlag GmbH & Co. KGaA, pp. 279-322, 2007.

[88]   JGC, "NEDO's Application of Arkenol's Concentrated Acid Hydrolysis Technology for the Conversion of Biomass to Ethanol," http://bfreinc.com/docs/IZUMI_Status_2004_for_BlueFire_051606.pdf (accessed April, 2015).

[89]   ZHU, L.,O'DWYER, J. P.,CHANG, V. S.,GRANDA, C. B.,HOLTZAPPLE, M. T., "Structural features affecting biomass enzymatic digestibility," Bioresour. Technol., vol. 99, no. 9, pp. 3817-3828, 2008.

[90]   HALL, M.,BANSAL, P.,LEE, J. H.,REALFF, M. J.,BOMMARIUS, A. S., "Cellulose crystallinity - a key predictor of the enzymatic hydrolysis rate," Febs J, vol. 277, no. 6, pp. 1571-1582, 2010.

[91]   SRIBALA, G.,VINU, R., "Unified Kinetic Model for Cellulose Deconstruction via Acid Hydrolysis," Ind Eng Chem Res, vol. 53, no. 21, pp. 8714-8725, 2014.

[92]   KANCHANALAI, P.,REALFF, M. J.,KAWAJIRI, Y., "Solid-Phase Reactive Chromatographic Separation System: Optimization-Based Design and Its Potential Application to Biomass Saccharification via Acid Hydrolysis," Ind Eng Chem Res, vol. 53, no. 41, pp. 15946-15961, 2014.

[93]   KANCHANALAI, P.,REALFF, M. J.,KAWAJIRI, Y. "Dynamic Modelling and Optimal Design of the Solid-Phase Reactive Chromatographic Separation System for Biomass Saccharification via Acid Hydrolysis," 12th International Symposium on Process Systems Engineering (PSE) and 25th European Symposium on Computer Aided Process Engineering (ESCAPE), Copenhagen, Denmark, Gernaey, K. V.,Huusom, J. K.,Gani, R., Eds. Elsevier B.V, 2015.

[94]   DE PAULA, M. P.,LACERDA, T. M.,ZAMBON, M. D.,FROLLINI, E., "Adding value to the Brazilian sisal: acid hydrolysis of its pulp seeking production of sugars and materials," Cellulose, vol. 19, no. 3, pp. 975-992, 2012.

[95]   LACERDA, T. M.,ZAMBON, M. D.,FROLLINI, E., "Effect of acid concentration and pulp properties on hydrolysis reactions of mercerized sisal," Carbohyd Polym, vol. 93, no. 1, pp. 347-356, 2013.

[96]   CAMACHO, F.,GONZALEZTELLO, P.,JURADO, E.,ROBLES, A., "Microcrystalline-cellulose hydrolysis with concentrated sulphuric acid," J. Chem. Technol. Biotechnol., vol. 67, no. 4, pp. 350-356, 1996.

[97]   FARONE, W. A.,CUZENS, J. E., "Strong acid hydrolysis of cellulosic and hemicellulosic material," U.S. Patent 5,597,714, Jan 28, 1997.

[98]   ZHANG, J. H.,ZHANG, J. Q.,LIN, L.,CHEN, T. M.,ZHANG, J.,LIU, S. J.,LI, Z. J.,OUYANG, P. K., "Dissolution of Microcrystalline Cellulose in Phosphoric Acid-Molecular Changes and Kinetics," Molecules, vol. 14, no. 12, pp. 5027-5041, 2009.

[99]   ZHANG, Y. H. P.,LYND, L. R., "Determination of the number-average degree of polymerization of cellodextrins and cellulose with application to enzymatic hydrolysis," Biomacromolecules, vol. 6, no. 3, pp. 1510-1515, 2005.

[100]   KANG, Y. Z.,BANSAL, P.,REALFF, M. J.,BOMMARIUS, A. S., "SO2-catalyzed steam explosion: The effects of different severity on digestibility, accessibility, and crystallinity of lignocellulosic biomass," Biotechnol Progr, vol. 29, no. 4, pp. 909-916, 2013.

[101] SAEMAN, J. F., "Kinetics of Wood Saccharification - Hydrolysis of Cellulose and Decomposition of Sugars in Dilute Acid at High Temperature," Ind Eng Chem, vol. 37, no. 1, pp. 43-52, 1945.

[102] LEE, Y. Y.,WU, Z. W.,TORGET, R. W., "Modeling of countercurrent shrinking-bed reactor in dilute-acid total-hydrolysis of lignocellulosic biomass," Bioresour. Technol., vol. 71, no. 1, pp. 29-39, 2000.

[103] GIRISUTA, B.,JANSSEN, L. P. B. M.,HEERES, H. J., "A kinetic study on the decomposition of 5-hydroxymethylfurfural into levulinic acid," Green Chem, vol. 8, no. 8, pp. 701-709, 2006.

[104] KUMAR, R.,HU, F.,SANNIGRAHI, P.,JUNG, S.,RAGAUSKAS, A. J.,WYMAN, C. E., "Carbohydrate derived-pseudo-lignin can retard cellulose biological conversion," Biotechnol Bioeng, vol. 110, no. 3, pp. 737-753, 2013.

[105] HANSEN, P. C., "Discrete Inverse Problems: Insight and Algorithms," Society for Industrial and Applied Mathematics, Denmark, 2010; p 1-213.

[106] BRENNAN, M. A.,WYMAN, C. E., "Initial evaluation of simple mass transfer models to describe hemicellulose hydrolysis in corn stover," Appl Biochem Biotech, vol. 113, pp. 965-976, 2004.

[107] KARIMI, K.,KHERADMANDINIA, S.,TAHERZADEH, M. J., "Conversion of rice straw to sugars by dilute-acid hydrolysis," Biomass Bioenerg, vol. 30, no. 3, pp. 247-253, 2006.

[108] LENIHAN, P.,OROZCO, A.,O'NEILL, E.,AHMAD, M. N. M.,ROONEY, D. W.,WALKER, G. M., "Dilute acid hydrolysis of lignocellulosic biomass," Chem Eng J, vol. 156, no. 2, pp. 395-403, 2010.

[109] HEINONEN, J.,TAMMINEN, A.,UUSITALO, J.,SAINIO, T., "Ethanol production from wood via concentrated acid hydrolysis, chromatographic separation, and fermentation," J. Chem. Technol. Biotechnol., vol. 87, no. 5, pp. 689-696, 2012.

[110] KIM, B. J.,LEE, Y. Y.,TORGET, R., "Modified Percolation Process in Dilute-Acid Hydrolysis of Biphasic Hemicellulose," Appl Biochem Biotech, vol. 45-46, no. 1, pp. 113-129, 1994.

[111] WRIGHT, J. D.,BERGERON, P. W.,WERDENE, P. J., "Progressing Batch Hydrolysis Reactor," Ind Eng Chem Res, vol. 26, no. 4, pp. 699-705, 1987.

[112] LEE, Y. Y.,IYER, P.,TORGET, R. W., "Dilute-Acid Hydrolysis of Lignocellulosic Biomass," Recent Progress in Bioconversion of Lignocellulosics, Springer Berlin Heidelberg, vol. 65, pp. 93-115, 1999.

[113] SONG, S. K.,LEE, Y. Y., "Countercurrent Reactor in Acid-Catalyzed Cellulose Hydrolysis," Chem Eng Commun, vol. 17, no. 1-6, pp. 23-30, 1982.

[114] KIM, S. B.,YUM, D. M.,PARK, S. C., "Step-change variation of acid concentration in a percolation reactor for hydrolysis of hardwood hemicellulose," Bioresour. Technol., vol. 72, no. 3, pp. 289-294, 2000.

[115] JANGA, K. K.,HAGG, M. B.,MOE, S. T., "Influence of Acid Concentration, Temperature, and Time on Decrystallization in Two-Stage Concentrated Sulfuric Acid Hydrolysis of Pinewood and Aspenwood: A Statistical Approach," Bioresources, vol. 7, no. 1, pp. 391-411, 2012.

[116] KOCHERGIN, V.,KEARNEY, M., "Existing biorefinery operations that benefit from fractal-based process intensification," Appl Biochem Biotech, vol. 130, no. 1-3, pp. 349-360, 2006.

[117] KEARNEY, M.,KOCHERGIN, V.,HESS, R.,FOUST, T.,HERBST, R.,MANN, N., "Industrial Membrane Filtration and Short-bed Fractal Separation Systems for Separating Monomers from Heterogeneous Plant Material: Final Report (2005), US Department of Energy (DOE)," http://www.osti.gov/scitech/biblio/838864 (accessed August, 2014).

[118] LODE, F.,MAZZOTTI, M.,MORBIDELLI, M., "A new reaction-separation unit: The simulated moving bed reactor," Chimia, vol. 55, no. 10, pp. 883-886, 2001.

[119] MAZZOTTI, M.,STORTI, G.,MORBIDELLI, M., "Optimal operation of simulated moving bed units for nonlinear chromatographic separations," J Chromatogr A, vol. 769, no. 1, pp. 3-24, 1997.

[120] DA SILVA, E. A. B.,PEDRUZZI, I.,RODRIGUES, A. E., "Simulated moving bed technology to improve the yield of the biotechnological production of lactobionic acid and sorbitol," Adsorption, vol. 17, no. 1, pp. 145-158, 2011.

[121] KAWASE, M.,SUZUKI, T. B.,INOUE, K.,YOSHIMOTO, K.,HASHIMOTO, K., "Increased esterification conversion by application of the simulated moving-bed reactor," Chem Eng Sci, vol. 51, no. 11, pp. 2971-2976, 1996.

[122] MINCEVA, M.,RODRIGUES, A. E., "Simulated moving-bed reactor: Reactive-separation regions," Aiche J, vol. 51, no. 10, pp. 2737-2751, 2005.

[123] RAY, A. K.,CARR, R. W.,ARIS, R., "The Simulated Countercurrent Moving-Bed Chromatographic Reactor - a Novel Reactor Separator," Chem Eng Sci, vol. 49, no. 4, pp. 469-480, 1994.

[124] DA SILVA, E. A. B.,SOUZA, D. P.,DE SOUZA, A. A. U.,SOUZA, S. M. A. G. U.,RODRIGUES, A. E., "Analysis of the behavior of the simulated moving bed reactor in the sucrose inversion process," Separ Sci Technol, vol. 40, no. 12, pp. 2373-2389, 2005.

[125] SHIEH, M. T.,BARKER, P. E., "Combined bioreaction and separation in a simulated counter-current chromatographic bioreactor-separator for the hydrolysis of lactose," J. Chem. Technol. Biotechnol., vol. 66, no. 3, pp. 265-278, 1996.

[126] SHIEH, M. T.,BARKER, P. E., "Saccharification of Modified Starch to Maltose in a Semicontinuous Countercurrent Chromatographic Reactor-Separator (Sccr-S)," J. Chem. Technol. Biotechnol., vol. 63, no. 2, pp. 125-134, 1995.

[127] ZHANG, Y.,HIDAJAT, K.,RAY, A. K., "Modified reactive SMB for production of high concentrated fructose syrup by isomerization of glucose to fructose," Biochem Eng J, vol. 35, no. 3, pp. 341-351, 2007.

[128] RAY, A. K.,CARR, R. W., "Experimental-Study of a Laboratory-Scale Simulated Countercurrent Moving-Bed Chromatographic Reactor," Chem Eng Sci, vol. 50, no. 14, pp. 2195-2202, 1995.

[129] HASHIMOTO, K.,ADACHI, S.,NOUJIMA, H.,UEDA, Y., "A New Process Combining Adsorption and Enzyme Reaction for Producing Higher-Fructose Syrup," Biotechnol Bioeng, vol. 25, no. 10, pp. 2371-2393, 1983.

[130] DA SILVA, E. A. B.,DE SOUZA, A. A. U.,DE SOUZA, S. G. U.,RODRIGUES, A. E., "Analysis of the high-fructose syrup production using reactive SMB technology," Chem Eng J, vol. 118, no. 3, pp. 167-181, 2006.

[131] DA SILVA, E. A. B.,DE SOUZA, A. A. U.,RODRIGUES, A. E.,DE SOUZA, S. G. U., "Glucose isomerization in simulated moving bed reactor by Glucose isomerase," Brazilian Archives of Biology and Biotechnology, vol. 49, no. 3, pp. 491-502, 2006.

[132] DA SILVA, E. A. B.,DE SOUZA, A. A. U.,DE SOUZA, S. G. U.,RODRIGUES, A. E., "Simulated moving bed technology in the reactive process of glucose isomerization," Adsorption, vol. 11, pp. 847-851, 2005.

[133] MINCEVA, M.,GOMES, P. S.,MESHKO, V.,RODRIGUES, A. E., "Simulated moving bed reactor for isomerization and separation of p-xylene," Chem Eng J, vol. 140, no. 1-3, pp. 305-323, 2008.

[134] HASHIMOTO, K.,ADACHI, S.,NOUJIMA, H.,MARUYAMA, H., "Models for the separation of glucose-fructose mixture using a simulated moving bed adsorber," J. Chem. Eng. Jpn., vol. 16, no. 5, pp. 400-406, 1982.

[135] LAATIKAINEN, M.,HEINONEN, J.,SAINIO, T., "Modeling of chromatographic separation of concentrated-acid hydrolysates," Sep Purif Technol, vol. 80, no. 3, pp. 610-619, 2011.

[136] AGUILAR, R.,RAMIREZ, J. A.,GARROTE, G.,VAZQUEZ, M., "Kinetic study of the acid hydrolysis of sugar cane bagasse," J Food Eng, vol. 55, no. 4, pp. 309-318, 2002.

[137] GURGEL, L. V. A.,MARABEZI, K.,ZANBOM, M. D.,CURVELO, A. A. D., "Dilute Acid Hydrolysis of Sugar Cane Bagasse at High Temperatures: A Kinetic Study of Cellulose Saccharification and Glucose Decomposition. Part I: Sulfuric Acid as the Catalyst," Ind Eng Chem Res, vol. 51, no. 3, pp. 1173-1185, 2012.

[138] LU, Y. L.,MOSIER, N. S., "Kinetic Modeling Analysis of Maleic Acid-Catalyzed Hemicellulose Hydrolysis in Corn Stover," Biotechnol Bioeng, vol. 101, no. 6, pp. 1170-1181, 2008.

[139] EKEN-SARACOGLU, N.,MUTLU, S. F.,DILMAC, G.,CAVUSOGLU, H., "A comparative kinetic study of acidic hemicellulose hydrolysis in corn cob and sunflower seed hull," Bioresour. Technol., vol. 65, no. 1-2, pp. 29-33, 1998.

[140] KIM, B. J.,LEE, Y. Y.,TORGET, R., "An Optimal Temperature Policy of Percolation Process as Applied to Dilute-Acid Hydrolysis of Biphasic Hemicellulose," Appl Biochem Biotech, vol. 39, pp. 119-129, 1993.

[141] GIRISUTA, B.,JANSSEN, L. P. B. M.,HEERES, H. J., "Kinetic study on the acid-catalyzed hydrolysis of cellulose to levulinic acid," Ind Eng Chem Res, vol. 46, no. 6, pp. 1696-1708, 2007.

[142] KAWAJIRI, Y.,BIEGLER, L. T., "Optimization strategies for simulated moving bed and PowerFeed processes," Aiche J, vol. 52, no. 4, pp. 1343-1350, 2006.

[143] GUIOCHON, G.,FELINGER, A.,SHIRAZI, D. G.,KATTI, A. M., "Fundamentals of Preparative and Nonlinear Chromatography," 2nd ed., Academic Press, Boston, 2006.

[144] MINCEVA, M.,RODRIGUES, A. E., "Modeling and simulation of a simulated moving bed for the separation of p-xylene," Ind Eng Chem Res, vol. 41, no. 14, pp. 3454-3461, 2002.

[145] SILVA, V. M. T.,MINCEVA, M.,RODRIGUES, A. E., "Novel analytical solution for a simulated moving bed in the presence of mass-transfer resistance," Ind Eng Chem Res, vol. 43, no. 16, pp. 4494-4502, 2004.

[146]   KAWAJIRI, Y.,BIEGLER, L. T., "Large scale optimization strategies for zone configuration of simulated moving beds," Comput Chem Eng, vol. 32, no. 1-2, pp. 135-144, 2008.

[147]   KAWAJIRI, Y.,BIEGLER, L. T., "Nonlinear programming superstructure for optimal dynamic operations of simulated moving bed processes," Ind Eng Chem Res, vol. 45, no. 25, pp. 8503-8513, 2006.

[148]   AGRAWAL, G.,KAWAJIRI, Y., "Comparison of various ternary simulated moving bed separation schemes by multi-objective optimization," J Chromatogr A, vol. 1238, pp. 105-113, 2012.

[149]   SCHMIDT-TRAUB, H.,SCHULTE, M.,SEIDEL-MORGENSTERN, A., "Prepartive Chromatography," 2nd ed., Wiley-VCH, Germany, 2013.

[150]   MOSIER, N.,WYMAN, C.,DALE, B.,ELANDER, R.,LEE, Y. Y.,HOLTZAPPLE, M.,LADISCH, M., "Features of promising technologies for pretreatment of lignocellulosic biomass," Bioresour. Technol., vol. 96, no. 6, pp. 673-686, 2005.

[151]   CARRASCO, F.,ROY, C., "Kinetic-Study of Dilute-Acid Prehydrolysis of Xylan-Containing Biomass," Wood Sci Technol, vol. 26, no. 3, pp. 189-208, 1992.

[152]   MITTAL, A.,CHATTERJEE, S. G.,SCOTT, G. M.,AMIDON, T. E., "Modeling xylan solubilization during autohydrolysis of sugar maple and aspen wood chips: Reaction kinetics and mass transfer," Chem Eng Sci, vol. 64, no. 13, pp. 3031-3041, 2009.

[153]   DASARI, R. K.,BERSON, R. E., "The effect of particle size on hydrolysis reaction rates and rheological properties in cellulosic slurries," Appl Biochem Biotech, vol. 137, pp. 289-299, 2007.

[154]   SEIDEL-MORGENSTERN, A.,KESSLER, L. C.,KASPEREIT, M., "New developments in simulated moving bed chromatography," Chem Eng Technol, vol. 31, no. 6, pp. 826-837, 2008.

[155]   KAWAJIRI, Y.,BIEGLER, L. T., "Comparison of configurations of a four-column simulated moving bed process by multi-objective optimization," Adsorption, vol. 14, no. 2-3, pp. 433-442, 2008.

[156]   CHEN, R. F.,WU, Z. W.,LEE, Y. Y., "Shrinking-bed model for percolation process applied to dilute-acid pretreatment hydrolysis of cellulosic biomass," Appl Biochem Biotech, vol. 70-2, pp. 37-49, 1998.